1990

Topics in theoretical surface science: I Structures of clean and adsorbate covered surfaces II Epitaxy of metals on metal surfaces

Todd Joseph Raeker
Iowa State University

5

91

10554

INFORMATION TO USERS

The most advanced technology has been used to photograph and reproduce this manuscript from the microfilm master. UMI films the text directly from the original or copy submitted. Thus, some thesis and dissertation copies are in typewriter face, while others may be from any type of computer printer.

The quality of this reproduction is dependent upon the quality of the copy submitted. Broken or indistinct print, colored or poor quality illustrations and photographs, print bleedthrough, substandard margins, and improper alignment can adversely affect reproduction.

In the unlikely event that the author did not send UMI a complete manuscript and there are missing pages, these will be noted. Also, if unauthorized copyright material had to be removed, a note will indicate the deletion.

Oversize materials (e.g., maps, drawings, charts) are reproduced by sectioning the original, beginning at the upper left-hand corner and continuing from left to right in equal sections with small overlaps. Each original is also photographed in one exposure and is included in reduced form at the back of the book.

Photographs included in the original manuscript have been reproduced xerographically in this copy. Higher quality 6" x 9" black and white photographic prints are available for any photographs or illustrations appearing in this copy for an additional charge. Contact UMI directly to order.

U·M·I

University Microfilms International
A Bell & Howell Information Company
300 North Zeeb Road, Ann Arbor, MI 48106-1346 USA
313/761-4700 800/521-0600

Order Number 9110554

Topics in theoretical surface science: I. Structures of clean and adsorbate-covered surfaces. II. Epitaxy of metals on metal surfaces

Raeker, Todd Joseph, Ph.D.

Iowa State University, 1990

U·M·I
300 N. Zeeb Rd.
Ann Arbor, MI 48106

Topics in theoretical surface science
I. Structures of clean and adsorbate covered surfaces
II. Epitaxy of metals on metal surfaces

by

Todd Joseph Raeker

A Dissertation Submitted to the
Graduate Faculty in Partial Fulfillment of the
Requirements for the Degree of
DOCTOR OF PHILOSOPHY

Department: Chemistry
Major: Physical Chemistry

Approved:

Signature was redacted for privacy.

In Charge of Major Work

Signature was redacted for privacy.

For the Major Department

Signature was redacted for privacy.

For the Graduate College

Iowa State University
Ames, Iowa
1990

TABLE OF CONTENTS

FORMAT OF THE DISSERTATION

Three areas in the theoretical chemistry of metal surfaces are investigated in this dissertation. First, extensions of the general N-body corrected effective medium (CEM-N) theory are derived for the special high symmetry cases of bulk metal (CEM-B) and clean surfaces (CEM-S). The structure and energetics of various clean metal surfaces are then predicted using the CEM-S formalism and discussed. Second, a further extension from the clean surface CEM-S formalism is derived for atomic chemisorption on metal surfaces (CEM-A). And third, a modified CEM theory (MD/MC-CEM) is used to examine the dynamics of the initial stages of epitaxial deposition of metals on metal surfaces. The ultimate goal of the molecular dynamics calculations was the determination of the mechanisms behind the formation of equilibrium structures.

This dissertation follows the alternative style format. The work on bulk metals and their clean surfaces is contained in Paper I, entitled "*Corrected effective-medium method. IV. Bulk cohesive and surface energies of second- and third-row metals and multilayer relaxation of Al, Fe, and Ni.*" The work on chemisorption is contained in Paper II, entitled "*Corrected effective medium method calculations of the Chemisorption of H and N on Fe(100), (110), and W(110).*" The work on the deposition of metals on metal surfaces is contained in Papers III and IV, which are entitled "*Molecular dynamics simulations of metal adsorbates on metal surfaces: Rh on Ag(100).*" and "*Theoretical studies of dynamical phenomena in epitaxial surface systems.*", respectively.

Paper I has been published in Physical Review B; Paper II has been published in Surface Science; Paper III has been published in the Journal of Vacuum Science Technology A, and lastly; Paper IV has been submitted to Surface Science.

GENERAL INTRODUCTION

Many significant technological advances in surface science have been made over the past decade. These have provided a wealth of information concerning the atomic and electronic structure of surfaces. It is the atomic structures of metal surfaces that are of particular interest in this dissertation. Many metals exhibit surface structures different from that expected from a simple termination of the bulk lattice. This is important since the catalytic activity (or reactivity) of many metals depends significantly on the structure of their surfaces.

Accurate theoretical descriptions of the factors influencing the structures and reactivities of metal surfaces is an essential ingredient in understanding surface properties of technological importance. One important factor to understand is the energetic driving forces involved in the structural changes that surfaces can undergo. Many theoretical tools used to examine surfaces have already been developed and are well established. The further development and utilization of one such tool is the major purpose of the present dissertation.

The use of Quantum Theory in describing bonds between atoms has evolved to the point where accurate calculations on small molecules is now routine. It is however a very difficult task to calculate accurately the energetics and forces in multi-atom metal systems using quantum mechanics. The delocalized nature of the electrons in metals makes the task very laborious. This, coupled with the many electrons present in heavy elements, makes the effort impractical without the aid of approximations and extremely fast computers. The treatment of the extremely large number of electrons present in extended systems by a many electron wave function is the most serious of the problems that must be dealt with. Some appropriate approximations to reduce the complexity of a calculation must be developed as alternatives.

One approach that has proven quite useful is to reformulate the quantum mechanical wavefunction problem into an electron density-functional method. This then attempts to treat the total electron density as a variable rather than treating each electron separately. Density-Functional Theory became a complete and rigorous theory in the early 1960s with the famous works of Kohn and Sham [1]. Since then,

Density-Functional Theory has become quite useful and applicable to many systems [2]. One must however still expend a considerable amount of effort to treat heavy metal atoms as discussed by Salahub and Zerner [3].

There has emerged over the past few years a set of very promising alternatives to the costly first principles methods. These enable workers to quickly evaluate the interaction energy of a many atom system. These methods are categorized as Effective-Medium type theories which all make use of the important work of Puska *et. al* [4].. They calculated the high symmetry Kohn-Sham self-consistent LD solution [1] of an atom interacting with jellium[1]. The central idea behind any effective-medium type method is to replace the many body interactions among atoms by those of the above atom-jellium interactions. This is qualitatively shown in the schematic below.

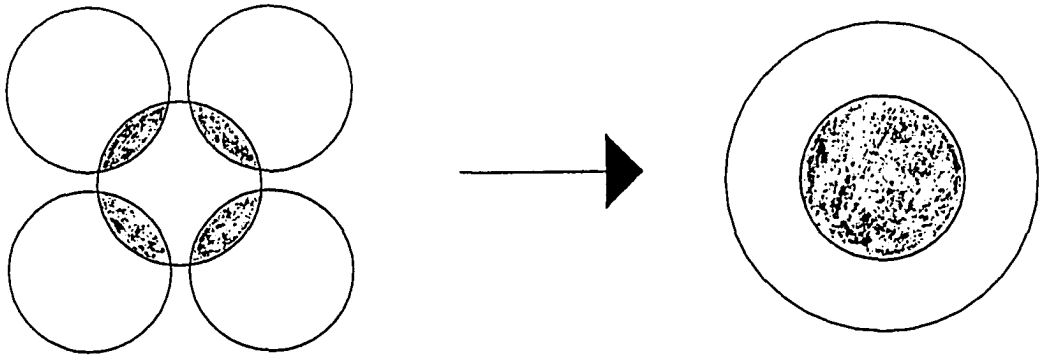

Fig. 1. Schematic drawing of the atom-atom and atom-jellium interactions

[1] Jellium is a three dimensional infinite homogeneous electron gas with a uniform positive density providing charge neutrality. Upon embedding an atom in jellium, the electron density becomes inhomogeneous.

In mathematical terms, the interaction energy of the system on the left is calculated by using as a reference state the atom-in-jellium system. This is in contrast to the usual reference of the vacuum. I introduce a general equation that employs this reference state from which all effective medium type methods can be derived. First label the atoms by $\{A_i,\ i=1,...N\}$ where the A_i can be any type of atom. The interaction energy in the N-atom system, denoted $\Delta E(\{A_i\})$, is written as

$$\Delta E(\{A_i\}) = \sum_{i=1}^{N} \Delta E_j(A_i;n_i) + corrections \qquad (1)$$

The $\Delta E_j(A_i;n_i)$ term is the embedding energy of atom A_i in jellium with an electron density n_i. The corrections represent the non-self-consistent energy that corrects for the use of the reference state of the atom-jellium system to that of the vacuum reference state. This is what characterizes the effective-medium type theories. Note that Eq. (1) is exact only if the above correction is self-consistently evaluated.

It is the particular choice of the jellium electron densities and the form of the corrections that distinguishes the various effective-medium type theories based on Eq. (1). In addition, the empirical theories use different embedding energy functions altogether. Regardless of the particular method, the energy terms have a few general features:

1. The embedding energies are functions of only the identity of the atom and the jellium electron density, and can be calculated once and for all and tabulated;

2. The corrections incorporate the differences between the more localized electron density and nuclear charges in the real N-atom system compared to the many atom-jellium systems.

Note that a self-consistent solution to Eq. (1) would require more effort than a self-consistent solution of the original N-atom system. Because of this fact, I reemphasize that the effective-medium type methods are not self-consistent (although a variational approach can not be ruled out). One then hopes that the corrections are relatively

small. However, I stress that the non-empirical theories based on Eq. (1) use real atoms and their electron densities. The jellium interaction is really only used to translate an electron density environment into an energy via the embedding energy function.

In what follows I derive the N-body CEM energy relations from which further developments and extensions are introduced and discussed in Papers I through IV. My major professor and I have recently published a review paper [5] providing general derivations of all current effective-medium type theories. The reader is encouraged to use this as a resource to gain a general understanding of each method. Some of the calculations that are presented in Papers I and II are compared to some results of the other methods. An understanding of all these methods would enable differences in results and the later discussions to be better understood.

The results presented in Papers I and II are both tests of the CEM method and predictions. Predictions that are compared favorably to experimental results lend support of predictions for which experimental data are unavailable. In contrast, the results in Papers III and IV are mostly predictive with a qualitative comparison to experimental data.

CORRECTED EFFECTIVE MEDIUM (CEM) THEORY

General Derivation

The derivation that I present follows that of Kress and DePristo [6] to which the reader is referred for further details. As discussed in the previous introduction, I consider an N-body system consisting of atoms $\{A_i,\ i=1,...,N\}$ where the A_i can be any type of atom. The nuclear positions are $\{\vec{R}_i\}$, nuclear charges are $\{Z_i\}$, and the electronic coordinates relative to each nuclear position are $\{\vec{r}_i\}$. The spin-up, spin-down and total electron densities around each atom are denoted by $n^+(A_i;\vec{r}_i)$, $n^-(A_i;\vec{r}_i)$ and $n(A_i;\vec{r}_i)$, respectively.

The desired quantity is the energy difference between the interacting and non-interacting systems of atoms, denoted by

$$\Delta E(\{E_i\}) = E(\sum A_i) - \sum_{i=1}^{N} E(A_i) \tag{2}$$

To evaluate this energy difference, I make use of the interaction energy of each atom embedded into jellium [4], defined by:

$$\Delta E_j(A_i;n_i) = E(A_i+n_i) - E(A_i) - E(n_i) \tag{3}$$

Here, $E(n_i)$ and $E(A_i+n_i)$ are the total energies of the jellium and jellium plus atom A_i systems, respectively. Solving Eq. (3) for the atom energy, $E(A_i)$, and subsequent substitution into Eq. (2) leads one to the first fundamental relationship of the CEM theory:

$$\Delta E(\{A_i\}) = \sum_{i=1}^{N} \Delta E_j(A_i;n_i) + E(\sum A_i) - \sum_{i=1}^{N} [E(A_i+n_i) - E(n_i)] \tag{4}$$

In Eq. (4), the first term on the right hand side is the sum of the embedding energies for each atom in jellium of some (as yet unspecified) electron density n_i. These energies can be evaluated from the SCF-LD calculations of Puska *et al.* [4] or from other, semi-empirical, methods as discussed in Papers I and II. I shall not distinguish between these two functions until then. The form of the remaining terms in Eq. (4) and the choice of the electron densities n_i are addressed in the remainder of this subsection.

The total energy is composed of coulombic, kinetic, exchange and correlation parts. I denote this separation by

$$E(\{A_i\}) = V_c(\{A_i\}) + G(\{A_i\}) \tag{5}$$

where V_c is the coulombic energy and G is the sum of the kinetic and exchange-correlation energies, T and E_{xc}, respectively. Substitution of Eq. (5) into Eq. (4) yields the second fundamental relationship of CEM theory,

$$\Delta E(\{A_i\}) = \sum_{i=1}^{N} \Delta E(A_i;n_i) + \Delta V_c(\{A_i\}) + \Delta G(\{A_i\}) \tag{6}$$

where

$$\Delta G(\{A_i\}) = G(\sum A_i) - \sum_{i=1}^{N} [G(A_i+n_i) - G(n_i)] \tag{7}$$

The ΔV_c term can be written exactly as Eq. (7) with V_c in place of G everywhere in the equation. Eq. (6) is in the same form as Eq. (1) where the last two terms correspond to the corrections.

Specifically Eq. (6) expresses the stabilization energy of the N-body system as a total of three terms:

1. The sum of the embedding energies for the separated atoms in jellium;
2. The difference in the coulombic energy between the real system and all the separated atoms in jellium;

3. The difference in the sum of the kinetic, exchange, and correlation energies between the real system and all the separated atoms in jellium.

The ΔV_e term accounts for two physical effects. The first is the difference in the homogeneity of the electron density distributions in the real and atom-in-jellium systems. The second is the difference between the uniform positive background in the jellium and the point nuclear charges in the real system. For the ΔG term there are also two effects. The most important is the difference in the uniformity of the electron density distributions. The second is the (possible) difference in spin-polarization between the real system and the unpolarized atom-in-jellium one.

So far, in the energy terms just discussed above, I have not specified electron density distribution of the many atom system. I am at liberty to choose what ever electron density I wish. However, if one expects reasonably accuracy in describing the real many atom system, the correct electron density must either be constructed or determined through the calculation itself, as done in fully self-consistent methods. Since the CEM method is not a self-consistent method, the easiest solution to this is to assume a simple construction of the electron density distribution. However, I would like to retain the essence of real atoms.

At the moment I do not need the exact form of the atomic electron densities. However in order to continue with the derivation, I must decide on a basic construction of the electron density distribution of the whole system. The approach I take makes use of the assumption of a superposition of atomic electron densities. This simply states that the electron density at any point in space, $\vec{r}$, is the sum of the electron spin-densities from each atom:

$$n^{\pm}(\vec{r}) = \sum_{i=1}^{N} n^{\pm}(A_i;\vec{r}-\vec{R}_i) \tag{8}$$

Even with this approximate approach the effects of electron inhomogeneity and spin-polarization do not vanish. Since the difference in energies of the real vs. jellium system is calculated, it is hoped that a lower sensitivity to the use of accurate electron densities will be obtained than the direct calculation of the energetics in either system by itself due to cancelation of errors. This is assuming of course that the proper electron density in the jellium is used. Thus, a self-consistent calculation or experimental data is employed via the $\Delta E(A_i;n_i)$. Only the corrections due to inhomogeneity of the electron and positive charge distributions are calculated non-self consistently. This includes the spin-polarization of the electron density.

Since the additive electron density approximation is assumed to hold for each atom in the jellium also, the coulombic interactions of an atom interacting with both the homogenous jellium electron density n_i and the positive background, cancel. This is a consequence of the coulomb potential being linear in the electron densities. The difference in coulombic energies is then just the interatomic coulomb terms:

$$\Delta V_c(\{A_i\}) = \frac{1}{2}\sum_{i=1}^{N}\sum_{i\neq j}^{N} V_c(A_i,A_j) \tag{9}$$

The coulombic energy can be broken into separate electron-electron and nuclear-nuclear repulsive and electron-nuclear attractive contributions;

$$\Delta V_c(i,j) = \int \frac{n(A_i;\vec{r}_1-\vec{R}_i)\,n(A_j;\vec{r}_2-\vec{R}_j)\,d\vec{r}_1\,d\vec{r}_2}{|\vec{r}_{12}|} + \frac{Z_i Z_j}{R_{ij}} - \int \frac{n(A_i;\vec{r}_1-\vec{R}_i)\,Z_j\,d\vec{r}_1}{|\vec{r}_1-\vec{R}_j|} - \int \frac{n(A_j;\vec{r}_2-\vec{R}_j)\,Z_i\,d\vec{r}_2}{|\vec{r}_2-\vec{R}_i|} \tag{10}$$

Where I have defined $\vec{r}_{12}=\vec{r}_1-\vec{r}_2$ and $R_{ij}=|\vec{R}_i-\vec{R}_j|$.

This result is quit appealing. The additive atomic electron densities produce a very simple pairwise coulombic interaction that does not depend on the jellium electron density. If appropriate forms of the atomic electron densities $n(\vec{r})$ are used, these electron-electron and electron-nuclear integrals can be evaluated quite easily. I shall

discuss the specific forms of atomic electron densities in the computational details section later.

To continue with the evaluation of the correction energy, accurate electron spin-density energy functionals must be utilized for the kinetic, exchange and correlation energies. The functional G is written as:

$$G = \int [\tau(n^+(\vec{r})) + \tau(n^-(\vec{r})) + \epsilon_{xc}(n^+(\vec{r}), n^-(\vec{r}))] d\vec{r} \tag{11}$$

To ensure that the atomic energies can be eliminated between Eqs. (2) and (3) the same kinetic-exchange-correlations energy functionals as used in the SCF-LD calculations of the atom embedded in jellium system must be used. The SCF-LD calculations utilized the local Dirac [7] exchange and local Gunnarsson-Lundqvist [8] correlation functionals. However, the exact kinetic energy within the Kohn-Sham formalism was used, which is not possible within the electron density based CEM method. Instead, an accurate Pade representation of the full gradient expansion [9] is used.

I reproduce the kinetic and exchange energy functionals here since these have consequences when the superposition of atomic electron density approximation is imposed. Also they will be useful in determining the jellium electron densities used in Eqs. (6) and (7). First let us examine the kinetic energy functional where we write the total kinetic energy:

$$T = \int [\tau(n^+(\vec{r})) + \tau(n^-(\vec{r}))] d\vec{r} \tag{12}$$

The Pade representation is written as

$$\tau(n^\pm(\vec{r})) = \tau_0(n^\pm(\vec{r})) \frac{(1+0.95x+14.2811x^2-19.57962x^3+26.64777x^4)}{(1-0.05x+9.99802x^2+2.96085x^3)} \tag{13}$$

where

$$\tau_0(n^{\pm}(\vec{r})) = \frac{3}{10}(6\pi^2)^{\frac{2}{3}}\, n^{\pm}(\vec{r})^{\frac{5}{3}} \tag{14}$$

is the local kinetic energy functional as originally used in Thomas-Fermi theory [10]. The gradient contribution comes in via

$$x = \frac{5}{108}(6\pi^2)^{-\frac{2}{3}} \frac{|\nabla n^{\pm}(\vec{r})|^2}{n^{\pm}(\vec{r})^{\frac{8}{3}}} \tag{15}$$

The total exchange energy

$$E_x = \int [\varepsilon_x(n^{+}(\vec{r})) + \varepsilon_x(n^{-}(\vec{r}))]\, d\vec{r} \tag{16}$$

uses the local energy density functional written as

$$\varepsilon_x(n^{\pm}(\vec{r})) = -\frac{3}{2}\left(\frac{3}{4\pi}\right)^{\frac{1}{3}} n^{\pm}(\vec{r})^{\frac{4}{3}} \tag{17}$$

The ± for the kinetic and exchange functionals represents a separate calculation of the up(+)/down(-) electron spin density energies.

Since these energy terms are not linear in the electron density, the correction energy functional ΔG, does not simplify to pairwise interactions under the superposition approximation. This is another point in the CEM theory where many-body interactions arise. The other is, of course, the embedding energy. The interactions in a real many-body system are indeed many-body in nature.

To finish the derivation, one must determine the jellium electron densities that are employed in Eqs. (6) and (7). I have already alluded to this determination in the diagram on page 3 where the surrounding atoms in some way provide the background electron density in which an atom is embedded. The proper choice of this electron density is important. Since the non-self-consistent part of the CEM formalism is expected to be less accurate than the self-consistent part ($\Delta E_i(A_i;n_i)$), I minimize the

$|\Delta G|$ term[2] with respect to the n_i. Since G is a complicated functional of both the electron spin-densities and their gradients, an analytic minimization of $|\Delta G|$ is not possible in the current form. In addition, a numerical minimization does not provide insight into the proper choice of the jellium densities. However, upon examining the variation of the sum of the leading terms, which are local kinetic-exchange energy, one can make progress. The integrand in Eq. (11) (excluding the correlation energy functional) can be approximated quite closely by a quadratic in n^+ as shown by DePristo and Kress [9] and reproduced in Figure 2.

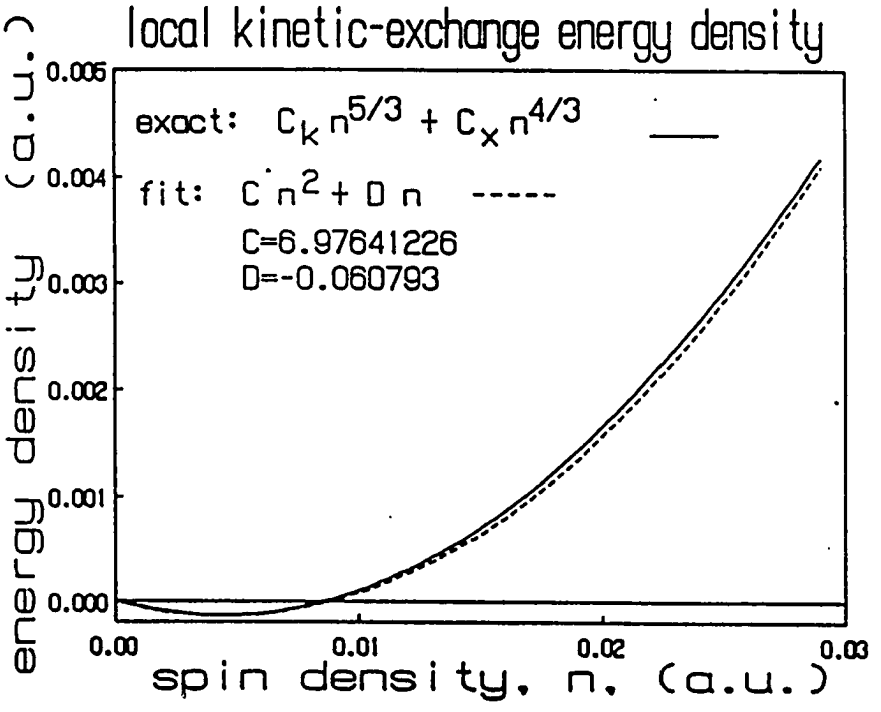

Fig. 2. Local kinetic-exchange spin-up energy density, $C_k(n^+)^{5/3} + C_x(n^+)^{4/3}$ with $C_k=(3/10)(6\pi^2)^{2/3}$ and $C_x=-(3/2)(3/4\pi)^{1/3}$, as a function of spin-up density n^+. Exactly the same function holds for n^-. A quadratic fit, based upon duplication of the exact position and depth of the minimum, is also shown

[2] Minimization of the sum $\Delta V_c+\Delta G$ can result in negative values for the jellium density since the coulombic energy can be quite negative.

Within this quadratic approximation for the energy functional in both the spin up and down electron densities , n^+ and n^-, we have

$$G(n) \approx C\int[n^+(\vec{r})^2 + n^-(\vec{r})^2]d\vec{r} + D\int[n^+(\vec{r}) + n^-(\vec{r})]d\vec{r} \tag{18}$$

where C and D are the coefficients of the quadratic fit.

Now using Eq. (7) and the atomic electron density superposition approximation we can now rewrite ΔG after some algebra as

$$\begin{aligned}\Delta G = C\sum_i\sum_{j\neq i}\int[n^+(A_i;\vec{r}-\vec{R}_i)n^+(A_j;\vec{r}-\vec{R}_j) + n^-(A_i;\vec{r}-\vec{R}_i)n^-(A_j;\vec{r}-\vec{R}_j)]d\vec{r} \\ -2C\sum_i\int[n^+(A_i;\vec{r}-\vec{R}_i)n_i^+ + n^-(A_i;\vec{r}-\vec{R}_i)n_i^-]d\vec{r}\end{aligned} \tag{19}$$

where the linear contribution completely cancels. Since the SCF-LD jellium utilizes an unpolarized electron gas, let $n^+_i = n^-_i = n_i/2$ in Eq. (19), yielding:

$$\begin{aligned}\Delta G = C\sum_i\sum_{j\neq i}\int[n^+(A_i;\vec{r}-\vec{R}_i)n^+(A_j;\vec{r}-\vec{R}_j) + n^-(A_i;\vec{r}-\vec{R}_i)n^-(A_j;\vec{r}-\vec{R}_j)]d\vec{r} \\ -C\sum_i Z_i n_i\end{aligned} \tag{20}$$

Setting $\Delta G=0$ of Eq. (20) leads to solutions for n_i which are <u>independent</u> of the coefficient C. The most symmetric solution is

$$n_i = \frac{\sum_{j\neq i}\int[n^+(A_i;\vec{r}-\vec{R}_i)n^+(A_j;\vec{r}-\vec{R}_j) + n^-(A_i;\vec{r}-\vec{R}_i)n^-(A_j;\vec{r}-\vec{R}_j)]d\vec{r}}{Z_i} \tag{21}$$

This possesses several reasonable physical properties that are worth discussing. First, the jellium electron density on atom A_i due to atom A_j is proportional to the electron spin-density of atom A_j averaged over atom A_i with the weight function equal to the (normalized) electron spin-density of A_i. Since the size of atom A_i can be characterized by the atomic electron spin-density, such an average makes good physical sense. Second, for the case of <u>spin-unpolarized</u> atoms, n_i becomes

$$n_i = \frac{\sum_{j \neq i} \int [n(A_i;\vec{r}-\vec{R}_i)\, n(A_j;\vec{r}-\vec{R}_j)\, d\vec{r}}{2Z_i} \tag{22}$$

This is half of the total electron density average because of a division of electron density between the two atoms, an effect which is analogous to dividing up a pair potential, V_{ij}, into $\frac{1}{2}V_{ij} + \frac{1}{2}V_{ji}$ and which thus eliminates over counting of embedding energies. Note that for a given pair of atoms, i and j, the electron density overlap contribution (numerator of Eqs. (21) and (22)) is always equal on each atom but the jellium electron density contribution may differ because of the inverse weighting by the atomic number. Third, the integrals in Eqs. (21) and (22) are positive for all well behaved atomic electron densities.

It should be noted that the CEM energies are not invariant to arbitrary changes in n_i because the ΔG terms are not calculated self-consistently. Because of this, an optimal choice of n_i is important to achieve. Small variations in n_i do not alter significantly the CEM energies because of a cancellation between the embedding energies and ΔG. The quadratic approximation is only used to find an analytic choice for the n_i. In all actual calculations, the original kinetic-exchange-correlation energy functionals are used in Eq. (7).

Papers I and II extend Eq. (6) by deriving CEM interaction energy relations specific for high symmetry cases in bulk lattices and surfaces. In both cases all the energy terms, including the jellium electron densities n_i, were evaluated in the same manner. The purpose of Paper I was to derive specific CEM relations for the bulk cohesive energy of any bulk lattice and extend this to surfaces. The possible multilayer relaxations and their driving forces were examined within the CEM formalism.

Paper II expanded on the surface relations of Paper I to cases of ordered overlayers of chemisorbed atoms on surfaces. The prediction of the binding energies and heights for the adsorbates were the primary purpose. The effect the adsorbates have on the structure of the surface was also examined.

While the calculations presented in Papers I and II are important they lacked at

least one important realistic aspect. In those calculations I assumed an equilibrium structure, based on only a few variable key structural parameters, then simply calculated its energy. The way in which an equilibrium structure is formed is disregarded. A next logical step in developing the CEM method was to incorporate it into molecular dynamics calculations so many more degrees of freedom can be varied. Papers III and IV present some of results of my work which involves the dynamics of metal adsorbates on metal surfaces.

The many degrees of freedom in a MD type calculation requires that the interaction potential be simple enough to evaluate many thousands of times for a single simulation. The numerical evaluation of the correction energy ΔG has two closely related and costly effects. The first is that the numerical evaluation is very slow for a many atom system. The second is that the derivatives of ΔG must be numerically evaluated and thus two evaluations per degree of freedom are required. This is not acceptable for even today's supercomputers. Thus to do molecular dynamics calculations the CEM method needed to be speeded up considerably. To achieve this, the CEM method was modified such that the correction energy functional, ΔG, was approximated as a simple empirical function of the jellium electron density. This is just like the embedding energy function. Thus the large amount of computer time involved in numerically integrating and differentiating the term ΔG accurately can be avoided. The derivation of this modified CEM method is shown in these papers where MD/MC-CEM denotes this new form of CEM.

SOME COMPUTATIONAL DETAILS OF CEM

The purpose of this section is to discuss some of the computational details of implementing CEM that have not been published before. In addition some details that have been published will be briefly mentioned to give the interested reader a better idea of what is involved in calculating CEM energies.

To keep the CEM method as accurate as possible accurate atomic electron densities are employed. To this end Hartree-Fock Slater-Type-Orbital (HF-STO) electron densities are employed. The following details the use of these electron densities in further calculations.

Gaussian Expansion of HF Electron Densities

The major impetus for developing the CEM method is to have a method in which the interaction potential can be calculated very quickly with reasonable accuracy. To help achieve this goal specific steps have been taken to make the method as computationally efficient as possible. To facilitate faster evaluations of the overlap and coulomb integrals in Eqs. (22) and (10) the radial part of the above mentioned HF-STO electron densities are fitted by an even tempered Gaussian expansion [11] in r (the radial distance from the nucleus). Using these Gaussians, the above integrals can be evaluated analytically [12].

Two sets of expansions are utilized for each atom. The first is for spherical type electron densities such as obtained from s-type orbitals. In addition, the d and f orbitals are forced to be spherical to simplify considerably the analytic overlap and coulomb integrals because the angular integration of d and f orbitals is very complicated. Since it is felt that the angular component of these orbitals do not contribute significantly to bonding in extended systems, sphericallization would not be a severe approximation. The second type of expansion is for non-spherical electron densities obtained from p-type orbitals. The basic form of the Gaussian expansion is given as

$$n_G(r) = \sum_{i=0}^{N} c_i r^i \exp(-\gamma \alpha^i r^2) \tag{23}$$

where the parameters γ, α, and the coefficients $\{c_i\}$ are different for each type of atom. The spherical and non-spherical electron densities have ℓ equal to 0 and 2, respectively. For the non-spherical (p-type) Gaussian electron densities, the angular contributions are also included as

$$\frac{3x^2}{r^2}\ ,\ \frac{3y^2}{r^2}\ ,\ \frac{3z^2}{r^2} \tag{24}$$

times the whole expansion to obtain the idividual p_x, p_y, p_z densities, respectively.

Use of an even tempered Gaussian expansion is very convenient since there are only two distinct adjustable non-linear parameters. These generate many exponents to ensure flexibility in fitting the HF-STO electron densities, as will be described shortly, or in minimizing the total energy as done by Schmidt and Ruedenberg [11].

The procedure for fitting the Gaussian expansion to existing HF electron densities is simple. We use a standard computer routine called 'STEPIT' [13] which minimizes any function with respect to a set of parameters. I shall go into more detail later but for now I just briefly describe the fitting process. The function we minimize is simply related to the square of the difference between the Gaussian and HF-STO electron density. Initial guesses of the parameters γ and α are inputed, and STEPIT iteratively changes these to appropriate values such that the difference function is minimized. In each iteration, the $\{c_i\}$ are obtained to achieve a best fit for each set of α and γ.

The quality of the above fit of the expansion to the HF-STO electron densities was quite good except at large distances from the nucleus. The Gaussian electron densities were typically up to 2 orders of magnitude higher than the HF-STO densities (10^{-6} vs. 10^{-8}) in this region and thus did not decay quickly enough. This did not cause significant errors in the CEM calculations but, as I shall discuss later, did have an effect on some physical properties that depend on very small energy differences and changes in the electron density distributions. Paper I utilized this particular form of the expansion but after publication, a new expansion was created. This new Gaussian expansion is currently in use and Papers II through IV of this dissertation have all used it.

The problem with the original Gaussian expansion in Eq. (23) was that it was not flexible enough in accurately fitting both the extremely high electron densities in the core region and the very low electron density far from the nucleus. To correct that problem two things were done. First, the flexibility was increased by adding a new parameter in the expansion:

$$n_{STO}(r) - n_G(r) - \sum_{i-0}^{N} c_i r^l \exp(-\gamma \alpha^{i^\beta} r^2) \; - \; \sum_{i-0}^{N} c_i r^l \phi_i \tag{25}$$

The additional parameter β can exert a considerable influence on the size and distribution of parameters generated from α in the expansion. Second, since the long range electron density behavior was a problem in the first expansion, specific steps were taken to ensure a better quality fit in this new expansion.

At large distances the Gaussian electron density must match the HF-STO electron densities. Consider two points: r_j is some radial point very far from the nucleus and r_{j-1} some point slightly closer. I require that the Gaussian electron density be equal to the HF-STO electron density at both points

$$\begin{aligned} n_G(r_{j-1}) &= n_{STO}(r_{j-1}) \\ n_G(r_j) &= n_{STO}(r_j) \end{aligned} \tag{26}$$

In these equations I employ a table containing a set of closely spaced radial distances r_j ($j=1,N_{sp}$ and typically N_{sp}=2000) ranging from $r_1=10^{-8}$ to some r_{max}. Here r_{max} is determined such that $r_{max}^2 n_{STO}(r)=10^{-5}$ *a.u.* The following discussion is completely general in the sense that fitting to spherical or non-spherical electron densities is transparent. One only needs to let ℓ equal the appropriate value for spherical (s) type or non-spherical (p) type electron densities. Note that only the radial part of the electron densities are fit. The angular parts of the electron density distributions are completely retained for the p type orbitals while the d and f orbitals are sphericallized in with the s type orbitals.

For large r, say r_j with j near N_{sp}, only the $i=0$ term in the Gaussian expansion contributes significantly to the total electron density when $\alpha>1$. Therefore Eq. (25)

can be truncated to

$$n_G(r_j) = c_o r_j^l \exp(-\gamma\ r_j^2) \tag{27}$$

This is very convenient since now I have a way in which γ can be easily determined.

Dividing the first equation in (26) by the second and replacing n_G with that given in Eq. (27) one obtains after some algebra

$$\exp(-\gamma\,(r_{j-1}^2 - r_j^2)) = \frac{n_{STO}(r_{j-1})\,r_j^l}{n_{STO}(r_j)\,r_{j-1}^l} \tag{28}$$

Solving this for γ gives

$$\gamma = \frac{\ln\left[\dfrac{n_{STO}(r_{j-1})\,r_j^l}{n_{STO}(r_j)\,r_{j-1}^l}\right]}{(r_j^2 - r_{j-1}^2)} \tag{29}$$

This determines γ much more reliably than simply allowing STEPIT to determine a value by a fit to the global electron density.

It remains to determine what α and β are for each type of Gaussian expansion. This is done by minimizing the function,

$$\sum_{j=1}^{N_\sigma} r_j^2 [n_G(j) - n_{STO}(j)]^2 \tag{30}$$

with respect to both α, β and the $\{c_i\}$. This function has two effects in the fitting process. First, the square of the difference matches the Gaussian electron density to the HF-STO electron density. Second, including r^2 has the effect of putting more weight on the difference term at large distances from the nucleus. This last feature provides an added measure of control on providing a better quality fit of the small electron densities far from the nucleus. Fortunately, this is not at the expense of a quality fit to the core electron densities. For each choice of α and β in the minimization procedure, the coefficients of the expansion in Eq. (25) are determined by

a least squares fit.

Multiply both sides Eq. (25) by ϕ_k and integrate over r^2dr to get

$$\theta_k = \sum_{i=0}^{N} c_i \chi_{ki} \tag{31}$$

where for convenience I let

$$\theta_k = \int \phi_k(r) n_{STO}(r) r^2 dr$$
$$\chi_{ki} = \int r^l \phi_k(r) \phi_i(r) r^2 dr \tag{32}$$

Doing this for every expansion function ϕ_k ($k=1,N$), I can then create the matrix equation

$$\underline{\Theta} = \begin{bmatrix} \theta_0 \\ \theta_1 \\ \cdot \\ \cdot \\ \cdot \\ \theta_N \end{bmatrix} = \begin{bmatrix} \chi_{00} & \chi_{01} & \cdot & \cdot & \cdot & \chi_{0N} \\ \chi_{10} & \cdot & \cdot & \cdot & \cdot & \cdot \\ \cdot & \cdot & \cdot & \cdot & \cdot & \cdot \\ \cdot & \cdot & \cdot & \cdot & \cdot & \cdot \\ \cdot & \cdot & \cdot & \cdot & \cdot & \cdot \\ \chi_{N0} & \cdot & \cdot & \cdot & \cdot & \chi_{NN} \end{bmatrix} \begin{bmatrix} c_0 \\ c_1 \\ \cdot \\ \cdot \\ \cdot \\ c_N \end{bmatrix} = \underline{\mathbf{X}}\underline{C} \tag{33}$$

The coefficients $\{c_i\}$ can then be readily found by numerically solving this set of linear equations by standard mathematical procedures.

I summarize the process of fitting the even tempered Gaussians as follows:

1. Obtain the HF-STO electron densities and set up a table of 2000 points spanning the whole range of the atomic electron density;
2. Obtain γ from Eq. (29);
3. Guess α and β;
4. Find the coefficients $\{c_i\}$ from Eqs. (31) through (33) and evaluate the Gaussian electron density in Eq. (25);

5. Determine the value of Eq. (30);

6. STEPIT changes α and β according to a modified Newton-Raphson procedure;

7. Repeat step 4 through 6 until Eq. (30) is minimized with respect to α, β and the $\{c_i\}$.

The above procedure is carried out twice for each atom. Once for the spherical (s and, if present, d and f type) electron densities and again for non-spherical (p-type) electron densities. In addition, the number of Gaussian functions are varied to further minimize Eq. (30). I have found the spherical density expansion required about 35 terms and the non-spherical density expansion required about 25 terms for Eq. (30) to be minimized. This provided electron densities in agreement with STO values usually to better than 0.1 % regardless of the magnitude of the electron density.

The following papers contain some of the initial developments and applications of the CEM method. Each paper refers to Papers I-IV that are not the same papers that are presented in the dissertation.

PAPER I

CORRECTED EFFECTIVE MEDIUM METHOD: IV. BULK COHESIVE AND SURFACE ENERGIES OF SECOND AND THIRD ROW METALS AND MULTILAYER RELAXATION OF AL, FE AND NI

Corrected Effective Medium method: IV. Bulk Cohesive and Surface energies of second and third row metals and multilayer relaxation of Al, Fe and Ni.

Todd J. Raeker
and
Andrew E. DePristo[1]
Department of Chemistry
Iowa State University
Ames, Iowa

[1] Camille and Henry Dreyfus Teacher-Scholar; Alfred P. Sloan Fellow

ABSTRACT

We provide a detailed analysis and discussion of the recently developed corrected effective medium method (CEM) as applied to the calculations of the bulk cohesive energies of the second and third row metals. The results demonstrate that a quantitatively accurate description of these quantities requires a new "covalent" embedding function instead of the SCF-LD Puska *et al.* [29] "ionic" embedding function. Construction of these covalent embedding functions from diatomic and bulk electron density binding potentials is detailed.

We present the formalism within the CEM method for the calculation of the surface energy of infinitely periodic two-dimensional solid surfaces. Calculations of the surface energies for the perfectly terminated low miller index faces of Na, Mg, Al, K, Ca, Fe, Ni and Cu are carried out. These results are compared to experimental measurements and very good agreement is found for almost all of these metals. More demanding multilayer surface relaxation calculations are performed for Al(111),(110),(100), Ni(110),(100), and Fe(100). Very good agreement with experimental observations is obtained for these systems with the exception of Al(111) and (100). Detailed analysis of these calculations leads to an explanation of the relaxation process and its driving components.

1. INTRODUCTION

The experimental and theoretical study of metal surfaces has produced a wealth of information concerning the electronic and structural properties of metal surfaces. Of particular interest for the present paper are the geometric deviations of surfaces from that of the truncated bulk arrangement. Observations of large multilayer relaxations have been made for a number of systems such as Al(110) [1,2] and Ni(110) [3-6]. Smaller relaxations limited to the top surface layer have also been reported for Al(100) [7,8], Ni(100) [9] and Fe(100) [10].

First principles self-consistent calculations using a local-density functional formalism [11,12] have been carried out for a small number of systems, obtaining good agreement with experiment. These calculations, though accurate and very informative, are computationally very time consuming and difficult to carry out. Thus a large variety of simpler theoretical models [13-21] have also been developed in an attempt to predict and explain these dramatic deviations from that of the ideal surface. Some of these simplistic models are unable to accurately predict the magnitude and sometimes even the direction of the relaxation process. By contrast, the previously developed embedded-atom method EAM of Daw and Baskes [22] has recently been applied to surfaces of fcc transition metals [23] and though not being self-consistent produced relatively good agreement with experimental observations and measurements for surface energies and multilayer relaxations. In addition, the related effective medium EM theory [24-25] has been applied to the relaxation of Al surfaces [25] with some success.

Recently three articles [26-28] (referred to as Papers I, II and III) have been published detailing the development and applications of the corrected effective medium CEM method for the calculation of the interaction energies of small and large systems, including diatomic molecules, metal clusters, and bulk solids. In the present paper, we apply the CEM method to the calculation of the surface energy of a variety of metal surfaces. The CEM method is not entirely self-consistent but it does, as will be discussed in Section III, have a basic component of self-consistency. Like the effective medium theory, the CEM method begins by replacing the interaction energy of the

multi-atom system by the summation of the embedding energies for each atom in jellium having an effective electron density provided by the rest of the atoms in the system. The energy of embedding an atom in jellium is known from the SCF-LD calculations of Puska *et al.* [29] as a function of the homogeneous electron gas density. In CEM, one goes further by introducing and evaluating numerically the explicit *corrections* which describe the coulombic-kinetic-exchange-correlation energies in the multi-atom and jellium systems.

It is worthwhile to discuss briefly the relationship between the EM, CEM and EAM methods. It is important to emphasize that the CEM formalism was not developed as an explicit correction to either of the other theories, but was derived from a consistent replacement of the fundamental relationship between the interaction energy of an N-body system and the embedding energy of each atom in jellium. The derivation is completely different from that of either of the EM or EAM theories. Nevertheless, by suitable approximations to the CEM formula, one can derive either EM or EAM theory. For EM, one neglects the correction for the kinetic - exchange - correlation energy; approximates the coulombic correction via an induced polarization formula; uses the SCF-LD embedding functions; and, uses a slightly different choice for the density of the jellium. For EAM, one also neglects the correction for the kinetic-exchange-correlation energy; replaces the coulombic correction by an empirical function; uses empirical embedding functions; and, uses a particularly simple choice of the jellium density. More details of these relationships can be found in Papers I and II, with some further remarks in Paper II.

One of the important points to come from Paper II was that the Puska *et al.* embedding curve reflects a rather ionic interaction of the atom with jellium. For homonuclear systems this is not quite correct and one should introduce another correction to reflect this fact. The form and implementation of this correction is still under active investigation, and at present a (semi-empirical) covalent embedding function is used to replace the ionic Puska *et al.* interaction in order to be quantitatively accurate for homonuclear systems. These curves were constructed from knowledge of the experimental diatomic binding curves in Paper II.

In Paper III the N-body formalism was derived for an infinitely periodic 3D bulk

metal system with one atom per unit cell. Applications to the binding in Mg_N and Cu_N clusters with N=2,3...13,19 were presented. The covalent embedding functions for these two metals were constructed from knowledge of both the diatomic and bulk binding curves. It was suggested that these embedding functions were not functions of the number of atoms in the system but instead were universal for any one type of atom in a homogeneous system.

The present article is divided into four sections. In Section II we derive the CEM-N relation for infinite systems with 2D translational symmetry (e.g., surfaces). In Section III we present calculated bulk cohesive energies for the metals of the second and third rows. The covalent embedding functions for Al, Na, K, Ca, Fe and Ni are constructed. We then present and discuss results for the calculated surface energies of the perfectly terminated (111), (100), (110) faces of these metals. Following this, the multilayer relaxation of Al(111),(100),(110), Ni(100),(110) and Fe(100) is discussed in detail. Finally Section IV contains a summary and conclusions of the method as applied to surfaces.

2. THEORY

The full details of the CEM method, especially CEM-N, are contained in Papers I-III, to which the reader is referred. Here, we shall only present the features necessary to understand the extension and application to surfaces. The starting point is the interaction energy for a system of N-atoms,

$$\Delta E(\{A_N\}) = E\left(\sum_{i=1}^{N} A_i\right) - \sum_{i=1}^{N} E(A_i) \tag{1}$$

which within the CEM-N formalism is rewritten in the equivalent form,

$$\Delta E(\{A_N\}) = \sum_{i=1}^{N} \Delta E_J(A_i;n_i) + \Delta V_c + \Delta G(\{A_N\}) \tag{2}$$

where all summations extend over the number of atoms in the system. The first term in eq. (2) is the sum of the embedding energies in jellium of all the atoms of the system; two different types of embedding functions are considered in this paper and they are denoted as the covalent, $\Delta E_C(A;n)$, and Puska *et al.* [29], $\Delta E_P(A;n)$, functions respectively. The second term is the difference in coulomb energy between the multi-atom system and all the atoms in jellium. The last term is the difference in kinetic-exchange-correlation energy between the multi-atom system and all the atoms in jellium, written as

$$\Delta G(\{A_N\}) = G\left(\sum_{i=1}^{N} A_i\right) - \sum_{i=1}^{N} [G(A_i + n_i) - G(n_i)] \tag{3}$$

where G denotes the sum of kinetic, exchange and correlation energy functionals of the density and n_i is the density of the jellium for the i^{th} atom.

Eq. (2) is not solved self-consistently but instead utilizes the approximation of superposition of atomic densities to form the total system density. Minimizing the effect of this approximation on the non-self-consistent ΔG term in eq. (2) yields a prescription for the choice of the jellium density for each atom [27], which for non-

spin-polarized atomic densities is

$$n_i = \frac{\sum_{j=1}^{N} (1-\delta_{ij}) \int n(\vec{r}_i) n(\vec{r}_j) d\vec{r}}{2Z_i} \tag{4}$$

The generalization to spin-polarized densities is presented in Paper II, but this is not necessary for the present article. Here, $n(\vec{r}_i)$ is the unpolarized electron density distribution and Z_i is the atomic number of atom i. Use of the superposition approximation simplifies the coulombic correction ΔV_c to be the sum of the atom-atom coulomb interactions.

Now, we invoke periodicity to simplify the evaluation of eq. (2). The formalism for an infinite bulk system having 3D translational periodicity with one atom per unit cell has been presented previously [28] and thus will be merely outlined here. The cohesive energy is defined to be $E_{coh} = \Delta E(\{A_N\})/N$ in the limit $N \rightarrow \infty$. Using the fact that all atoms in the system are equivalent in this limit, we can rewrite eq. (2) for the cohesive energy as

$$E_{coh} = \Delta E_f(A_b; n_b) + \Delta G_b + \frac{1}{2}\sum_{j \neq b}^{N} \Delta V_{jb} \tag{5}$$

where ΔV_{jb} is the coulomb interaction between atom j and the bulk atom b, and

$$\Delta G_b = G_b(bulk) - [G(A_b + n_b) - G(n_b)] \tag{6}$$

The subscript "b" refers to any <u>one</u> of the bulk atoms. The evaluation of $G_b(bulk)$ involves an integral over the Wigner-Seitz cell of the atom A_b (see Paper II). The task of calculating the energy of the infinite N-body system is now reduced to the calculation of the interaction energy of a bulk atom (A_b) in the electron density environment due to the rest of the atoms in the metal.

In the case of surfaces, we can also simplify the evaluation of Eq. (2) but are restricted to use of 2D translational periodicity rather than the 3D periodicity in the bulk. Assuming no in-planar reconstruction, this periodicity implies that for surfaces we may consider the atoms within a particular layer as being equivalent (i.e., having

the same electron density environment). In this case we calculate the cohesive energy of an atom in the i^{th} layer as

$$E_i = \Delta E_J(A_i;n_i) + \Delta G_i + \frac{1}{2}\sum_{j\neq i}^{N} \Delta V_{ji} \tag{7}$$

To be more explicit, we pick a 'focus' atom in layer i and calculate its cohesive energy via Eq. (7). The evaluation of ΔG_i entails a generalization to the simple integration over a Wigner-Seitz cell in the calculation of ΔG_b: the integration is over all spatial points which are closer to the focus atom 'i' than to any other atom (just as in the general case for systems without any symmetry described in Paper II).

For surfaces the fundamental quantity of interest is the surface energy, defined as σ=*[E(bulk system) - E(two cleaved surface systems)] /total surface area.* We can obtain this quantity by calculating ΔE_i for each layer leading into the bulk and by using the fact that $\Delta E_i \rightarrow E_{coh}$ as i gets large. Since only one type of atom is considered here, there is only one atom per surface unit cell yielding the total surface area as $2N_sA_c$ for N_s surface atoms and unit cells each with area A_c. (Remember that two surfaces are formed from cleavage of one bulk system.) Combining this definition with Eq. (7) yields the final formula within the CEM formalism for the surface energy:

$$\sigma = \frac{\sum_i (\Delta E_i - E_{coh})}{A} \tag{8}$$

The summation over 'i' extends over the layers and not over the individual atoms. To determine the extent of surface layer relaxation, we minimize the surface energy in Eq. (8) with respect to the displacement of one or more lattice planes in a direction perpendicular to the surface.

All that remains is to choose the energy density functionals and the atomic densities. The kinetic energy density functional used was a Pade' summation of the gradient series [30] in $|\nabla(n)|/n^{4/3}$. The local Dirac exchange functional [31] and the local Gunnarsson-Lundqvist [32] correlation energy functional were used. As a representation of the atomic densities we have generated an even-tempered Gaussian basis [33] from Slater-type atomic Hartree-Fock densities [34]. This allows convenient

analytic evaluations of the coulomb integrals and the density overlaps [35] (i.e., Eq. (4) for the jellium density). Following Paper II on diatomic molecules and subsequent (unpublished) studies by us of a variety of metals (including those under study in the present paper), we utilized a non-spin-polarized atomic density since this yielded the most accurate energies within the CEM formalism. In addition, we have forced all the 3d transition metals to have a ($3d^n$,$4s^2$) rather than a ($3d^{n+1}$,$4s^1$) configuration; it was seen in Paper III that the semi-empirical embedding function using two diffuse 4s electrons allowed for a much smoother match of the bulk and diatomic contributions to the curve. We have also restricted the 3d shell to be spherically symmetric which has a negligible effect on the total electron density distributions at the atomic separations of interest in this article.

3. RESULTS

3.1. Bulk Metal Cohesive Energies

We have calculated the CEM bulk cohesive energies using the SCF-LD Puska *et al.* embedding functions for the second and third row metals by minimizing Eq. (5) with respect to the lattice constant of the metal system. In the case of the hcp lattice, calculations were carried out by constraining the ratio $^c/_a$ to that which is observed experimentally [36]. The atomic density around each atom was cut-off at a radial distance (R) such that R^2*(atom density) < 10^{-5} a.u., and all atoms within 2R of the focus atom were used to represent the infinite lattice. Inclusion of atoms outside this range and use of a larger cutoff radius resulted in negligible change in the calculated energies.

In Figure 1a, we show both the minimized CEM and experimental cohesive energies vs. atomic number. A similar plot for the equilibrium nearest neighbor distances (NNDs) is shown in Figure 1b. For the second row metals, the CEM predictions are nearly quantitative for both the cohesive energies and NNDs. However, for the third row metals the situation is less satisfactory with predictions of the cohesive energy being accurate for K $\rightarrow$ V only and with predictions of the NNDs all being contracted considerably with the exception of K where an expansion is predicted. Clearly there is some aspect of the interaction that is not described adequately using the Puska *et al.* embedding function for the third row metals.

We have further investigated the above problem by considering some relevant properties of atoms and jellium. First, we have also plotted the Pauling [37] electronegativity for the free metal *atoms* in Figure 1a, indicated as stars. An interesting correlation appears between the variation of the CEM calculated energies and the electronegativity as a function of the atomic number in each row. But this is not the sole reason for the inaccuracy of the Puska *et al.* functional for the 3d elements since even for Al and Si having relatively large electronegativities the predictions are still good.

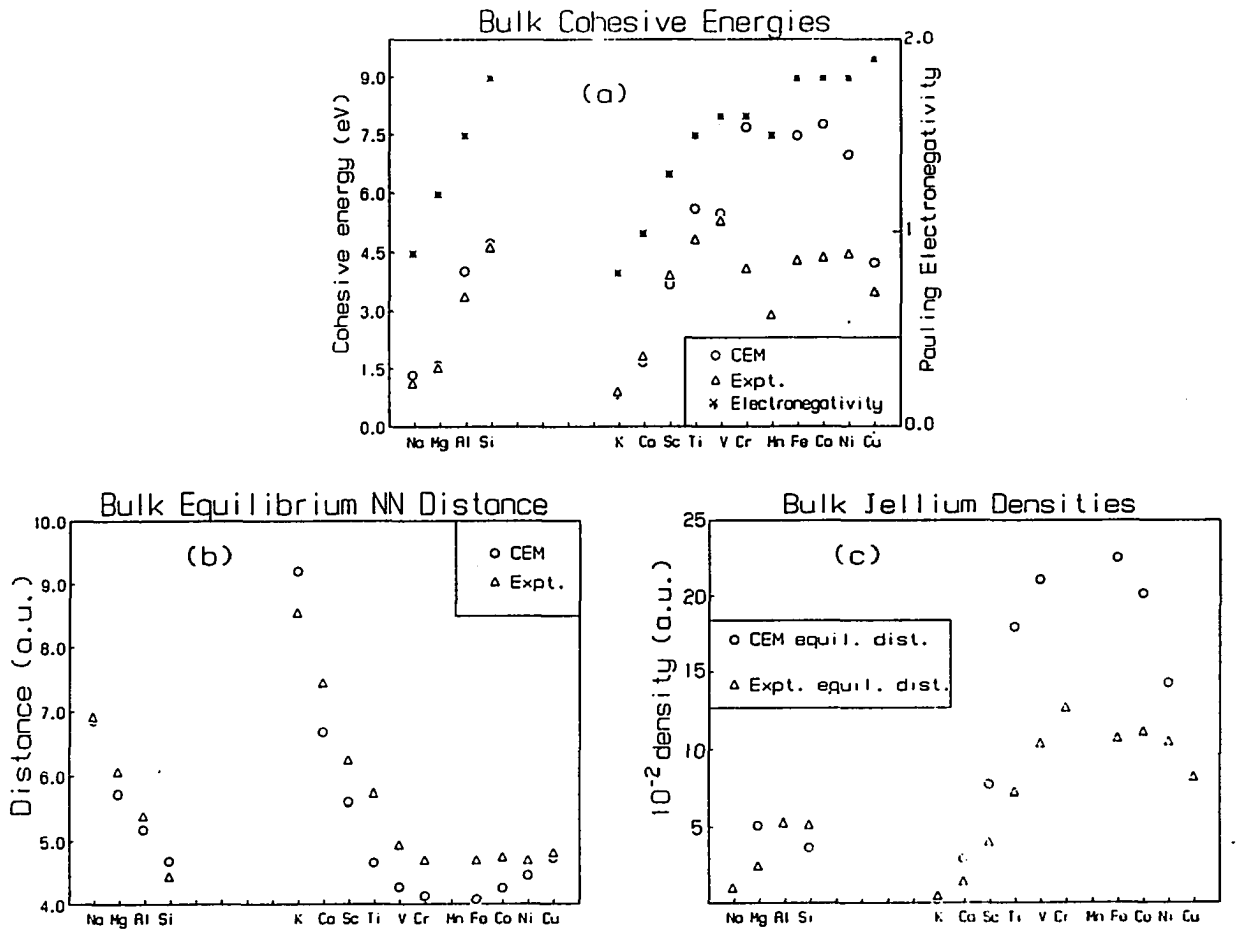

Fig. 1. **Calculated bulk metal cohesive energies and nearest neighbor distances along with the experimental values [36] are shown. Also Pauling's free atom electronegativity [37] is plotted for a comparison of ionic characteristics of the embedding functions. (a) CEM and experimental cohesive energies. Electronegativities are symbolized by stars. (b) CEM and experimental nearest neighbor distances. (c) Sampled jellium densities at the CEM and experimental equilibrium distances**

A second important point involves the variation of the work function for jellium, which is basically an increasing function from densities of 0 to 0.0018 au, with a peak of 2.4 eV, and then a linearly decreasing function of density thereafter, becoming negative after 0.0163 au. Figure 1c is a plot of the bulk jellium sampling densities for both the CEM and experimental NN distances as a function of the atomic number. One immediately notes that in general the density sampling increases as one proceeds across the second row metals for both cases. For the transition metals we note that the density peaks at about V to Co and then decreases as the 3D shell is continually filled. From these considerations, the predicted results seen in Figures. 1a and 1b can be understood in terms of the overemphasis on an ionic interaction which is inherent in the Puska *et al.* SCF-LD embedding curve for an electronegative atom in a high density jellium system.

Let us consider the above points in more detail. For the second row metals the density sampled by the atoms in the bulk is relatively low and thus the work function of jellium is high ensuring that the degree of ionic interaction is small. This results in the general agreement found with experiment for both the cohesive energy and the NND distance. In the case of the third row metals for Ti to Cu the sampling density is considerably larger resulting in a lowering of the work function of jellium. Therefore one would expect the ionic interaction with jellium to be significant and that the use of the Puska *et al.* functional will predict a substantial ionic component to the bonding, especially for the right-half transition metals. Since the experimental trend in binding energy does not follow the CEM predictions, we must conclude that a substantial ionic bonding component is not correct. These results support our initial argument in the theory section that in order to obtain quantitative binding energies an alternative embedding function must be used. The use of a corrected embedding function will allow us to adequately describe the correct type of interaction occurring on clean metal surfaces.

3.2. Covalent Embedding Functions

Paper II presented semi-empirical covalent embedding functions which were constructed solely by inverting the experimental binding potential curves for

homonuclear diatomics [38]. These covalent embedding functions are determined by solving Eq. (2) (with $J=C$) for $\Delta E_C(A;n)$,

$$\Delta E_C(A;n) = \frac{[\Delta E(A_2) - \Delta G(A_2) - \Delta V_c(A_2)]}{2} \tag{9}$$

For $\Delta E(A_2)$ a Morse potential representation of the experimental data [38] was used. Following Paper III, we also utilize the bulk cohesive energy to determine the covalent embedding function via Eq. (5):

$$\Delta E_C(A;n) = E_{coh} - \Delta G_b - \frac{1}{2}\sum_{j \neq b} \Delta V_j b \tag{10}$$

In this analysis, the bulk experimental binding potential is obtained from a harmonic expansion about the equilibrium lattice constant with the bulk modulus providing the second derivative of the cohesive potential. Table I contains the experimental data used to construct the bulk portion of the embedding functions for the atoms considered in this paper.

Included in this table is the bulk data for other metals for which we have constructed covalent embedding functions but which are not discussed in this paper. Once the two portions of the embedding curves are constructed they are combined to form one covalent embedding function that we propose will be universal with respect to the number (N) of atoms in the system of a particular element as applied with the CEM approach.

This universality implies that the effects of all other variations with number of atoms in the system are incorporated into the coulombic and correction terms. The latter is particularly important to discuss since the reader may question the requirement of a correction term (which is time consuming to compute) when the embedding functions are determined semi-empirically. First, note that the correction term is determined by the spatial variation of the electron density, becoming small as a system becomes more homogeneous. In particular, the correction is most important for diatomics and becomes rather small for bulk systems (both assumed to be near the equilibrium distance). By contrast, the embedding energy (per atom) is smallest for

diatomics and becomes rather large for bulk systems due to the increasing number of neighbors. Thus, the correction term cannot be incorporated into a semi-empirical embedding function. To test this argument, we have determined new embedding functions in exactly the same manner as described above but without the correction term; the results for the surface energies and relaxations were considerably poorer than those in which the correction term is retained (and which will be presented in part C). For transition metal surface energies, including relaxation, typical errors are on the order of 5% with the correction energy and 20% without the correction energy.

Table I Cohesive energies and lattice constants from Eq.(5) using the embedding functions of Puska *et al.*(Ref.29)

	CEM			Experiment[a]		
	a (au)	E_{coh} (eV)	Structure	a (au)	E_{coh} (eV)	Bulk Modulus[b] (1011 N/m2)
Na	7.94	1.38	BCC	7.98	1.113	0.68
Mg	5.76	1.62	HCP[c]	6.07	1.53	3.54
Al	7.35	4.05	FCC	7.65	3.39	7.22
K	10.65	0.88	BCC	9.87	0.934	0.32
Ca	9.49	1.71	FCC	10.54	1.84	1.52
Fe	4.75	7.52	BCC	5.42	4.28	16.83
Ni	6.32	7.00	FCC	6.65	4.44	18.6
Cu	6.72	4.26	FCC	6.82	3.50	13.7
Si[d]	10.88	4.76	DIA[e]	10.25	4.63	9.88
Sc	5.63	3.66	HCP	6.25	3.90	4.35
Ti	4.68	5.62	HCP	5.74	4.85	10.51
V	4.98	5.52	BCC	5.73	5.31	16.19
Cr	4.79	7.71	BCC	5.44	4.71	19.01
Co	4.27	8.80	HCP	4.74	4.39	19.14

[a] All experimental values obtained from ref. [36].

[b] The Bulk modulus provides the second derivative for the harmonic expansion of the cohesive energy in construction of covalent embedding function.

[c] The ratio of c/a was held constant for HCP structures.

[d] The surface energies or relaxation of the metals under the dashed line are not studied. Thus a covalent embedding function is not constructed in this paper for these metals. The Mg and Cu functions were constructed in Paper III.

[e] The diamond lattice structure was used for Si.

These quantities are rather sensitive to the difference in inhomogeneity of the electron density between bulk and surface atoms. For quantities which may not be so sensitive to such inhomogeneity (e.g., composition of bimetallic systems or even the desorption energy of a surface metal atom), it may be possible to eliminate the correction term. We illustrate the construction of the semi-empirical embedding functions by providing a step by step analysis for the construction of the covalent embedding function for Al. The semi-empirical embedding curves for the rest of the metals will simply be presented and discussed since the construction procedure is the same for all atoms.

In Figure 2a, we have plotted the harmonic binding potential for bulk Al as a function of both the lattice constant and the sampled jellium electron density. Figure 2b is an analogous plot for the binding potential of Al_2. The five points shown in Figure 2a correspond to lattice constants of 90, 95, 100, 105 and 110 percent of the experimental equilibrium lattice constant.

In Figure 3, we have plotted the covalent embedding function resulting from the application of Eqs. (9-10) to these data. The Puska *et al.* embedding function for Al is also shown. Only the high density (90% $\rightarrow$ 105%) bulk points were retained since the true binding curves are expected to be softer than harmonic for the very expanded low density geometries. These points correspond to the four points labeled to the left of and including the point indicated by an arrow on Figure 2a and with the corresponding embedding energies labeled N=∞ on Figure 3. The diatomic points for bond lengths less than the point indicated by a closed square on Figure 2b were not retained since the Morse potential is not expected to be accurate in this region. The two vertical arrows in the low and high density regions of Figure 3 indicate the location of the diatomic and bulk densities on the embedding curves corresponding to the experimental equilibrium bond distance and lattice constant, respectively.

Examination of these Figures demonstrates that the diatomic and bulk systems correspond to separate regions of sampled density. Hence, the smoothness of the interpolation between these two regions provides strong evidence for the *universality* of the covalent embedding curve. One should also note the excellent qualitative agreement between the two embedding curves in Figure 3.

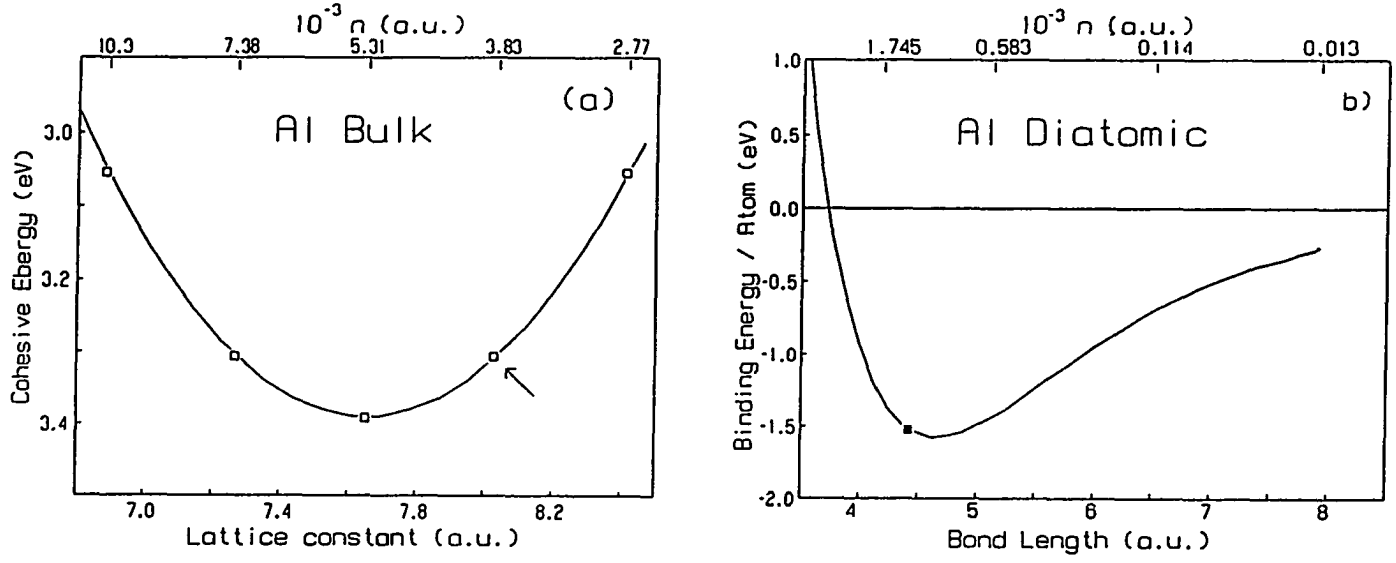

Fig. 2. **The experimental potentials for Al (from which the Al semi-empirical covalent embedding function is derived) are plotted as a function of both the internuclear spacing (lattice constant for the bulk; bond length for the diatomic) and the corresponding sampled jellium density n. (a) Bulk metal, (b) Diatomic molecule**

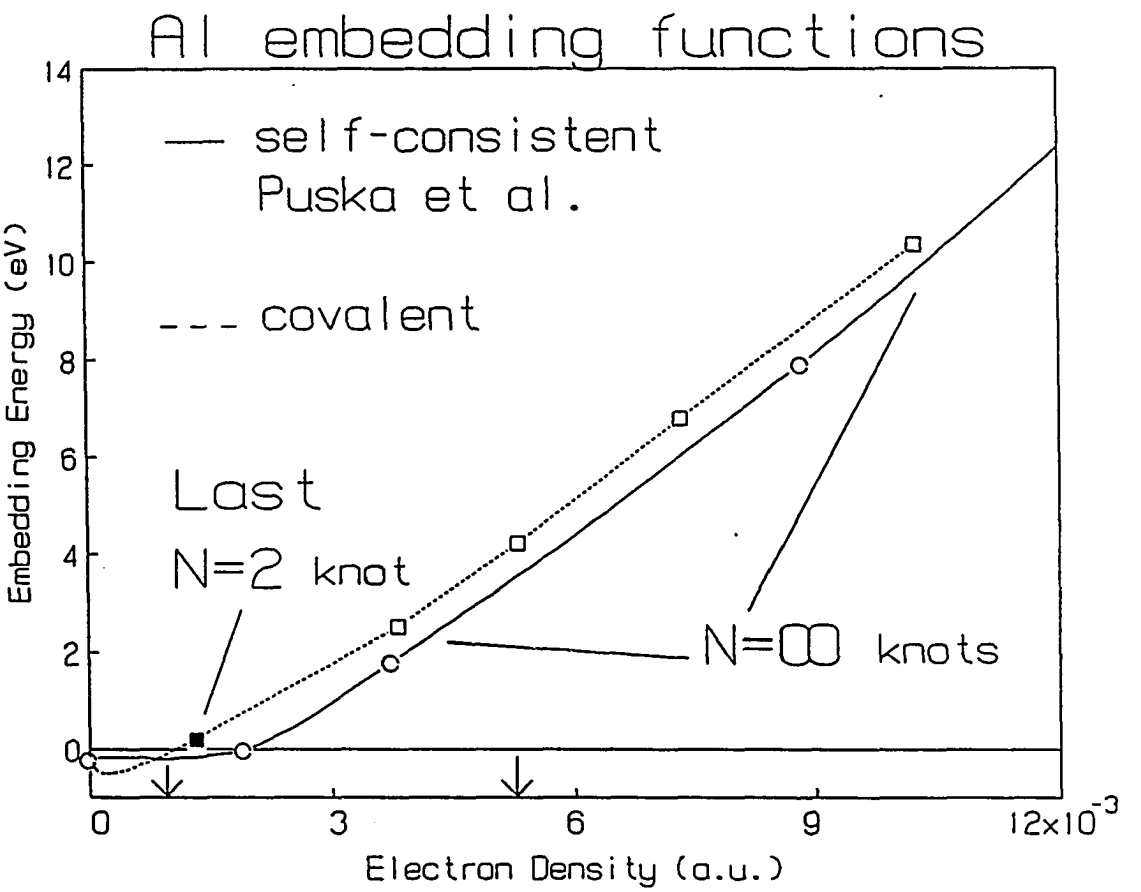

Fig. 3. The semi-empirical covalent embedding function (squares) for Al is shown. Also shown is the SCF-LD embedding function (open circles) as calculated by Puska *et. al.* [29]. The embedding energy is plotted as a function of the jellium density. The vertical arrows in the low and high density regions indicate the location of the equilibrium diatomic and bulk points, respectively

The two differ by a constant for almost all densities with the Puska *et al.* curve lying below the covalent curve. This is characteristic, as seen in Paper II, of a partial ionic interaction for the (partially negative) charged atom in jellium. The fact that the slopes are almost the same is reflected in the excellent agreement of the Al NND in Table I with experiment. Another important distinction between the two embedding curves is that the Puska *et al.* embedding function is drawn to the negative of the electron affinity of the free atom in the zero embedding density limit [29] while the covalent embedding function is drawn to zero. This will be the case for all atoms with a positive electron affinity [24,29].

Carrying out the same procedure for Na we show in Figure 4 both the Puska *et al.* and the covalent embedding function. In this case only the three highest bulk electron density points were used in order to obtain a smooth fit and as can be seen even this leaves a somewhat non-smooth curve. This will be seen later to lead to difficulties in accurately calculating the energies of Na surfaces. In comparison to Al, we find that the Puska *et al.* Na embedding function is closer to the covalent curve throughout the whole density range, indicating that Na is slightly less negative in jellium. This is expected since not only is the electronegativity of Na lower but the sampled electron density is also much lower, yielding a higher jellium work function. Also note that there is only one calculated Puska *et al.* embedding energy point in this lower density region.

For K we show in Figure 5 both the Puska *et al.* and the resulting covalent embedding curves. The bulk points in this case were also truncated at the 100% lattice value. Although the Puska *et al.* curve is slightly above the covalent curve, this is not of concern since the Puska *et al.* embedding function in this region is an extrapolation from a calculated high density point to the negative of the electron affinity, and is thus quite uncertain. With no real data points this region of the embedding curve is unknown self-consistently and thus the covalent embedding function not only provides the correct type of interaction but it also fills in the gap in the Puska *et al.* calculations.

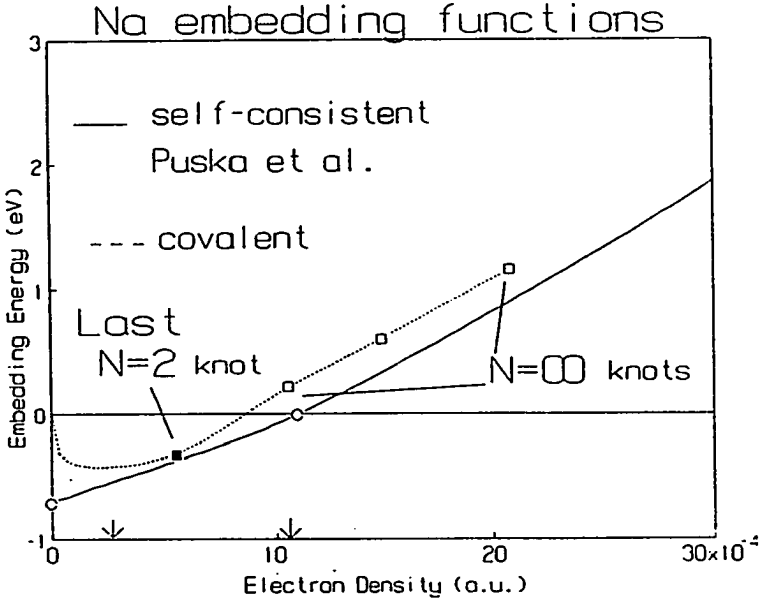

Fig. 4. Same as Fig. 3 except for Na

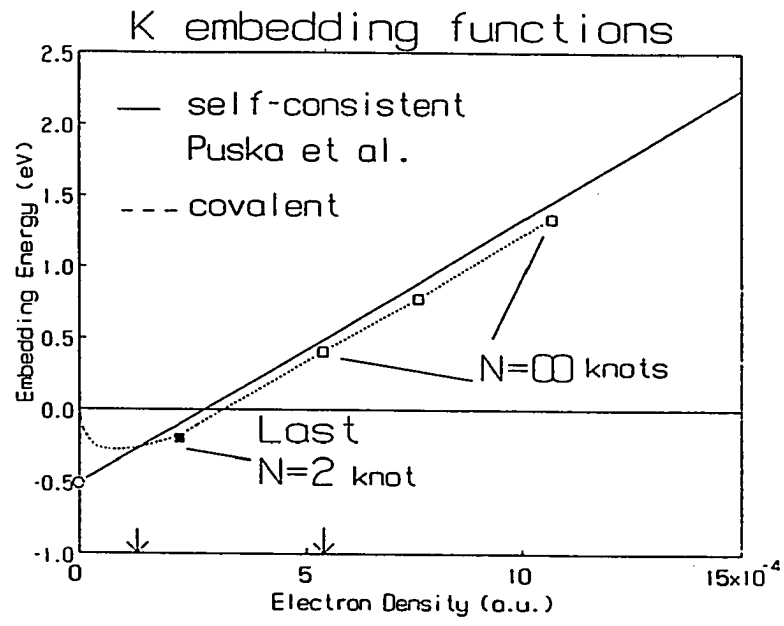

Fig. 5. Same as Fig. 3 except for K

This also indicates that the calculated bulk cohesive energy and NN distance shown in Figures 1a and 1b for K should not be taken very seriously.

In the case of Ca we see in Figure 6 a smooth curve again with truncation at the 100% bulk lattice point. Like K, the Puska *et al.* embedding curve for Ca is very slightly above the covalent curve and is mainly an extrapolation in the zero density. As in the case of K the covalent embedding function fills in the gap in the Puska *et al.* embedding function.

Moving now to Fe we see in Figure 7 that in the covalent embedding curve the smooth interpolation between the diatomic and bulk regions is quite remarkable. We were able to retain many more diatomic points (e.g., note the last diatomic point relative to the first vertical arrow) without any loss of smoothness. We were even able to retain the 105% lattice value in the bulk region as well. We also see a dramatic transition in the ionic character of Fe in jellium indicated by the increasing separation of the covalent and Puska *et al.* embedding curves as the density is increased. The increased density results in a lower work function for jellium suggesting that Fe is slightly negative in jellium at such densities. Since there are a number of Puska *et al.* points in the region of interest the bulk calculation can be considered reliable.

Finally we examine the embedding functions of Ni in Figure 8. We see that the covalent embedding function is above that of the Puska *et al.* embedding function throughout the whole range of densities in contrast to that seen in Fe. Even though they both have the same electronegativities the Ni atom has a greater tendency to fill its 3d shell than Fe does. In the case of Ni we had to again truncate the high density diatomic and low density (>100%) bulk contributions to the embedding curve to obtain a smooth interpolation of the diatomic and bulk regions. Again the bulk calculation can be considered reliable as there are plenty of Puska *et al.* points in this region.

The covalent embedding functions of both Cu and Mg were presented in Paper III where the same procedures as above were carried out. The characteristics seen for these two metals are very similar to Ca for Mg and Ni for Cu. In the case of Cu the Puska *et al.* and covalent embedding function were very close indicating only a very small ionic interaction of Cu in jellium.

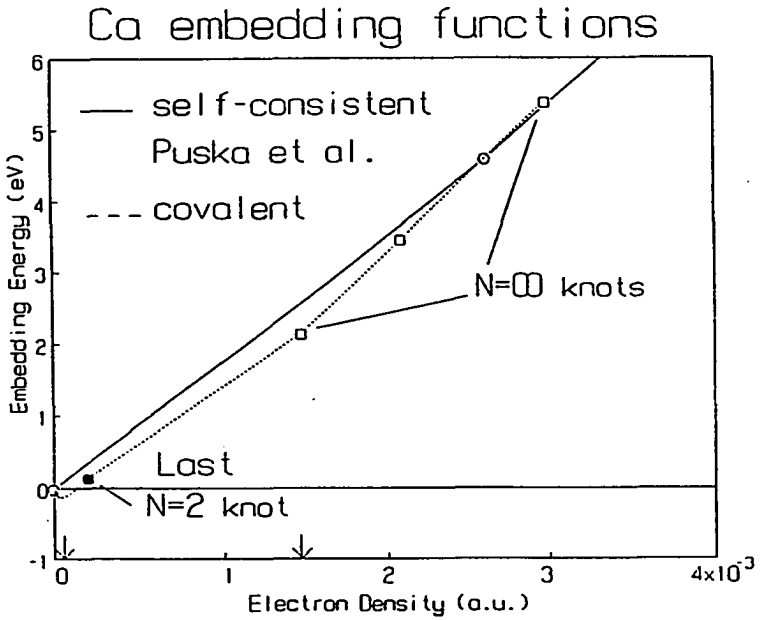

Fig. 6. Same as Fig. 3 except for Ca

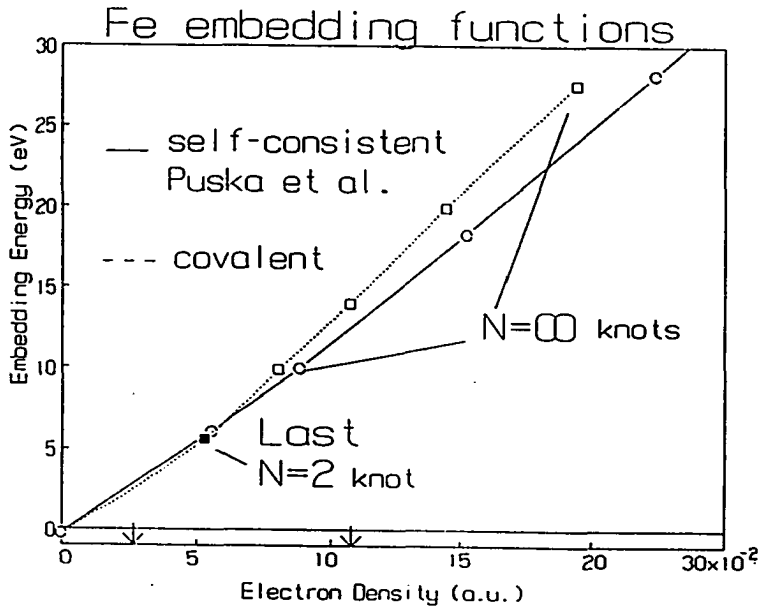

Fig. 7. Same as Fig. 3 except for Fe

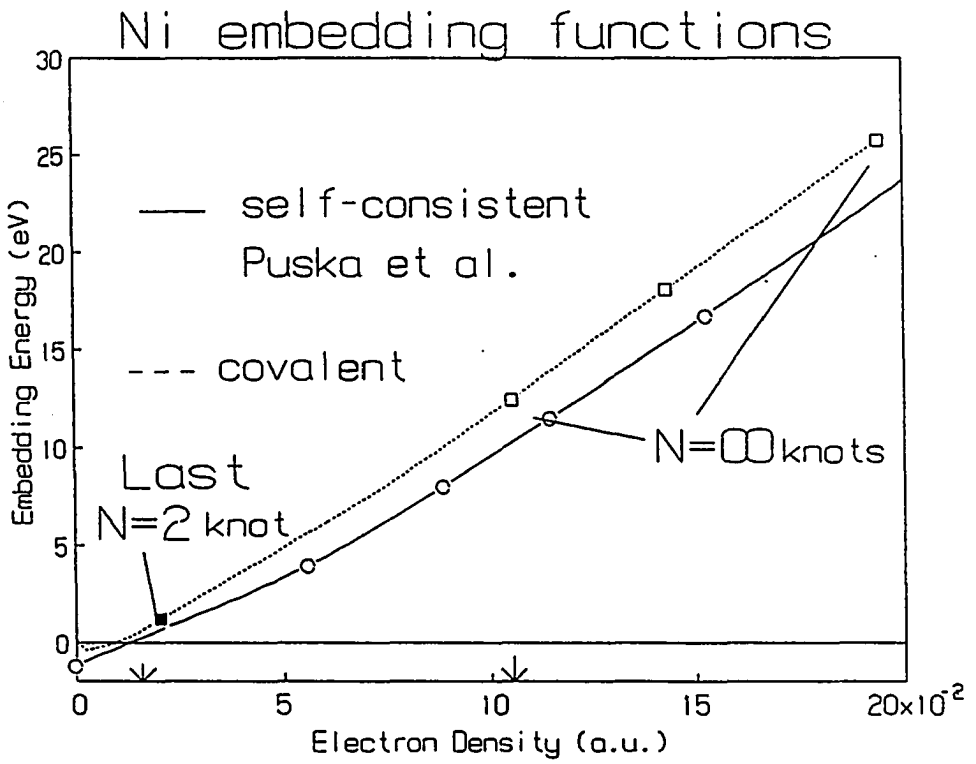

Fig. 8. Same as Fig. 3 except for Ni

3.3. Surface Energies and Relaxation

As described previously, an accurate calculation of the bulk cohesive energy and lattice constant requires the use of the covalent embedding functions. With these functions at hand, we can predict a number of properties of the metal, and in this subsection, we have calculated the surface energies of a number of perfectly terminated low Miller index faces of Na, Mg, Al, K, Ca, Fe, Ni and Cu from Eqs. (7-8).

Later, we will consider the multilayer relaxations of a select few of these surfaces, but we emphasize that the surface energy is only slightly affected by such relaxation.

As in the calculations for bulk systems, the total number of atoms must be large enough such that the electron density sampled by the focus atom in each layer is unaffected by the addition of more atoms. In addition for surfaces, the summation in Eq. (8) over the energy of each layer must be converged with respect to the number of layers. For the closely packed surfaces, it was found that only 4 layers were needed for convergence of Eq. (8) to be obtained while, for more open surfaces, 5-6 layers were needed. In all cases the total number of layers in the system was constrained to 2n+1 where n is the number of focus layers indicated above. This ensured that the energy of the n^{th} focus atom was equal to E_{coh} within numerical accuracy.

Before discussing the results we feel that a few general points concerning the various contributions to the surface energy is in order. First, we expect the embedding energy contribution to be negative since the embedding energy repulsion is smaller due to the lowered electron density at the surface relative to the bulk. This also implies that the more open the surface is, the more negative this contribution will become. Second, we expect that the coulombic contribution will be positive and dominant since the surface atoms have completely lost the longer range electrostatic interactions with the atoms above the plane of the surface. Note also that the more open surfaces will have a larger coulombic energy contribution than the more closely packed surfaces. The trend of the correction energy contribution is difficult to predict but we do expect that it will be relatively small for the simple free electron like metals.

In Table II we show the CEM predictions for the surface energies along with its energy components (with obvious notation) for the low index faces of various metals. Due to the unavailability of experimental data on isolated surface planes direct comparison is only semi-quantitative. In general though, very good agreement with experiment is obtained for almost all of these metals and if the experimental data is assumed to be mainly for the most close packed surfaces, the predictions are nearly quantitative. One also notes immediately the difference in magnitudes for the simple metals as compared to the transition metals. Also, as expected, the trend of increasing

surface energy with increasing openness of the surface is seen for these cases. During the calculations we also noted that the contributions to the total surface energy arose from deeper layers for the more open surfaces.

Table II Calculated surface energies and energy components in J/m^2 of the low-index-surface faces

		CEM				Other	Exp.[a]
		σ_{Ehom}	σ_{γ_c}	σ_{Cor}	σ_{Tot}	theory	
Na	100	-0.484	0.570	0.053	0.139	0.270[b]	
	110	-0.407	0.484	0.069	0.147	0.248[b]	0.261
	111	-0.473	0.583	0.048	0.158	0.305[b]	
Mg	1000	-1.403	1.999	0.048	0.643	0.629[b]	0.785
Al	100	-4.061	5.456	-0.160	1.230	1.701[b]	
	110	-4.275	5.812	-0.183	1.353	2.964[b]	1.143
	111	-3.732	4.938	-0.110	1.096	0.852[b]	
K	100	-0.306	0.383	0.013	0.090	0.161[b]	
	110	-0.270	0.322	0.029	0.081	0.147[b]	0.145
	111	-0.304	0.386	0.013	0.095	0.176[b]	
Ca	100	-0.866	1.461	-0.017	0.578	0.615[b]	
	110	-0.920	1.563	-0.020	0.622	0.737[b]	0.578
	111	-0.795	1.307	0.010	0.523	0.472[b]	
Fe	100	-14.970	17.537	-0.135	2.429		
	110	-12.651	15.245	-0.105	2.489		2.417
	111	-15.106	17.978	-0.181	2.690		
Ni	100	-13.106	15.935	-0.207	2.622	1.580[c]	
	110	-13.935	17.073	-0.259	2.878	1.730[c]	2.380
	111	-11.899	14.596	-0.135	2.561	1.450[c]	
Cu	100	-9.731	11.775	-0.321	1.722	1.280[c]	
	110	-10.350	12.551	-0.388	1.813	1.400[c]	1.790
	111	-8.756	10.640	-0.259	1.625	1.170[c]	

[a] Average of a polycrystalline surface, ref. [39].

[b] Variational jellium calculations with weak ion pseudopotentials for nuclear core roles from ref. [40].

[c] Embedded-Atom-Method results from ref. [23].

This trend agrees with the experimental finding that multilayer relaxations can occur for the open surfaces while for the more closely packed surfaces the relaxation is limited to the top layer and in some cases the second layer as well. We shall have more to say about this aspect of the surface energy and relaxation.

In comparison to the variational jellium with ion core pseudopotential model results of Sahni *et al.* [40] we note that agreement is not very good for Na,Al and K where CEM consistently underestimates the surface energy. This is especially true for Na and K. Even then, recall that their calculations were a variational treatment of the surface and thus would represent an upper limit on the surface energy of these simple metals. Comparison to the embedded-atom-method calculations [23] that included planar relaxation for Ni and Cu shows that EAM considerably underestimates the surface energy. EAM can be considered a simpler CEM method without the correction term and with parametrized forms for the homogeneous and coulombic energy terms. Since σ_{Cor} is negative, its neglect would increase σ_{Tot}, and thus the errors in EAM must come from parametrizing the homogeneous and coulombic energies.

Of the metals studied in this paper the cases of Na and K show calculated surface energies that are in significant disagreement with both experiment and Sahni *et al.* To understand why this occurs we examined more closely the embedding energy contributions and noted that the top layer atoms of any metal sample a jellium density that is between the last diatomic point and the first bulk point as seen in Figures 3-8 of the embedding functions. As mentioned in the previous section this area of the embedding curve is the least known due to the unavailability of experimental data for systems that would have sampling densities in this region. With this in mind a quantitatively accurate calculation of surface energies would support confidence in the universality of the embedding function.

For Na we find that the jellium density for the top layer atoms correspond to a point just below the upward hump of the embedding curve, thereby causing the embedding energy for these atoms to be artificially lowered relative to the bulk. This lowered embedding energy would result in a more negative surface energy contribution and thus tend to lower the total surface energy for sodium. Because of this we feel

that in order to describe accurately the Na surfaces we need to have a much smoother embedding function in this region of the surface density. This non-smoothness, we believe, may be a result of the restriction to non-polarized atom densities which will be more severe for low atomic number atoms. By contrast, for K such non-smoothness for the embedding function does not occur. But we do note that the correction energy contribution is significantly less for K than it is for Na and the magnitude of the difference between the experimental and CEM results is not very large.

For the rest of the metals there are no dramatic deviations from experiment. We see that the coulombic contribution to the surface energy is indeed dominant and that the correction energy contribution is non-negligible ($\approx$ 10 - 20% of σ_{Tot}) and negative for the more inhomogeneous transition metals, and also surprisingly for Al as well.

Now we examine in detail the multilayer relaxations of some of the surfaces studied above. The more closely packed surfaces will be studied first leading into more open surfaces where large relaxations are expected to take place and to extend deep into the subsurface layers.

The Al(111) surface has been studied experimentally a number of times with nearly all results indicating an expansion of only the top layer, with values ranging from Δd_{12}=3±2% [41] to Δd_{12}=0.5±0.5% [42]. There is one instance where a very large contraction, Δd_{12}=-7.7±2%, has been observed [8]. A recent theoretical study [18] has reported a slight contraction, Δd_{12}=-0.4%, while we have found a larger top layer contraction, Δd_{12}=-3.0±1%. To see if an expansion is possible for this surface we allowed small expansions of the first interlayer spacing, but this always yielded a larger surface energy compared to the ideal surface.

In Figures 9a-d we show a plot of the CEM energy components ($\Delta E_C(Al;n)$, ½ $\Sigma_j \Delta V_{ij}$, ΔG_i and the sum) for each layer-atom from Eq. (9) for the ideal and contracted surface of Al(111). Examining these plots one notes immediately that the largest changes as a result of the contraction are in the embedding and coulomb energies. The embedding energy becomes more repulsive due to the increased electron density during contraction, but at the same time the coulombic attraction between these layers increases due to the decreasing separation.

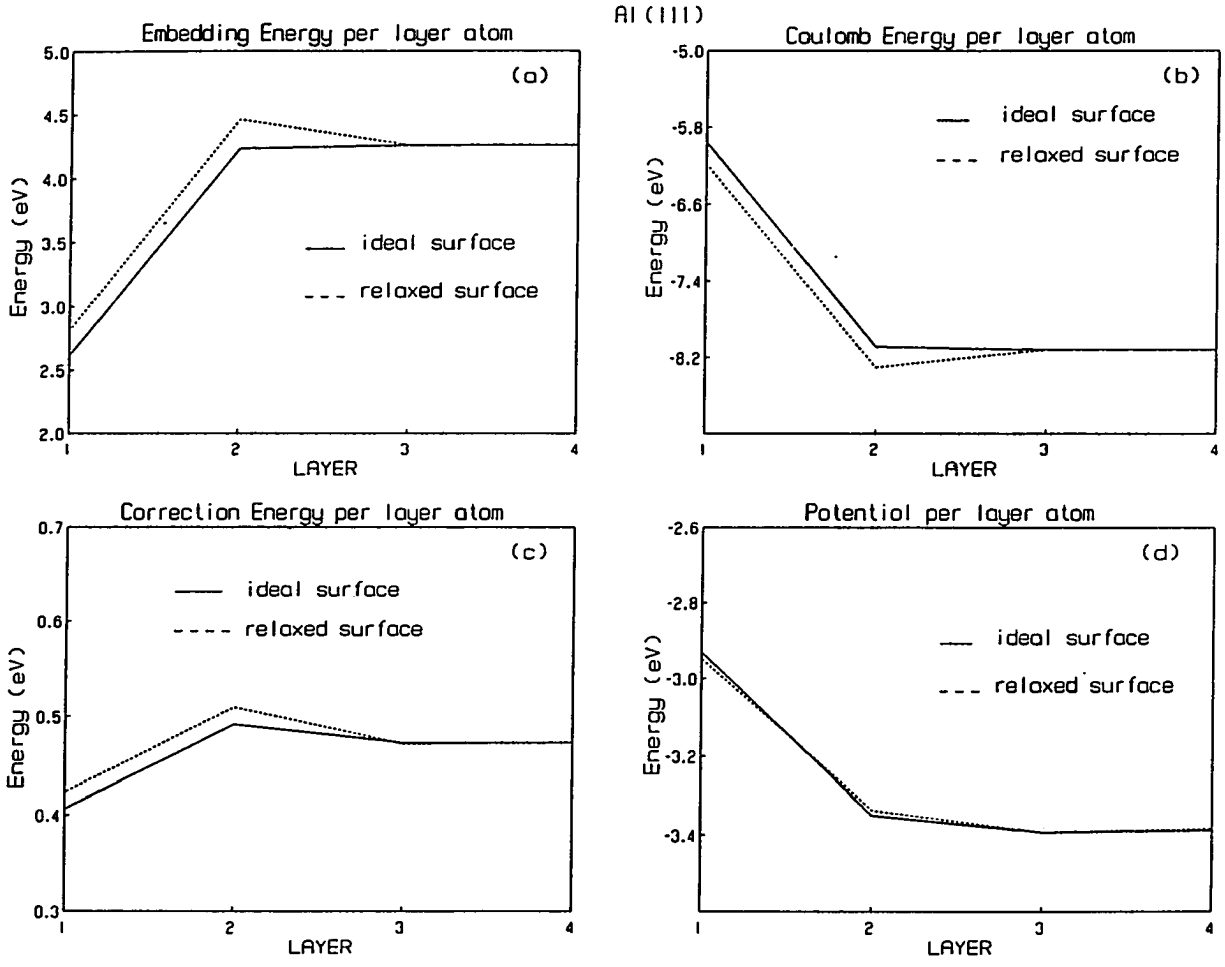

Fig. 9. **The energy components for the ideal and relaxed Al(111) surface as a function of the layer are shown. (a) Homogeneous embedding energy. (b) Coulombic Energy. (c) Correction energy. (d) Sum of components a+b+c**

Also note that the correction energy in Figure 9c ends up being slightly more repulsive for this surface indicating that the electron gas density is more inhomogeneous after contraction has occurred. The potential per layer-atom shown in Figure 9d indicates that even though the individual energy components change significantly during relaxation, these changes tend to cancel. Indeed the minimized surface energy for the contracted geometry is 1.076 j/m2 compared to 1.096 j/m2 for the ideal surface. This change in surface energy is so small that it pushes the limits of precision of our calculations. In view of this difficulty, a smaller contraction certainly could be possible. For larger changes in the surface energy, this will not be a problem, and it will be seen next that the slightly more open (100) surface falls into this category.

We show in Table III the results of the multilayer relaxation of Al(100) in comparison to experimental values. The correct direction of relaxation is predicted but again the magnitude is much larger than is observed experimentally. Also note that we find that the second interlayer distance has significantly expanded where the experimental study seemed to have not take into account or observed a possible relaxation of this spacing.

Table III Multilayer percent of bulk relaxation of Al(100), Fe(100), and Ni(100)

	Al			Fe		Ni	
	CEM	EXP.	EM[a]	CEM	EXP.	CEM	EXP.
Δd_{12} %	-5.0	-2.2[b]	-3.0	-1.5	-1.0[c]	-3.5	-3.2[d]
Δd_{23} %	+3.5	0.0	0.0	+0.5	0.0	+2.0	0.0
Δd_{34} %	+0.5	0.0	0.0	0.0	0.0	0.0	0.0
σ_I[e]	1.230			2.461		2.621	
σ_R[f]	1.158		0.830	2.399		2.320	

[a] Ref. [25].

[b] This is an upper limit to the contraction as provided in ref. [8]. In ref. [7] a value of -1.5% is reported.

[c] Ref. [10].

[d] Ref. [9].

[e] Surface energy for the ideal surface in j/m2.

[f] Surface energy for the relaxed surface in j/m2.

To see if this expansion effects the top layer contraction we allowed only the top layer to relax with the result being the same, Δd_{12}=-5.0% contraction, indicating that for this surface the magnitude in relaxation of the top layer is independent of the relaxation of the second or deeper interlayer distances.

In Figure 10 we show the components of the energy contribution to the cohesive energy for each layer-atom. For the top two layers, the embedding energy has increased, but the expansion of the second interlayer spacing leads to a significantly lower electron density for the third layer atoms which results in a lowering of their embedding energy. The analogous behavior is also apparent for the coulomb and correction energies. Note that the magnitude for these changes in the first and third layers are almost the same but opposite in direction. Inspection of Figure 10c shows that the correction energy has increased with relaxation for the top two layers and then has decreased dramatically for the third layer. The increased repulsion seen in the correction for the first two layers seems to be a characteristic of Al surfaces and will be seen later to reflect the lack of 3d electrons.

Although the change in the surface energy is not very large in total, the variation in the potential per layer is much larger than for Al(111). From Figure 10d, we see that the potential has been lowered in the top and third layer atoms. The contraction between the first two layers results in a lower first layer potential while the second layer potential is raised, and the latter is lowered again by expanding the distance between the second and third layers. This decrease in interaction does not however raise the potential of the third layer over that of the ideal surface, but on the contrary is more stable after relaxation. Closer inspection shows that while the expansion between the third and second layers has decreased the attractive coulomb interaction, it has also decreased the embedding energy by a slightly larger amount. This feature along with the decrease in the correction energy for this layer accounts for most of the lowering in the layer potential. Through these plots we are able to see a simple picture of the oscillatory behavior of the relaxation process beginning to appear.

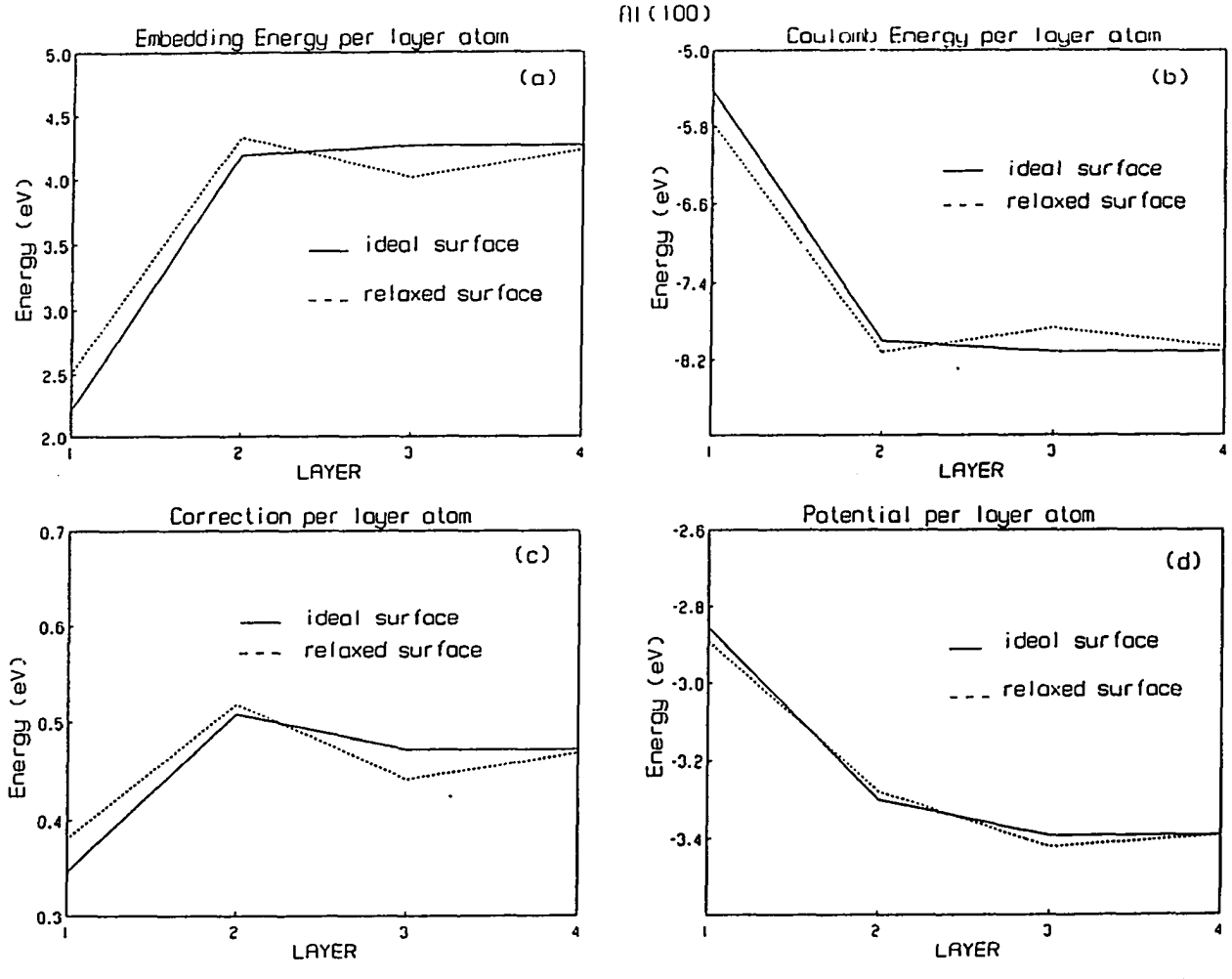

Fig. 10. Same as Fig. 9 except for Al(100)

Next, we show in Table III the results of the multilayer relaxation of Fe(100). We find very good agreement with experiment but, as can be seen, the change in the surface energy is small enough that the accuracy of the calculations might be in question. Indeed, during the analysis the surface energy oscillated a considerable amount within this range and it was found that an expanded first interlayer distance was more favorable than the ideal surface but not the contracted surface. Examination of Figure 11 shows that all the energy components remain essentially constant during the contraction, and therefore not much can be said about this surface at this time.

We also show in Table III the results of the multilayer relaxation of Ni(100) finding very good agreement with experimental results. While Δd_{12}=-3.5% in both studies, we find a corresponding expansion of 2.0% for the second interlayer spacing. The experimental study did not mention this possible expansion, and when only the top layer were relaxed we still obtained Δd_{12}=-3.5% . This indicates that as in Al the relaxation of the top layer seems to be rather independent of the relaxations of other layers in the subsurface. The energy of relaxation for this surface is very large and thus the results can be considered very reliable since this energy is well outside the precision limits of the calculations.

In Figure 12 we show the energy components for this surface as a function of layer. s a result of the contraction we see the expected increase in the embedding energy for the top two layers, and also the expected corresponding decrease for the third layer atoms due to the expansion. The coulomb energy shows the same trend as Al(100) but now the correction energy decreases upon relaxation for all the layers, in contrast to the oscillatory behavior that is seen for the same Al face. Despite this difference the potential in Figure 12d again reveals the oscillatory behavior of the relaxation process as explained in detail for the Al(100) surface.

Earlier we mentioned that the increase in ΔG_i with decreasing Δd_{12} for the first two layers in Al(111) and Al(100) was due to the lack of 'd' electrons. To confirm this we removed the 3d shell electrons from Ni by contracting them into the nucleus and thereby reducing the atomic number by eight.

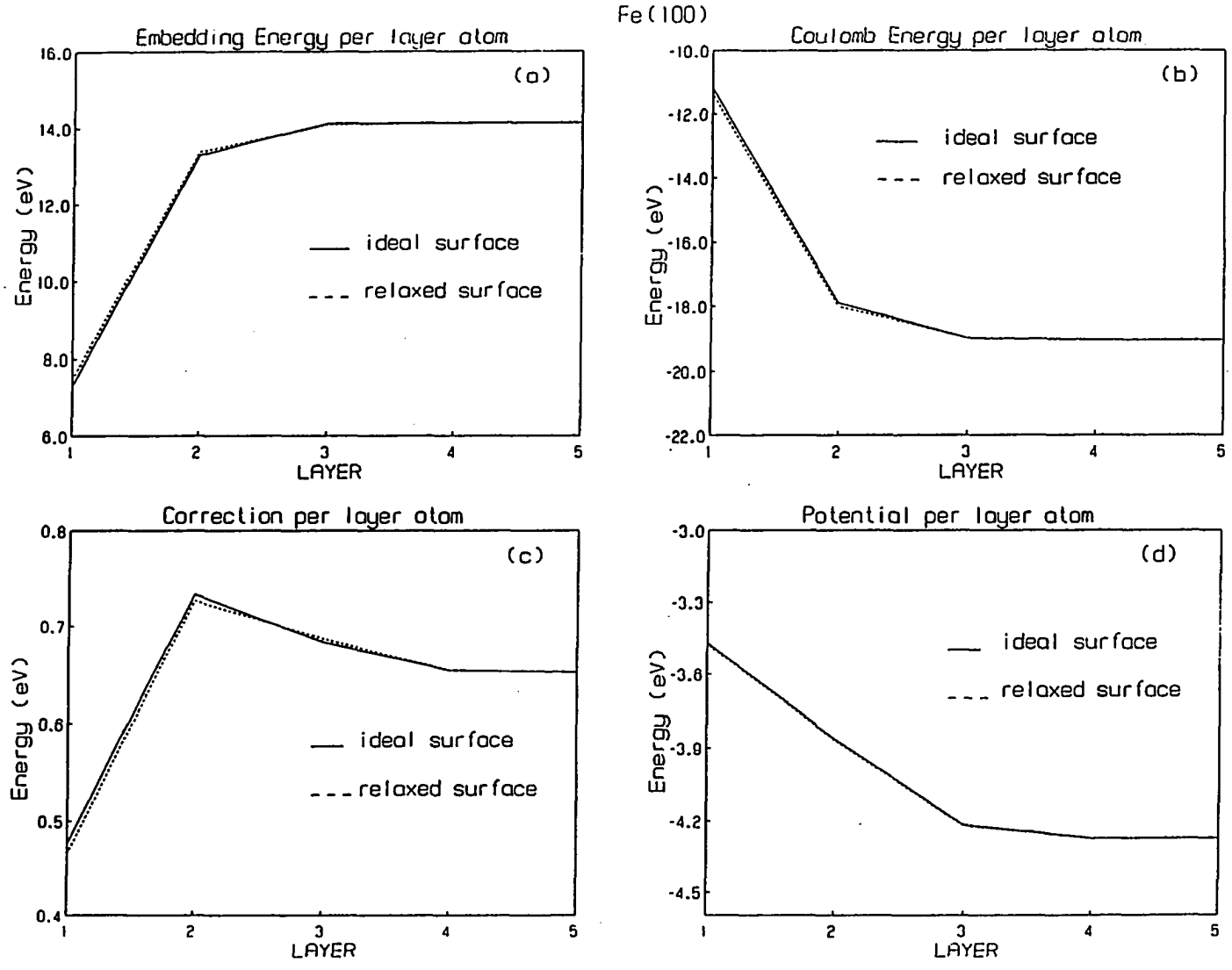

Fig. 11. Same as Fig. 9 except for Fe(100)

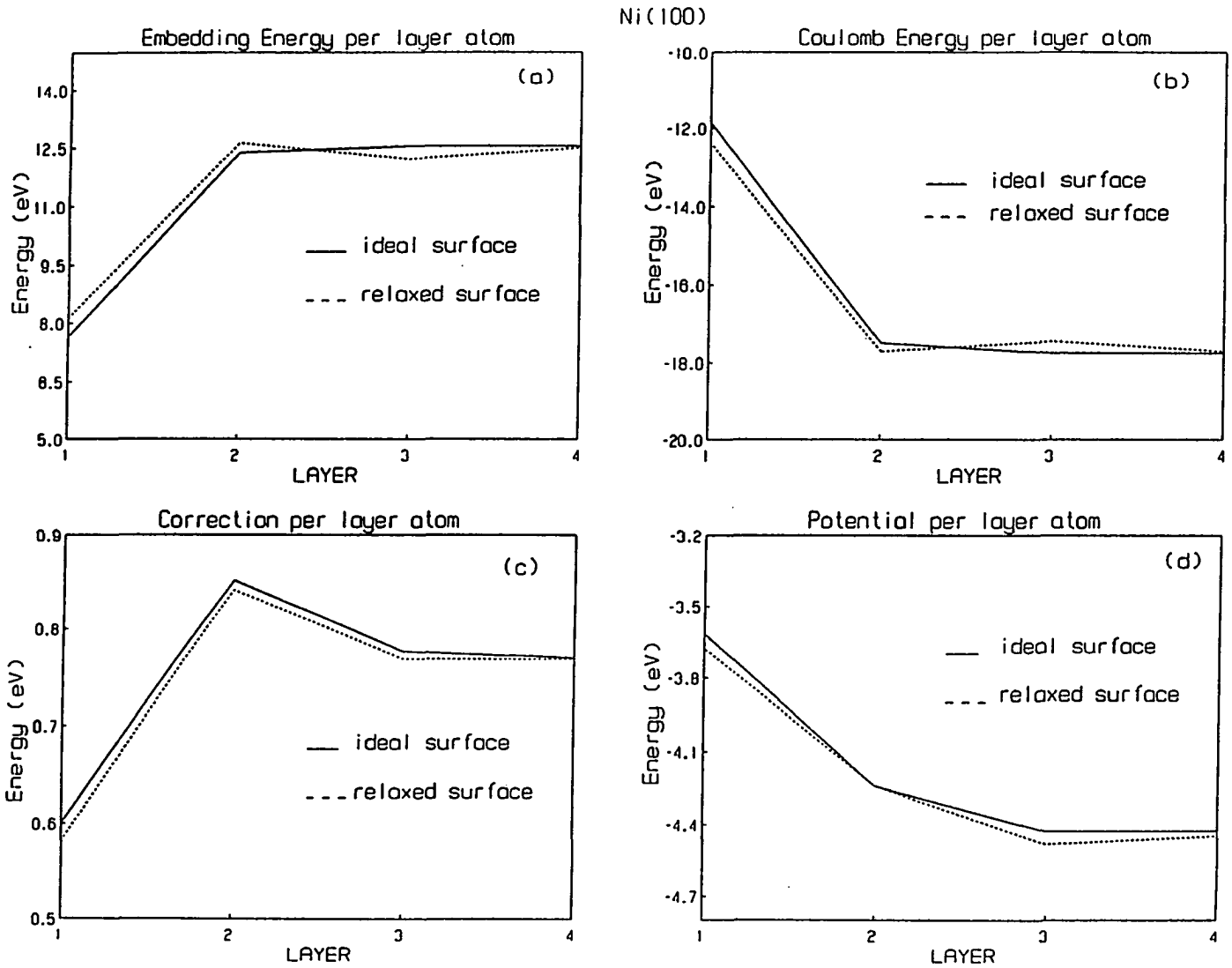

Fig. 12. Same as Fig. 9 except for Ni(100)

Using the Puska *et al.* embedding function, we found a=7.3 bohr and E_{coh}=2.8 eV resulting in an expanded and weakly bound solid. This clearly indicates the significant bonding nature of the 3d electrons. Calculations for the ideal and relaxed surfaces showed that the correction energy now increases upon relaxation and exhibits the oscillatory behavior as observed in the Al surfaces. This indicated that the 3d electrons are an important factor in the difference between the relaxation process in simple vs. transition metal surfaces. A similar finding occurred if we did not use the Puska *et al.* embedding function but instead created a new covalent embedding curve using the same experimental diatomic and bulk data as before in part B of this section.

Returning to computations of surface relaxations, we consider the more open fcc(110) surface for both Al and Ni. The ideal surface energy seen in Table II is much larger than for the fcc(100) face, and thus we expect the multilayer relaxations to be more pronounced. In Table IV we present the CEM results for Al(110) in comparison to experimental data and theoretical EM [25] and SCF-LD [12] calculations. We obtain very good agreement with experiment and relatively good agreement with the self-consistent calculations for all interlayer spacings. In comparison to the EM values we find that CEM is more sensitive to the relaxation process and that the surface energy of the relaxed surface is much more in agreement with that seen by the SCF-LD calculations and experiment. The energy of relaxation is small but, keeping in mind that the surface area of the unit cell is quite large, is none the less large enough to lie outside the precision limits in the calculations.

During the analysis we also allowed only the top layer to relax obtaining a Δd_{12}=-10% contraction, again indicating that the top layer relaxation is relatively independent of other interlayer relaxations. The situation is quite different for the remaining layers where large correlations between the relaxations were observed. The relaxation of the second interlayer spacing was difficult to determine without a corresponding contraction of the third interlayer spacing which in turn was dependent on the fourth interlayer spacing expansion. Basically, since the surface is so open the interactions between layers becomes more sensitive to changes in the local environment of atoms in each layer.

Table IV Percent of bulk multilayer relaxation of Al(110) and Ni(110)

	Al(110)				Ni(110)		
	CEM	SCF-LD[a]	EM[b]	Exp.[c]	CEM	Exp.	
Δd_{12} %	-9.5	-6.8	-7.0	-8.6 ± 0.8	-9.5	-9.0[d] ±1.0	-8.7[e]
Δd_{23} %	+5.5	+3.5	+1.0	+5.0 ± 1.1	+4.0	+3.5±1.5	+3.0
Δd_{34} %	-1.5	-2.0		-1.6 ± 1.2	-1.5		-0.5
Δd_{45} %	+1.0	+1.6			+1.0		
σ_I[f]	1.353	≈1.2			2.879		
σ_R[g]	1.265	1.09	0.883		2.592		

[a] Ref. [12] indicated relaxation energy of ≈10meV.

[b] Ref. [25].

[c] Ref. [1].

[d] Ref. [4].

[e] Ref. [43].

[f] Surface energy for the ideal surface in j/m2.

[g] Surface energy for the relaxed surface in j/m2.

The above correlation can best be seen by examination of Figure 13. The embedding energy shows an increase for the top two layers but a decrease for the third and fourth layers. By contrast the coulomb energy is nearly constant after the first two layers, while the correction energy decreases after the first two layers. The plot of the potential in Figure 13d again reveals the oscillatory behavior of the relaxation process. When the top layer contracts so much, the second layer responds by increasing d_{23} in order to greatly decrease its interaction with the third layer. Now the third and fourth layer atoms compensate for this loss of interaction by contracting the third inter-layer spacing. This cycle continues in a decreasing manner as the layers progress inward towards the bulk.

For the relaxation of Ni(110), we present in Table IV a summary of the results from CEM in comparison to experimental data.

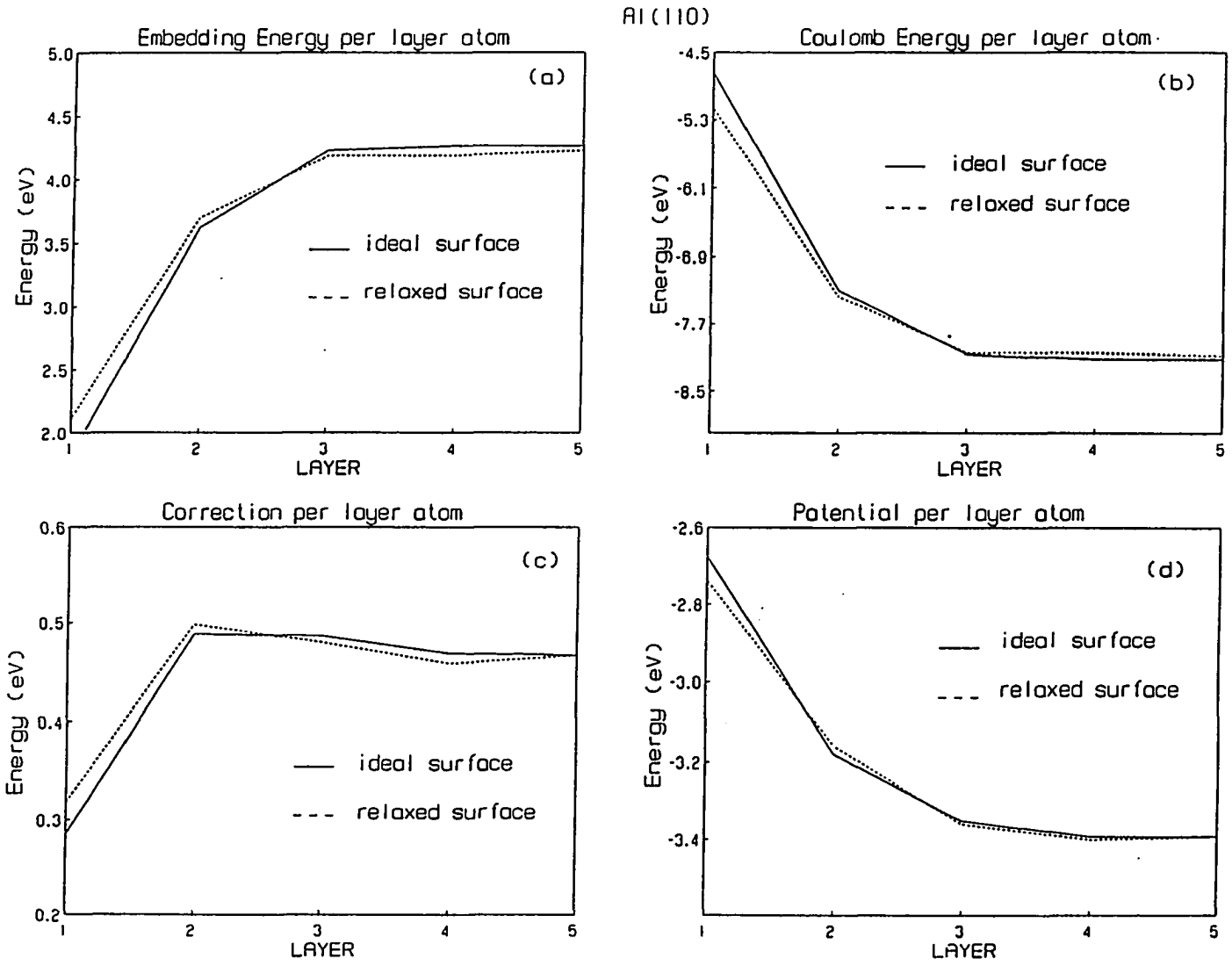

Fig. 13. Same as Fig. 9 except for Al(110)

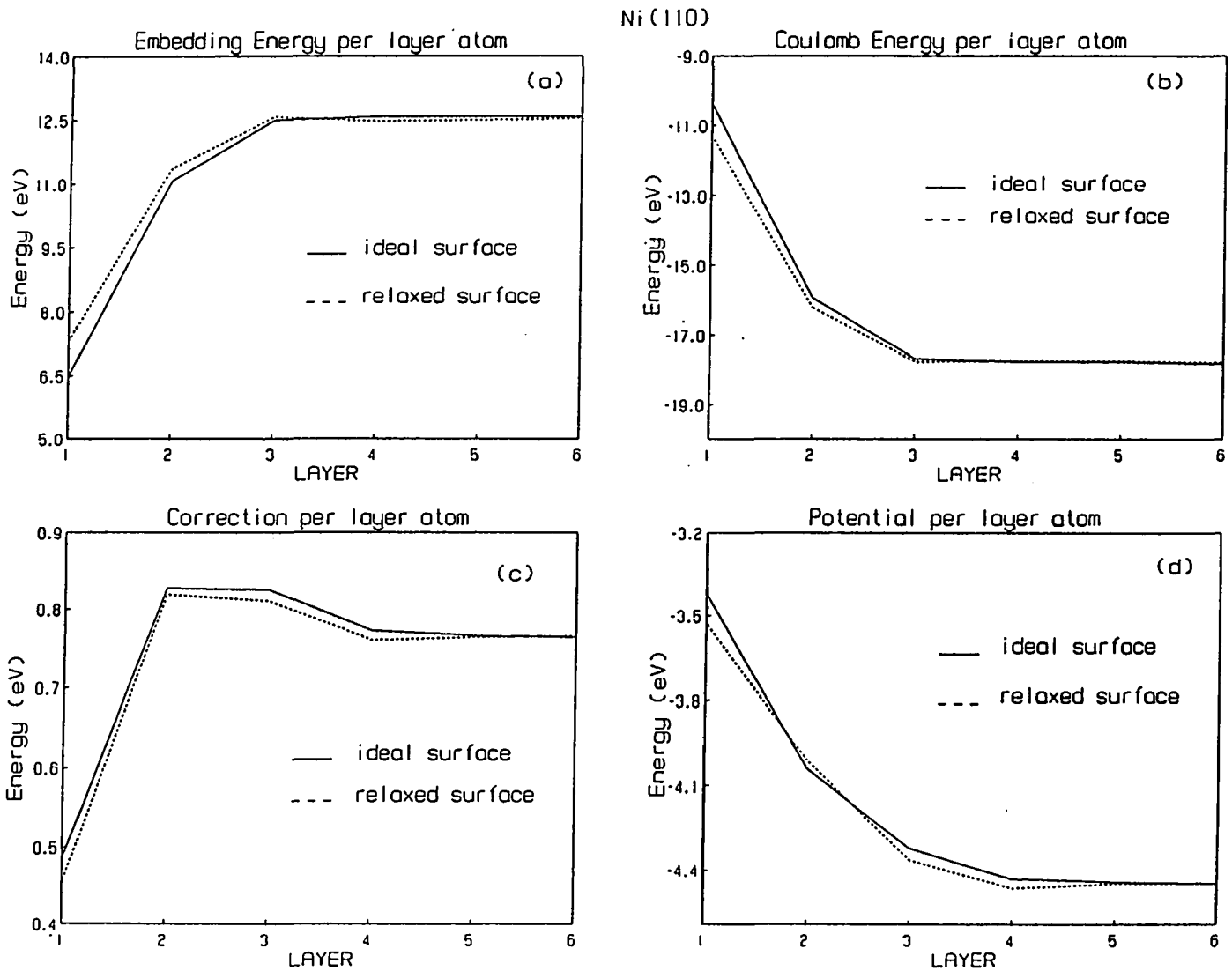

Fig. 14. Same as Fig. 9 except for Ni(110)

As in the case of Al(110) we obtain excellent agreement for the top two layers whereas the relaxations for the third and fourth layers were either not experimentally studied or not detected in the ref. [4] while in ref. [43] a very small contraction of the third interlayer spacing was reported. The calculated relaxation process showed a similar correlation between the relaxation of the layers as observed in Al(110). A plot of the energy components for Ni(110) is shown in Figure 14 and comparison to Figure 13 for Al(110) shows qualitatively similar features for both the embedding and coulomb energies in the top two layers with differences beginning in the third layer.The embedding energy for the third layer in the relaxed geometry is now larger than that of the ideal surface for Ni(110) whereas the opposite is true for Al(110). This feature may be a result of a smaller expansion in the third inter-layer spacing for Ni(110) than in Al(110). The most striking difference though lies in the correction energy, where all the layers in Ni(110) lower their respective correction energies as a result of the relaxation. This is especially true for the third and fourth layers. The resulting sum of the energy components yields the potential in Figure 14d. We see that the top layer potential is lowered while the second layer stays relatively stable. But surprisingly, the third and fourth layers give significant contributions to the relaxation process as reflected by their respective potentials.

With the above calculations we can now draw some important conclusions about the multilayer relaxation process. We have seen that the top layer contraction is independent to a significant degree of the relaxation of the rest of the layers below it. In contrast, the second inter-layer spacing expansion (if it is relatively large) is highly dependent upon the relaxation (contraction) of the third-layer spacing. This feature of the relaxation process can most likely be extended to the rest of the simple and transition metals and studies are underway to determine if this is indeed true.

4. SUMMARY AND CONCLUSIONS

Calculated cohesive energies for the second and third row metals were presented using the corrected effective medium CEM method with the Puska *et al.* embedding functions for the atoms in jellium. It was shown that these embedding functions do not provide an accurate description of the type of bonding occurring for such homonuclear systems. In an attempt to describe the correct type of interaction we have constructed (semi-empirical) covalent embedding functions using both the experimental diatomic binding potential and bulk cohesive energies. These two different types of systems determined different parts of the covalent embedding curve and a smooth interpolation between the two was obtained. This feature supported the postulated universality of this embedding energy as a function of the size of the system. It was also seen that for the electropositive atom the covalent embedding energy is lower than the ionic Puska *et al.* energy. This is in contrast to characteristics of the electronegative atoms studied in Paper II where the covalent embedding energy is larger than that of the Puska values.

We have presented the formalism for the calculation of the surface free energy of an infinitely periodic 2-D metal surface within the CEM method. Within this method, we used the covalent embedding functions to calculate the surface energy for a number of second and third row metals. The energies were shown to agree very well with experimental measurements and to predict the correct qualitative trend of increasing surface energy with increasing openness of the surface. We then carried out multilayer relaxation calculations of well known surfaces through minimization of the surface energy. Very good agreement was obtained for most of the surfaces studied. In our opinion these calculations are in general consistently more accurate and complete than those of other models presented to date in their ability to correctly describe the stability and structural features of various metal surfaces at modest computational expense (e.g., determination of an energy for Ni(110) required 125 minutes on a RIDGE 3200 which is approximately three times faster than a VAX 11/780).

With the ability to accurately describe the metal surface, calculations are currently

being carried out to determine the effect on relaxation of various chemisorbed atoms as a function of the coverage. These results will be presented in a future publication [44]. Also the method is being extended to include more complicated in-planar reconstructions of the metal surface. Improvements in computational methodology are being implemented which may greatly increase the speed of this method to the point where simulations of crystal and cluster growth and roughening may become feasible. If fundamental extensions can be developed to allow for a non-empirical correction between covalent and ionic bonding embedding functions, the CEM approach offers the real possibility of a consistent, accurate and fast computational scheme for the determination of the interaction energies of a collection of different types of atoms ranging from heteronuclear diatomics to large clusters of hundreds of atoms to bulk solids.

5. ACKNOWLEDGEMENT

This work was supported by NSF grant CHE8609832. One of us (TJR) is very pleased to acknowledge many beneficial conversations with Dr. Joel D. Kress.

6. REFERENCES

[1] J. N. Anderson, H. B. Nielson, L. Peterson and D. L. Adams, J. Phys. C 17 (1984) 173.

[2] J. R. Noonan and H. L. Davis, Phys. Rev. B 29 (1984) 4349.

[3] Y. Gauthier, R. Bauding, C. Gaubert and L. J. Clark, J. Phys. C 15 (1982) 3223 and 3231.

[4] Y. Gauthier, R. Bauding, Y. Joly, C. Gaubert and J. Rundgren, J. Phys. C 17 (1984) 4547.

[5] D. L. Adams, L. E. Peterson and C. S. Sorenson, J. Phys. C 18 (1985) 1753.

[6] S. M. Yalisove, W. R. Graham, E. D. Adams, M. Copel and T. Gustafsson, Surf. Sci. 171 (1986) 400.

[7] N. Masud, R. Bauding, D. Abedam and C. Gaubert, Surf. Sci. 133 (1983) 580.

[8] A. Bianconi and R. Z. Bachrach, Phys. Rev. Lett. 42 (1974) 104.

[9] J. W. M. Frenken, J. F. van der Veen and G. Allan, Phys. Rev. Lett. 51 (1983) 1876.

[10] R. Imbihl, R. J. Behm and G. Ertl, Surf. Sci. 123 (1982) 129.

[11] C. L. Fu, S. Ohnishi, E. Wimmer and A. J. Freeman, Phys. Rev. Lett. 53 (1984) 675.

[12] K. M. Ho, K. P. Bohnen, Phys. Rev. B6 32 (1985) 3446.

[13] G. Allan and M. Lannoo, Surf. Sci. 40 (1973) 375.

[14] R. N. Barnett, U. Landman and C. L. Cleveland, Phys. Rev. B 28 (1983) 1685 and Phys. Rev. Lett. 51 (1983) 1359.

[15] T. Halicioglu, H. O. Damuk and S. Erkoc, Surf. Sci. 143 (1984) 601.

[16] R. A. Johnson, Surf. Sci. 151 (1985) 311.

[17] D. Tomanek and K. H. Bennemann, Surf. Sci. 163 (1985) 503.

[18] P. Jiang, P. M. Marcus and F. Jona, Solid State Commun. 59 (1986) 275.

[19] M. Manninen, Phys. Rev. B 34 (1986) 8486.

[20] A. G. Equiluz, Phys. Rev. B 35 (1986) 5473.

[21] X. W. Wang and W. Weber, Phys. Rev. B 35 (1987) 7404.

[22] M. S. Daw and M. I. Baskes, Phys. Rev. B 29 (1984) 6443.

[23] S. M. Foiles, M. I. Baskes and M. S. Daw, Phys. Rev. B 33 (1986) 7983

[24] J. K. Norskov and N. D. Lang, Phys. Rev. B 21 (1980) 2136; M. J. Stott and E. Zarembra, Phys. Rev. B 22 (1980) 1564.

[25] K. N. Jacobson, J. K. Norskov and M. J. Puska, Phys. Rev. B 35 (1987) 7423 and references therein.

[26] J. D Kress and A. E. DePristo, J. Chem. Phys. 87 (1987) 4700.

[27] J. D Kress and A. E. DePristo, J. Chem. Phys. 88 (1988) 2596.

[28] J. D. Kress, M. S. Stave and A. E. DePristo, "Corrected Effective Medium Method: III. application to clusters of Mg and Cu", J. Phys. Chem. (submitted).

[29] M. J. Puska, R. M. Nieminen and M. Manninen, Phys. Rev. B 24 (1981) 3037; M. J. Puska (private communication).

[30] A. E. DePristo and J. D. Kress, Phys. Rev. A 35 (1987) 438.

[31] a) A. E. DePristo and J. D. Kress, J. Chem. Phys. 86 (1987) 1425;
b) J. P. Perdew, Phys. Rev. Lett. 55 (1985) 1665;
c) A. D. Becke, J. Chem. Phys. 84 (1986) 4524;
d) S. K. Ghosh and R. G. Parr, Phys. Rev. A 34 (1986) 785;
e) O. Gunnersson, M. Jonson and B. I. Lundqvist, Phys. Rev. B 20 (1979) 3136.

[32] O. Gunnarsson and B. I. Lundqvist, Phys. Rev. B 13 (1976) 4274.

[33] M. Schmidt and K. Ruedenberg, J. Chem. Phys. 71 (1979) 3951.

[34] E. Clementi, IBM J. Res. Develop. Suppl. 9 (1965); P. S. Bagus, T. L. Gilbert and C. J. Roothan, J. Chem. Phys. 56 (1972) 5159.

[35] S. Huzinaga, Prog. Theor. Physics Suppl. 40 (1967) 279.

[36] C. Kittel, "Introduction to Solid State Physics" (John Wiley, New York, 1986).

[37] L. Pauling, "The Nature of the Chemical Bond", (Cornell University Press, Ithaca, New York, 1960), p. 93.

[38] K. P. Huber and G. Herzberg, "Constants of Diatomic molecules" (Van Nostrand, New York, 1979).

[39] W. R. Tyson and W. A. Miller, Surf. Sci. 62 (1977) 267.

[40] V. Sahni, J. P. Perdew and J. Gruenebaum, Phys. Rev. B 23 (1981) 6512

[41] F. Soria, M. C. Munuz and J. L. Sacedon, Surf. Sci. 128 (1983) 424.

[42] H. B. Nielson and D. L. Adams, J. Phys. C 15 (1983) 615.

[43] D. L. Adams, L. E. Petersen and C. S. Sorensen, J. Phys. C 18 (1985) 1753

[44] T. J. Raeker and A. E. DePristo, Surf. Sci. 235 (1990) 84.

PAPER II
CORRECTED EFFECTIVE MEDIUM CALCULATIONS OF THE CHEMISORPTION OF H AND N ON FE(100),(110) AND W(110)

Corrected Effective Medium Calculations of the Chemisorption of H and N on Fe(100),(110) and W(110).

Todd J. Raeker
and
Andrew E. DePristo
Department of Chemistry
Iowa State University
Ames , Iowa 50010

ABSTRACT

We employ the recently developed corrected effective medium method (CEM) to study chemisorption of H and N atoms on low Miller index surfaces of Fe and W. The binding energy, height and adsorbate induced surface relaxation is investigated as a function of coverage via explicit treatment of the 2-D periodicity of an infinite surface with an infinitely ordered overlayer of chemisorbed atoms. There is no use of the approximation of a cluster model.

We find that the most stable site for both H and N on Fe(100) is the four-fold center; for H on Fe(110) and W(110), both the long-bridge and three-fold center sites are nearly equal in adsorption energy; for N on Fe(110), the three-fold center site is most stable; and, for N on W(110), the long-bridge site is most stable. Thus, H and N differ in their adsorption properties. Such differences are accentuated in the effect of chemisorption on surface relaxation. For example, the chemisorption of N induces a strong coverage dependent outward relaxation of the Fe(100) top metal surface layer distance while H induces a much smaller outward relaxation.

1. INTRODUCTION

Extensive experimental study of H_2 [1-4] and N_2 [5-9] on Fe surfaces has occurred over the past few years. A practical reason is to provide a better understanding of the mechanisms involved in the production of ammonia over Fe catalysts in which the dissociation of N_2 is thought to be the rate limiting step in the reaction process [10]. Theoretical research has lagged behind the experimental studies. To the best of our knowledge, there are no studies of these dissociative chemisorption reaction energetics using accurate first-principle or ab-initio methods. Such calculations are only now beginning to appear for less demanding transition metals such as Ni, Cu and Pt [11-14].

The theoretical treatment of atomic chemisorption is still a demanding problem due to the complexity and size of extended systems. As such, accurate first principle and ab-initio calculations are very few. Some examples include O/Fe(100) [15], H/W(100) [16], H/Ni(100) [17,18], S,P,Cl and Li on Rh(001) [19], S,P,C and H on Fe(001) [20] and Si/Al(001) [21]. In addition, there are cluster calculations for the H/Ni [22,23], O/Ni [22-24], H/Pd [25], and O/Ag [26,27] systems. Semi-empirical methods have been used more extensively and we just mention the relevant H/Fe cluster results [28]. Several studies based upon simpler models of adsorbate-substrate binding exist for H on metal surfaces, some of which can be found in refs. [29] and [30]. For N on metal surfaces, these are non-existent to our knowledge.

In the present article, we try to build on the above studies by employing the recently developed corrected effective medium (CEM) method [31-34] to study chemisorption of H and N on Fe(110), Fe(100) and W(110). The binding energy, height and adsorbate induced surface relaxation were investigated as a function of coverage via explicit treatment of the 2-D periodicity of an infinite surface with an infinitely ordered overlayer of chemisorbed atoms. A major focus was to examine in detail the effect that adsorbates can have on the structural geometry of the metal surface atoms. In general, relaxations and reconstructions can occur, but in this study we focus on the former.

The CEM theory was first presented in a one-body formalism in ref. [31], referred

to as Paper I from now on, as a method to calculate the chemisorption binding energies of single atoms on metal surfaces. The first fundamental idea, which originated with the effective medium theory [29,30,35], is to replace the atom-surface system with an effective medium, the atom embedded in jellium. The second idea in Paper I is to provide non-self-consistent corrections due to coulomb and kinetic-exchange-correlation energy differences between the effective medium and the real many atom system. This CEM method is quite accurate for adsorbates which do not interact too strongly with the substrate. However, it suffers from an inconsistent treatment between the inert surface atoms (i.e., not embedded in jellium) and the active adsorbate atom (i.e., embedded in jellium). In other words, it neglects the changes in bonding in the metal due to the adsorbate.

Removal of this inconsistency is provided by the N-body formalism in ref. [32], referred to as Paper II. In this theory, every atom in the system is embedded in an appropriate jellium whose density is determined by the remaining atoms. Again, non-self-consistent corrections due to coulomb and kinetic-exchange-correlation energy differences are calculated. Further extensions to bulk [33] and surface [34] systems, referred to as Papers III and IV respectively, have also been presented. The CEM method was shown to be accurate and reliable in its ability to describe and predict surface relaxations in Paper IV. In the present paper, we have extended the method yet again to include adsorbates on a metal surface.

This paper is divided into four sections with two major purposes in mind. In Section II, we develop the formalism to calculate the binding energy of an ordered layer of adsorbates on metal surfaces within the CEM method. This derivation uses previously developed CEM energy relations for extended surface and bulk systems. Section III includes a brief presentation of CEM results for the diatomics, HFe, NFe, HW and NW and extensive results for H and N chemisorption on Fe and W surfaces, including binding energies and adsorbate induced surface relaxation. Also within this section, results for the clean surface relaxation are discussed and related to those for the adsorbate covered surface. Following this, Section IV contains a summary and conclusion of the method as applied to chemisorption.

2. THEORY

The major developments, and illustrative applications, of the CEM method have been presented previously in Papers I-IV [31-34] and the reader is encouraged to refer to these papers. We start from the basic CEM relation for the interaction energy of N-atoms, as developed in Paper II:

$$\Delta E(\{A_N\}) = \sum_{i=1}^{N} \Delta E_J(A_i;n_i) + \Delta V_c + \Delta G(\{A_N\}) \tag{1}$$

where

$$\Delta G(\{A_N\}) = G(\sum A_i) - \sum_{i=1}^{N} [G(A_i+n_i) + G(n_i)] \tag{2}$$

A_i represents the i^{th} atom in the set of atoms $\{A_N\}$ in a specified geometry. The first term in Eq. (1) is the sum of the embedding energies of all the atoms in jellium, with each jellium having an electron density n_i. Each embedding function, ΔE_J, should be considered as a known function of the density, which we will discuss further later in this section. The second term is a coulombic correction that describes the different electrostatic interaction among the atoms compared to that between the atoms and jellium. Finally the last term describes the different kinetic-exchange-correlation energy in the N-atom system compared to that of the atom-jellium systems. Both corrections arise due to the difference between the homogeneity of the electron density in the N-atom and atom-jellium systems. The energy functional, $G(S)$, denotes the sum of the kinetic, exchange and correlation energy density functionals of the electron density for the system S. The energy density functionals we have used are the same as described in Papers II-IV: Pade' representation of the kinetic energy functional [36], local exchange and correlation with the Gunnarsson-Lundqvist form [37] for the latter. The latter are required by the use of the embedding functions of Puska et al. [38] which were determined from SCF-LD calculations with local exchange and Gunnarsson-Lundqvist correlation functions.

From the fundamental relation in Eq. (1), we extended the formalism to include

periodic systems in Papers III and IV. For an infinitely periodic three-dimensional homogeneous crystal, the cohesive energy is

$$E_{Coh} = \Delta E_J(A_b;n_b) + \Delta G_b + \frac{1}{2}\sum_{j\neq b}^{N} V_{bj} \tag{3}$$

where

$$\Delta G_b = G_b - [G(A_b+n_b) - G(n_b)] \tag{4}$$

The last term V_{bj} of Eq. (3) is the pairwise coulomb interaction between atoms b and j. The subscript "b" refers to any <u>one</u> bulk 'focus' atom in the system. The evaluation of G_b in Eq. (4) requires an integration over the Wigner-Seitz cell of atom b (see Paper II).

For a two-dimensional surface of a monatomic crystal, the basic idea is to use the fact that each atom in a particular layer is identical to any other atom in the layer. Thus, for surface structural energies one simply calculates the cohesive energy of <u>one</u> 'focus' atom in the i^{th} layer as;

$$\Delta E_i = \Delta E_J(A_i;n_i) + \Delta G_i + \frac{1}{2}\sum_{j\neq i} V_{ij} \tag{5}$$

The evaluation of G_i for surface and near-surface atoms involves an integral over a generalization to the Wigner-Seitz cell of atom i: one integrates over all spatial locations which are closer to atom i than to any other atom. With this formalism the task of calculating the energy of an infinite N-body surface system is reduced to a finite calculation over the layers of a surface system. We have found that Eq. (5) converges with 3-5 layers for the relatively close packed surfaces studied in Paper IV and in this paper. For very open surfaces, the summation will converge more slowly since many more layers lie close to the vacuum.

For chemisorption systems with an ordered and infinitely periodic overlayer, it is not each surface atom but each <u>unit cell</u> of the chemisorbed overlayer which is the periodic unit. Thus the cohesive energy of the <u>unit cell</u> can be obtained through calculation of the cohesive energy of each unique atom in a layer for the unit cell by

use of Eq. (5). (This is exactly equivalent to using a larger basis associated with the space lattice of the metal substrate, and will also occur for solids with more than one atom per unit cell.) This allows a simple calculation of the binding energy of a chemisorbed atom in an ordered overlayer without the use of a cluster model approximation. We sum the energies of Eq. (5) for all the atoms in the unit cell (N_u) for both the adsorbate covered and clean surface to obtain the adsorbate binding energy as;

$$E_B = \sum_{i=0}^{N_u} \Delta E_{ia} - \sum_{i=1}^{N_u} \Delta E_i \tag{6}$$

The first sum is the energy of the unit cell for the adsorbate covered surface where $i=0$ is the adsorbate atom, with one adsorbate atom per unit cell, and where $i=1,N_u$ includes the metal atoms. The second sum is the energy of the clean surface with the same unit cell but only includes the metal atoms $i=1,N_u$. We emphasize that each summation requires a separate calculation since the embedding energies of the surface change due to the adsorbate and since a full geometry optimization must be performed. Thus, one cannot calculate E_B directly.

The question of the choice of the jellium densities for each embedding energy now arises. In Paper II, we have shown that an elegant solution exists in which the correction energy, ΔG, is minimized with respect to all the densities $\{n_i\}$. This yields the CEM jellium density,

$$n_i = \frac{\sum_{j \neq i}^{N} \int n(\vec{r}_i) n(\vec{r}_j) d\vec{r}}{2Z_i} \tag{7}$$

where Z_i and $n(\vec{r}_i)$ are the atomic number and atom electron density, respectively. The integral in Eq. (7) is over all space with the electron densities centered on atoms A_i and A_j, respectively. It is thus an overlap of electron densities that determines n_i.

Finally, we must specify the embedding function. There are two distinct types of embedding energies available. The first is provided by first-principle SCF-LD calculations of Puska et al. [38] on atom-jellium systems. The second is constructed

semi-empirically from experimental binding curves as detailed below following papers III and IV. These are denoted by ΔE_P and ΔE_C, respectively. Papers II-IV suggested that the Puska et al. embedding energies describe an ionic interaction of the atom in jellium. For systems with a single type of atom, a different embedding energy function must be used to reflect correctly covalent or metallic bonding, thereby labelled ΔE_C. The ΔE_C function for N is presented in Paper II while that for Fe is presented in Paper IV. For easy reference, these are reproduced here along with introducing the ΔE_C function for W.

The H and N covalent embedding energy curves are constructed from Extended Rydberg [39] and Morse diatomic potentials [40] as discussed in Paper II. For the Fe system, the low density region of the embedding energy curve is constructed from Morse potentials fit to diatomic data [41]. The higher density region is generated from a Morse expansion (in the lattice constant [42]) of bulk data that includes the lattice constant, cohesive energy and the bulk modulus [43]. The ΔE_C curve for W is constructed as for Fe except that no diatomic data is used. Although first principles relativistic calculations [44] exist, we do not use these since there is no real evidence that they are of sufficient accuracy. For the lower density region of the embedding curve we instead rely on a smooth interpolation of a fourth order polynomial in the density between the bulk points and the zero embedding energy at zero density. The lack of good information about the low density area of the W covalent embedding energy function may have an effect on the results. This is because the surface atoms have an overlap embedding density between the bulk and diatomic limits of the respective metals.

We present in Figure 1 the ΔE_P and ΔE_C functions for H, N and Fe; for W, only ΔE_C is shown since ΔE_P is not available. From Figures 1a and 1b one can see that the H and N embedding functions have minima that are negative. This phenomena is characteristic [38] of electronegative atoms. The curves for Fe and W in Figures 1c and 1d by contrast show no minima and increase with density much faster than do H and N.

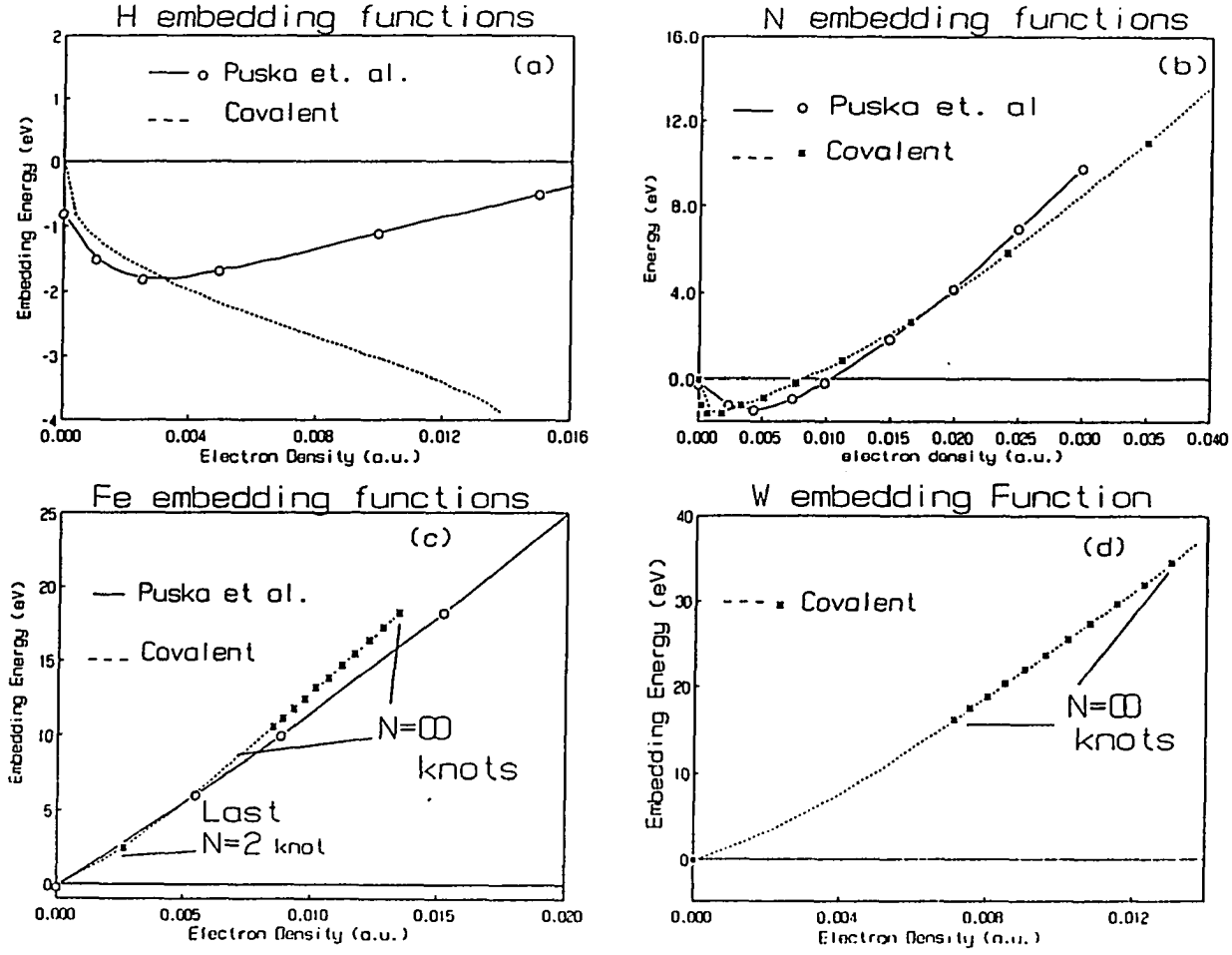

Fig. 1. **The semi-empirical covalent embedding energy ΔE_C (dashed line) and SCF-LD Puska et al. [38] embedding energy ΔE_P (solid line with circles) functions. (a) ΔE_C and ΔE_P functions for H; (b) ΔE_C and ΔE_P functions for N; (c) ΔE_C and ΔE_P functions for Fe; (d) ΔE_C function for W**

ΔE_C for H continues to decrease at high density; this occurs because ΔG remains nearly constant while the coulomb integral becomes more repulsive than the binding curve, and the sum of the three terms must equal the binding curve [32]. This behavior is unique to H because the difference between the H_2 molecule and the H-jellium system is particularly large. The differences for the N and Fe are less with both types of functions in qualitative agreement. Quantitatively, we note that use of the Fe ΔE_P would yield a contracted and overly bound Fe of a=4.75 a.u. and ΔE_{Coh}=7.52 eV compared to the experimental values of a=5.42 a.u. and ΔE_{Coh}=4.28 eV [43] which are duplicated by use of ΔE_C. A smaller overestimation of the binding energy also occurs for full SCF-LSD calculations [45] but as in most variational methods, the bond distances are much better.

One feature of all the embedding functions in Figure 1, except $\Delta E_C(H)$, is particularly interesting, namely the near-linearity of the function at high density. In this case, the embedding energy is nearly pairwise additive since the density on the i^{th} atom is a summation over pairwise overlap in Eq. (7). The two body potentials will be extremely complicated however since the electron density of each atom is represented by many Gaussian or Slater type functions. For example, in W there are 36 s-type and 26 p-type Gaussians used to represent the electron density. Thus, there are 1953 unique terms in both the overlap and coulomb integrals, which is why one does not want to utilize empirical two body functions as is done in the EAM method [46].

For the electron density of the i^{th} atom, we have used Slater-type atomic Hartree-Fock densities [47]. We then fit an even-tempered Gaussian basis [48] to the atomic electron densities. This allows simple analytical evaluations of the coulomb and density overlap [49] (i.e., for the sampled jellium density) integrals. The atomic density around each atom was cut off at a radial distance such that R^2*(atomic electron density) < 10^{-5} *a.u.* For all atoms in the present paper we utilized non-spin polarized atomic electron densities, (except as noted), since it was seen in Paper II that this yielded the most accurate energies within CEM.

A few computational details may be of interest. As described above, we do calculations for the 'focus' atoms in each layer of a periodic metal surface with a semi-infinite overlayer of adatoms. We used a large enough number of atoms around each

'focus' atom such that the 'focus' atoms did not 'feel' the edges of the lattice. To mimic an infinite surface for a 'focus' unit cell we swept out a volume of radius *1.5R* where *R* is the radial density cutoff distance as described above. Including atoms outside this range changed the surface unit cell energy by less than 0.005 eV. We used a slab of *2n* layers where the energy was calculated for the top "*n*" layers. A value of *n=3* yielded chemisorption binding energies converged to 0.01 eV. This procedure led to about 300 atoms interacting with each 'focus' atom.

It is worthwhile to reiterate the six steps in a CEM calculation:

1) construct atomic densities from Gaussian fit to HF values;
2) compute density overlap and evaluate n_i from Eq. (7);
3) evaluate the embedding energies;
4) compute coulomb energies;
5) calculate ΔG;
6) add embedding and coulomb energies and ΔG, as in Eq. (5).

For each additional geometry only steps 2-6 are repeated. The most time consuming step is "5" since it involves a three dimensional numerical integration over many centers. We emphasize here that there are no adjustable parameters or empirical constructs in this prescription once the embedding energies are known. These are constructed solely from diatomic and bulk data on the respective homonuclear systems or from the SCF-LD calculations of Puska et al. in ref. [38]. Any further calculation on heterogeneous systems is predictive, as is any other homogeneous calculation (e.g., surface energy).

3. RESULTS

In this section we first examine the binding potential of the diatomic molecules HFe, HW, NFe and NW as a prelude to discussing the chemisorption systems. From there we go on to discuss the results of our calculations on the chemisorption of H and N on various Fe and W surfaces. We consider both adsorption on surfaces which are not allowed to relax further and on those which are allowed to relax in response to the adsorption. These two cases are referred to as rigid and non-rigid surfaces, respectively. The reader should clearly understand that a rigid surface does not have perfectly terminated bulk positions but instead retains the fully optimized positions of the clean surface.

3.1. Diatomic Hydrides and Nitrides

As a severe test of the adequacy of the CEM calculated results, we have treated the above diatomics. In contrast to SCF ab-initio and first principle methods, the CEM method is least accurate for diatomics due to the significant deviation from the zero'th order model of atoms-in-jellium [32]. The known problems with the behavior of $\Delta E_P(A;n\rightarrow 0) = -IP(A)$ are also well illustrated by the errors in the curvature around the PES minimum in a diatomic molecule [32]. However, it is possible to utilize a comparison of CEM results with accurate diatomic information to gain some understanding of the adequacy of the former, and that is our main purpose in this subsection.

We have calculated the binding potentials of the HFe and HW molecules from Eq. (2) by using the ΔE_P function for H and the ΔE_C functions for Fe and W. The Puska et al. embedding function should be most appropriate for the interaction of a single H-atom with a metal. Calculations using $\Delta E_C(H)$ are not reported since this embedding function is pathological in Figure 1a. ΔE_C is used for the metals since we want to compare binding in diatomics to binding on surfaces. In Table I, we summarize our results for these two diatomics and compare to experimental data and other theoretical results when available.

In more detail, we note that the CEM binding energy for HFe is in good accord with one ab-initio result but too small compared to the other. The CEM bond length is too long by about 0.1 Å or about 7%. The major inaccuracy occurs for the frequency, which is only 62% of the experimental value. Both these errors are expected and are discussed further later. For the HW system, experimental data as well as other theoretical calculations are non-existent (to our knowledge). We however note that calculations for WH_6 are in somewhat good agreement with our results for the bond length. An important observation is that HW is more strongly bound than HFe.

Table I Results for HFe and HW

	r(Å)	D(eV)	$\omega(cm^{-1})$	
HFe	1.74	1.78	1040	CEM[a]
	1.56	1.65	1821	Other Theory[b]
	1.61	2.83	1605	Other Theory[c]
	1.63		1680	Experiment[d]
HW	1.77	2.29	950	CEM[a]
WH_6	1.80	2.8		CEM[a]
	1.85			Other Theory[e]

[a] H with Puska et al. embedding function and metal with covalent embedding function.

[b] CASSCF/MCPF calculations [50].

[c] CASSCF/CI calculations [51].

[d] Ref. [52] and refs. therein.

[e] Relativistic W-H bond length in WH_6 [53].

We examine HFe and HW bonding in more detail in Figure 2. In HFe at the equilibrium bond length, the coulomb and embedding energies contribute nearly equally to binding while the correction energy is slightly repulsive. The negative total

embedding energy arises because the H embedding energy is negative at these densities, $\Delta E_P(H;n=0.0094\ a.u.)=-1.3\ eV$, and because the contribution from Fe is positive and small, $\Delta E_C(Fe;n=0.00036\ a.u.)=0.30\ eV$. In HW, the embedding energy destabilizes the bond while the coulomb and correction energy stabilize the bond; the correction and embedding energy nearly cancel. The destabilization occurs because there is a much higher electron density on H from W which causes the embedding energy to rise much more quickly and is thus no longer in the negative region of the embedding curve of H, $\Delta E_P(H;n=0.0214\ a.u.)=0.09\ eV$). The W embedding energy is very similar in magnitude to that for Fe, $\Delta E_C(W;n=0.00028\ a.u.)=0.33\ eV$. The correction and coulomb energies in HW also change at a much faster rate than in HFe. The inhomogeneity in the electron density for HW is more pronounced, leading to the more significant contribution of the correction energy.

The above discussion leads to two important conclusions. First, even though the same $\Delta E_P(H)$ function is used for both HFe and HW, the CEM binding is substantially different due to the differences in the embedding functions and electron densities of the metals. It is not true that the binding potential reflects the H-embedding function. Second, despite the differences in the individual components, the resulting total binding potentials are very similar to each other. Both curves are very flat, making the location of the minimum very difficult to determine and the variation of ≈0.1Å in Tables I and II relatively insignificant. Bond lengths from these curves thus should not be taken as a definitive test of the ability of CEM to describe well the HFe and HW binding features. Furthermore, the inaccuracy of the frequency is a direct result of the flatness of $\Delta E_P(H)$ in the density range from zero up till the minimum. This arises because $\Delta E_P(H;n\rightarrow 0) \rightarrow -0.8\ eV$, the negative of the electronegativity of the H-atom, which is a significant fraction of the binding potential. This inaccuracy in the asymptotic variation of the embedding energy with density cannot be corrected at present, but does not cause significant inaccuracies in the values of the binding energy.

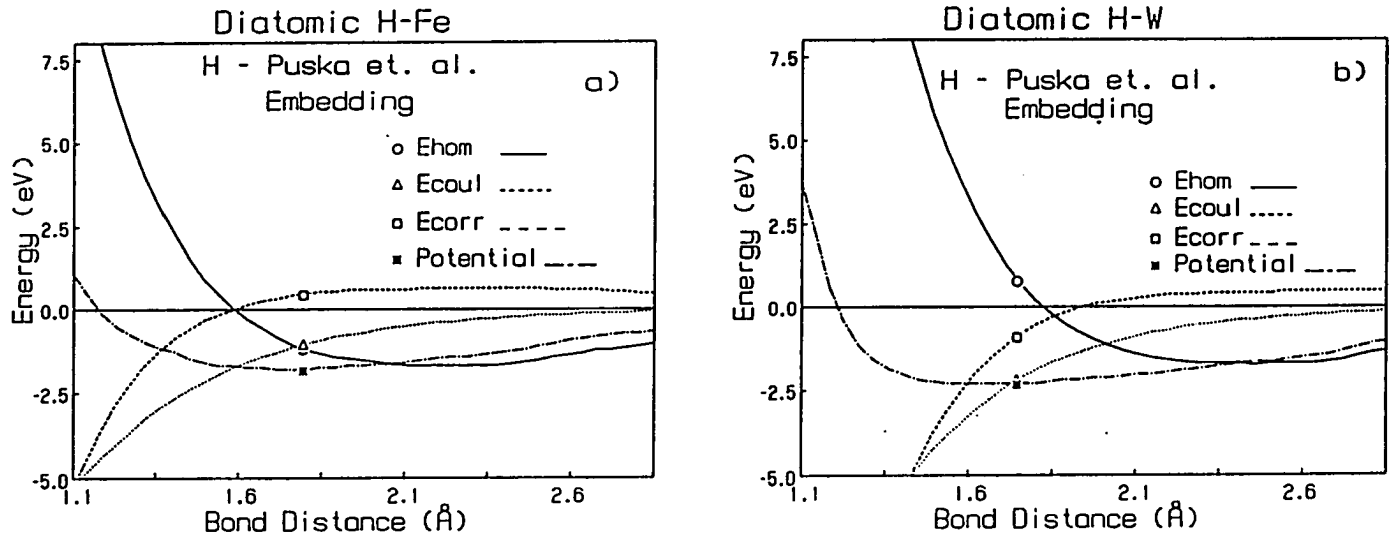

Fig. 2. **Calculated CEM energy components and the binding potential for diatomic HFe and HW using the ΔE_C function for the metals and ΔE_P function for H. The labeled points indicate the particular energy component curves and locate the equilibrium point of the binding potential. Embedding energy: solid line with circles; Coulombic energy: dotted line with triangles; Correction energy; dashed line with squares; binding potential: dot dashed line with stars. (a) HFe; (b) HW**

Although the Puska et al. embedding energy function accounts for a negatively charged H atom in jellium it is not completely correct for H^- interacting with Fe^+ or W^+. The approximation of not explicitly treating charge transfer also contributes to the inaccuracy in the frequency [32]. The lack of very good agreement with experimental data for diatomics is a known consequence of the approximations in the CEM formalism at present. Efforts to improve the situation are underway, but these will undoubtedly lead to a more complex and time-consuming theory.

We have calculated the binding potentials of the NFe and NW molecules from Eq. (2) by using both the ΔE_P and ΔE_C functions for N and the ΔE_C functions for Fe and W. We summarize our results in Table II and compare to experimental and other theoretical results. In general, we find that the bond energies for these two molecules are much larger than the hydrides. Also note that, as in the hydrides, NW is more strongly bound than NFe.

The difference in binding energy calculated with the two N embedding functions is small for NFe but not for NW. This can be understood by examining the N embedding energy function in Figure 1. Note that $\Delta E_C(N)$ is smaller than $\Delta E_P(N)$ for electron densities above 0.017 a.u. and that $\Delta E_C(N)$ rises at a slower rate. The electron density overlap in NFe (at the equilibrium bond length) lies in the region about where the curves cross. The increased atomic electron density from the much larger W atom causes the overlap electron density to be larger on N which leads to a significant separation between $\Delta E_C(N)$ and $\Delta E_P(N)$ with the former being less positive than the latter. The difference in bond length for both molecules is also in accord with the larger value of the Puska et al. embedding function for N. As for the hydrides, we expect that the results using $\Delta E_P(N)$ are more accurate since this functional should describe atom-metal binding.

In comparison to other results, we note that the CASSCF binding energy of Siegbahn and Blomberg [54] is smaller that either of our values by over 4 eV. We do not believe such a small value since, experimentally, several transition metal-nitrogen diatomics have been isolated with significant binding energies tabulated [40]. Some examples include CrN (≈3.87 eV), TiN (≈4.9 eV), and VN (≈4.9 eV). If indeed the bond of NFe is as strong as we predict here this molecule should be easy to isolate and

study experimentally. The CASSCF bond length is larger than the CEM value by 0.19 Å using $\Delta E_P(N)$. It would be reasonable to assume that the CASSCF results are a general reflection of the good bond lengths and poor energies provided by nearly all ab-initio calculations involving transition metals with partially filled d-shells. The comparison of our results of NW become even more difficult since not only are there no experimental data, but to our knowledge, no theoretical data exists for this molecule. However, we do observe that our bond lengths for NW are smaller by about 0.11 Å as compared with those of a molecular complex of W and N in ref. [55]. Finally, we note that the value of $\Delta E_P(N;n\rightarrow 0)$=-0.2 eV, which is only a small fraction of the binding energy. Thus, we expect that the frequencies of the diatomic nitrides should be much better than for the hydrides and also that the bond energy using $\Delta E_P(N)$ is reasonable.

Table II Results on NFe and NW

	r(Å)	D(eV)	ω(cm^{-1})	
NFe	1.48	5.25	1320	CEM ΔE_P[a]
	1.40	5.11	1410	CEM ΔE_C[b]
	1.67	0.90		Other Theory[c]
NW	1.56	7.93	1310	CEM ΔE_P[a]
	1.47	9.04	1702	CEM ΔE_C[b]
	1.68[d]			Experiment

[a] N Puska et al. embedding function.

[b] N Covalent embedding function.

[c] CASSCF results from ref. [54].

[d] Data for a complex of N and W from ref. [55].

In Figure 3 we show a plot of the total binding potentials and its CEM energy components of NFe and NW when using both N embedding energy functions. We examine NFe and NW bonding in more detail in Figure 3.

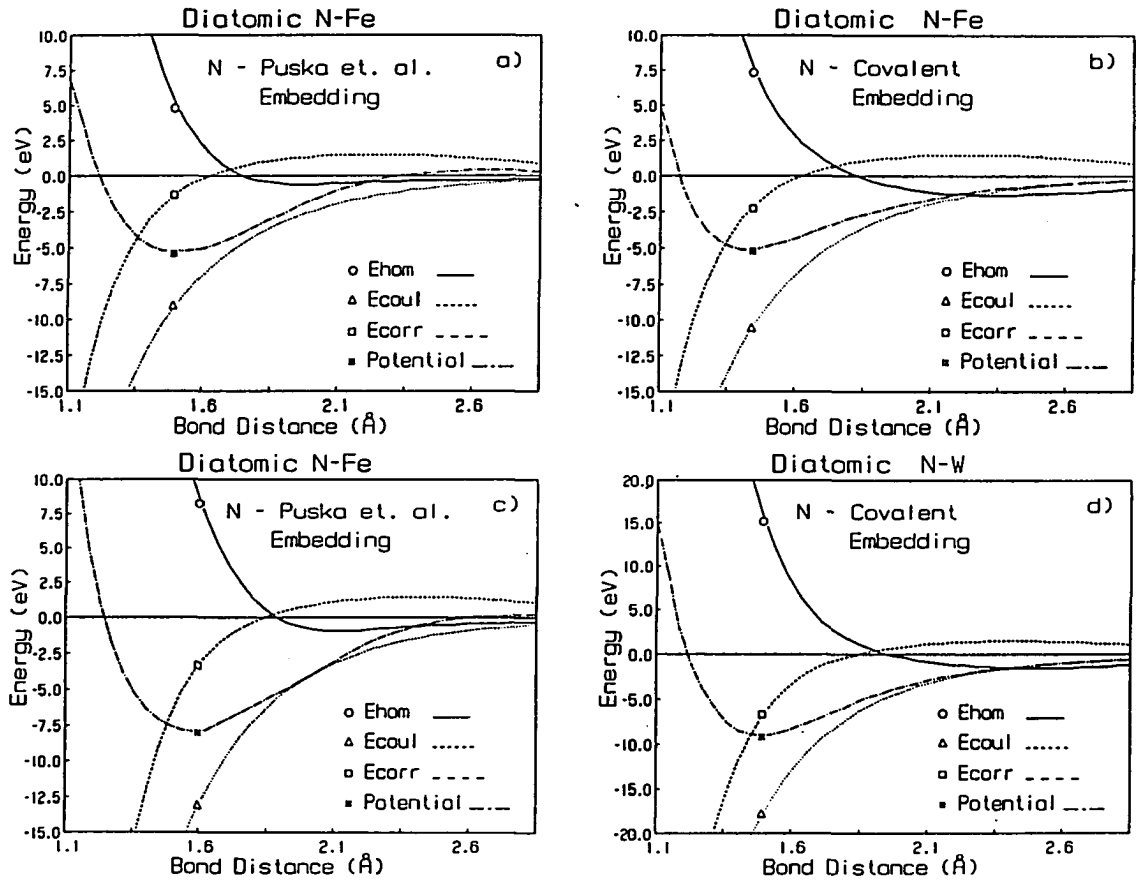

Fig. 3. **Calculated CEM energy components and the binding potential for diatomic NFe and NW using the ΔE_C function for the metals and both ΔE_P and ΔE_C functions for N. The labeled points indicate the particular energy component curves and locate the equilibrium point of the binding potential. Embedding energy: solid line with circles; Coulombic energy: dotted line with triangles; Correction energy; dashed line with squares; binding potential: dot dashed line with stars. (a) NFe with $\Delta E_P(N)$; (b) NFe with $\Delta E_C(N)$; (c) NW with $\Delta E_P(N)$; (d) NW with $\Delta E_C(N)$**

In all cases at the equilibrium bond length, the coulomb energy contributes most to binding; the correction energy contributes a smaller amount; and the embedding energy is quite repulsive. The difference from the hydrides is characteristic of all heavy adsorbates which have much larger coulomb attractions, substantially larger correction energies and also much larger and repulsive embedding energies.The binding energy curve is not determined by the N-embedding function since the corrections play a central role.

3.2. H and N Atomic Chemisorption

Now that we have examined the diatomics, we consider the bonding of H and N atoms on Fe and W surfaces. In Figure 4 we show the clean surface unit cells and the adsorbate binding sites for different coverages on the BCC (100) and (110) surfaces. Note that only a single type of adsorption site is illustrated for each surface in Figures 4c and 4d, but we have considered other sites such as the bridge on BCC(100) and short-bridge and three-fold sites on BCC(110) in this paper. The relative openness of these surfaces varies only slightly. We provide binding energies and heights. We do not report vibrational frequencies of the adatom on the surface for three reasons. First, these values are sensitive to the order of the polynomial used to represent the binding energy variation with height. Second, as discussed for the diatomics, the CEM frequencies will generally be too small, especially for H adsorption, because of the behavior of $\Delta E_P(H;n\rightarrow 0)$. Third, the motions of the surface layer and the adsorbate are strongly correlated which requires many calculations of extremely high accuracy to determine frequencies.

The effect of the adsorbates on the surface structure is examined in detail. In this regard, we emphasize that the CEM theory automatically incorporates both direct interactions between the adatoms via overlaps and coulomb integrals and indirect interactions via overlap with common substrate atoms. The correction term includes both direct and indirect interactions and thus cannot be separated in such an easy manner.

As indicated previously, two completely different types of calculations are performed. The first set is for adsorbates on a rigid (R) surface where no relaxation of

the surface is allowed. Calculations that allow the surface to relax in addition to varying the adsorbate binding height are referred to as non-rigid (NR).

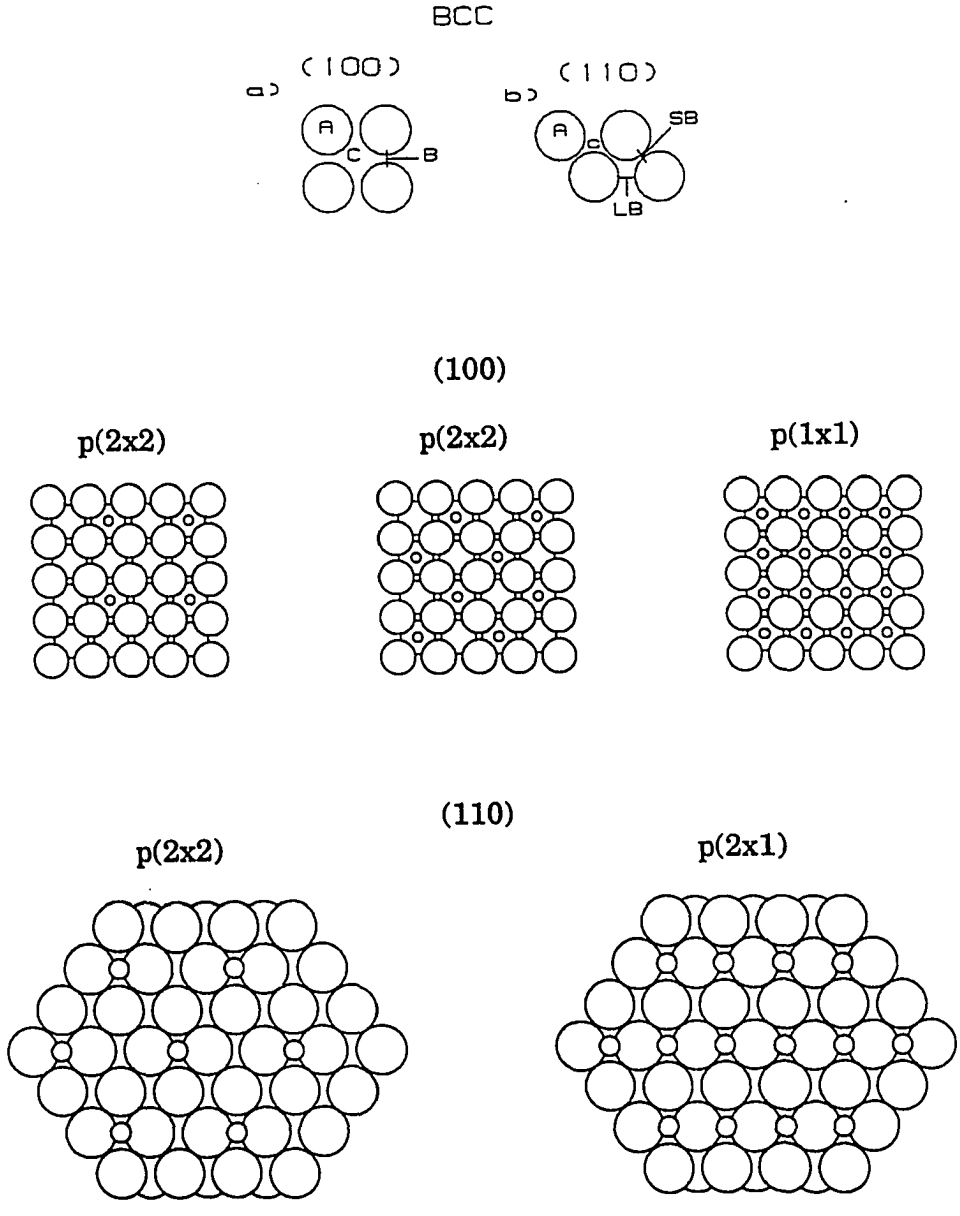

Fig. 4. BCC clean and adsorbate covered surface unit cells (a) (100) (b) (110) (c) p(2x2), c(2x2) and p(1x1) on BCC(100). (d) p(2x2) and p(2x1)

As a final general point of information, we note that, following the investigation on the diatomics, the Puska et al. embedding functions were used for H and N while the covalent embedding functions were used for Fe and W.

3.2.1. H and N on Fe(100)

The chemisorption of H and N on the rigid Fe(100) surface for various coverages θ is studied to help determine the extent of any interactions among the adatoms. The lowest coverage is θ=0.25 monolayer arranged in a p(2x2) structure, then θ=0.5 monolayer in a c(2x2) structure, and finally the highest coverage of θ=1.0 monolayer in a p(1x1) structure. These surface structures can be seen in Figure 4c.

Before studying the adsorbates on Fe(100) we first determine the extent of relaxation for the clean surface as predicted by the CEM method. We find a contraction between the first and second layers of 1.5% relative to the ideal bulk terminated distance. There is no variation in the second to third layer distance. These values agree with previous results by us [34] and experimental measurement [5].

We find that both H and N are most stable when bound in the four-fold center site at all coverages. With the adsorbate in the center site, in Table III we show the results for the minimum energy for rigid and non-rigid surfaces for all three coverages. There are several important general points illustrated by these values.

1) The chemisorption bond is less than half as strong for H than N.

2) The amount of relaxation of the metal surface increases with both the coverage and the binding strength of an adsorbate.

3) The induced relaxation of the metal surface increases slower than linearly with coverage (e.g., 3.5%, 5.5% and 8.5% for 0.25, 0.50 and 1.0 N-layers).

4) The energy variations with coverage are almost certainly too small to be predictable by the CEM method.

5) These binding energies do not contain vibration zero point energy which is also likely to change considerably with coverage. For H, we calculate the difference in energies between the center and bridge site binding to

be 0.16 eV for p(2x2) and c(2x2) structures and 0.20 eV for a full monolayer coverage. For N, the values are 0.50 eV and 0.76 eV. This variation in bridge vs. center binding will modify the in-plane vibrational frequencies and thus the zero-point energy contribution.

6) Dipole-dipole interactions are not included within the CEM method and these will vary substantially with coverage.

Hence, we need to investigate the general characteristics of coverage dependence and not focus on the small energy differences.

Table III Binding energies, heights and surface relaxation relative to the bulk terminated distances for H and N adsorption in four-fold sites on rigid and non-rigid Fe(100)

	H				N				
	BE(eV)	H(Å)	$\%\Delta d_{12}$	$\%\Delta d_{23}$	BE(eV)	H(Å)	$\%\Delta d_{12}$	$\%\Delta d_{23}$	
p(2x2)	2.73	0.77	-1.5	0	5.93	0.40	-1.5	0.0	R
	2.73	0.76	0	0	5.96	0.36	2.0	0.0	NR
c(2x2)	2.72	0.77	-1.5	0	5.92	0.41	-1.5	0.0	R
	2.73	0.73	1.0	0	5.94	0.34	4.0	-1.0	NR
					5.93	0.30	6.5	0.0	NR[a]
Expt					6.10[b]	0.27[c]	7.7[d]		
p(1x1)	2.74	0.78	-1.5	0	5.94	0.41	-1.5	0.0	R
	2.75	0.71	2.0	0	5.96	0.32	7.0	-1.5	NR
Expt[d]	2.87								
Other[e]	2.44	0.65	0	0					

[a] Calculations allowing only the adsorbate and first metal layer to move.

[b] Ref. [8].

[c] Ref. [5].

[d] Ref. [1].

[e] MINDO/SR calculations from ref. [28].

The calculated binding energy for H/Fe(100) is about 0.15 eV smaller than the experimental data. MINDO/SR calculations by Blyholder et al. [28] for H on a 12 atom Fe cluster, 6 atoms in the top layer and 6 atoms in the second layer, suggested that H prefers to bind in the bridge site with a binding energy of 2.60 eV compared to the center site of 2.44 eV. We obtain a bridge site binding energy of 2.57 eV in excellent agreement with their results. Their use of a cluster model limits comparison to our results. Some of the Fe atoms coordinated to H in the center site had a lower coordination than some of the bridge site Fe atoms did, this is especially for the case of the second layer atoms that had no Fe atoms below them. Recent ab-initio investigations [56] also indicate that for such small clusters one must carefully prepare a wavefunction with the proper symmetry for binding to the adsorbate to mimic the infinite surface results.

The calculated binding energy for N/Fe(100) is about 0.18 eV smaller than the experimental data while the binding height is 0.07 Å too large. Calculations using other methods for N on Fe(100) have not been done to our knowledge.

The lack of agreement for the experimental binding energies and heights is most likely due to the lack of a proper treatment of charge transfer from the surface to the adsorbates. Clearly the CEM method is not treating everything correctly but is retaining the most significant aspects involved in the interactions.

It is interesting to contrast the equal stability of the various coverages with the fact that the experimental [6] saturation limit of N on Fe(100) is at a half monolayer. First, once a half monolayer coverage is reached the metal surface is considerably less exposed, and in particular the absence of several contiguous exposed Fe atoms precludes dissociation of N_2 on the surface. The diffusion barrier is over 0.5 eV. Second, as mentioned earlier, repulsive dipole-dipole interactions would increase substantially past a half-monolayer.

Let us examine in detail the nature of the bonding of H and N with the Fe(100) rigid surface in the center site. Figure 5 shows plots of the center site binding potentials and their energy components for c(2x2) H and N using their respective ΔE_p functions. These curves are similar in shape but less rapidly changing than those in Figures 2a and 3a for the diatomics.

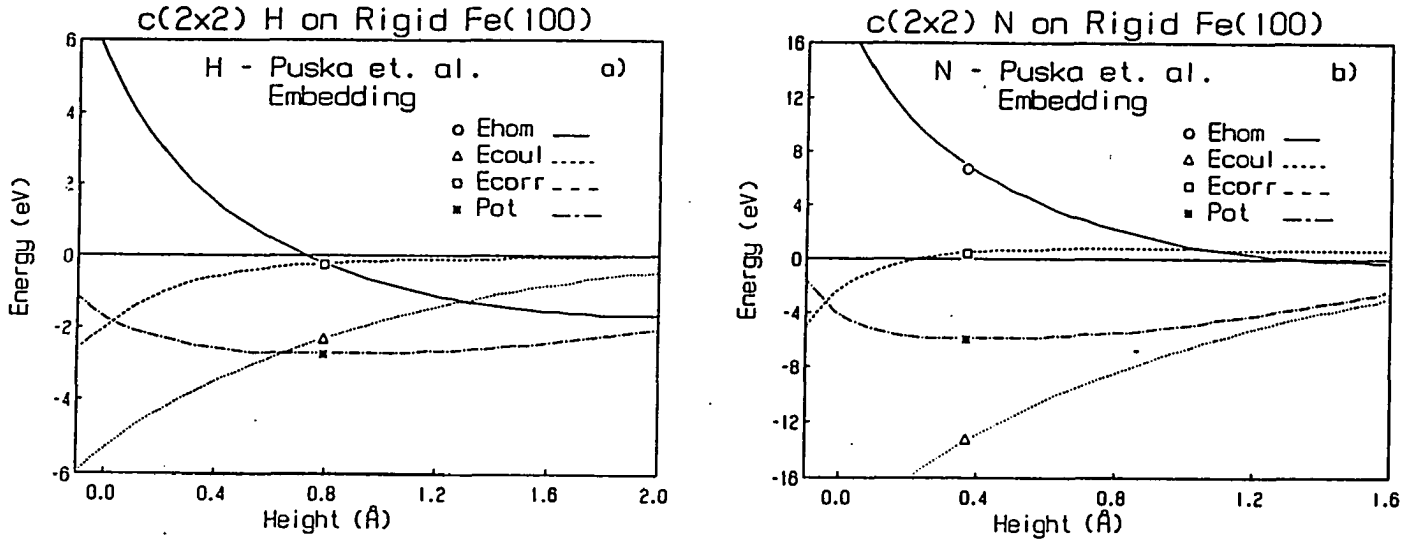

Fig. 5. Calculated CEM energy components and the binding potential for chemisorption on Fe(100) using the ΔE_C function for Fe and the ΔE_P function for H and N are used. Same labeling scheme as Fig. 2. (a) c(2x2) H on Fe(100). (b) c(2x2) N on Fe(100)

The correction energies are generally smaller in magnitude relative to the total potential. This is expected since the electron density distribution for the adsorbate-surface system is more homogeneous than for the diatomic, and ΔG is designed to correct the embedding energy for these inhomogeneities.

Along these lines, we determine the relevance of pair potential models for the adsorbate-surface interaction. From the binding heights, we determine the bond lengths of H and N to the nearest Fe atoms on the surface and in the second layer. Using these bond lengths in the pairwise energies from the diatomic binding potentials, we predict the chemisorption binding energies of H and N on Fe(100). From a H binding height of 0.8 Å, there are two very similar H-Fe bond lengths of 2.17 Å and 2.19 Å yielding a pairwise energy of 1.5 eV. With four top and one second layer atom, this predicts a H adsorption energy of 7.5 eV vs. ≈2.7 eV for the full CEM surface calculation. Clearly the bonding of H on the surface cannot be predicted correctly by using pairwise diatomic potentials. For N-Fe, the bond distances are 2.06 Å to the four nearest top layer Fe atoms and 1.83 Å to the second layer, yielding diatomic energies of 1.3 eV and 3.1 eV, respectively. This predicts a binding energy of 8.3 eV vs. ≈5.9 eV for the full calculation.

From the above results, we see that both H and N binding on Fe(100) is greatly overestimated by pairwise additive models with predictive ability (i.e., one can always fit a pairwise form to the CEM calculations after the latter are performed.) Many body repulsive contributions to the adsorbate binding potential are very important, and are due to the embedding and correction energies. This is why pairwise forms are non-transferable. However, we do find that the N-Fe(100) pairwise form is in better agreement with the CEM results than is the H-Fe(100) form. This can be traced to the fact that $\Delta E_p(H)$ varies non-linearly for densities around both the diatomic and surface minima. By contrast, $\Delta E_p(N)$ varies nearly-linearly for densities around both the diatomic and surface minima; a linear variation means that the embedding energy is proportional to the overlap which is in turn made up of summed pairwise overlaps.

Now we turn to analysis of the results in which the surface is allowed to relax upon adsorption of either H or N. On clean metal surfaces, experiment indicates that large relaxations occur for the more open clean surfaces; these persist perhaps two to

three layers down and exhibit oscillatory behavior (i.e., contraction of the top layer followed by an expansion of the layer below it). The results in Table III provide the first evidence for similar oscillatory behavior with an adsorbate covered surface: as the adsorbate binding height contracts, the top metal layer expands away from the second metal layer.

For p(2x2) H we observe a binding height contraction of 1.2% with a top layer expansion of 1.5% from the original rigid surface calculation. Upon doubling the coverage to the c(2x2) structure, the values are 5% and 2.5%, while for the full monolayer they are 9% and 3.5%. In all calculations, H is never observed to induce any relaxation in the second layer distance.

For N, the binding height contractions and top layer expansions are (10%, 3.5%), (17%, 5.5%) and (22%, 8.5%) for the p(2x2), c(2x2) and monolayer coverages, respectively. At the higher coverages, the N induces a second layer contraction of 1% and 1.5%, respectively. Thus, the N-atom induced changes are much larger than are the H-atom changes, which is in accord with the much larger strength of the N-Fe bonding.

For the c(2x2) N adsorption, the binding height of 0.34 Å is in better agreement (than the 0.41 Å for the rigid substrate) with the experimental value of 0.27 Å by Imbihl et al. [5]. The expanded distance between the first and second metal layers of 4.0% is also in reasonable agreement with the experimental value of 7.7%, both with respect to the ideal bulk terminated layer distance. However, we also find a contraction of the second layer, a possibility which was not taken into account in the analysis of the experimental data. To see the effect of this second layer contraction, we performed calculations in which only the top layer distance was allowed to relax with the second layer distance constrained to its ideal bulk value. In this case, we find a 6.5% expansion in the top layer distance relative to the ideal structure and a binding height of 0.30 Å, in much better agreement with experimental data. These calculations show a strong correlation between contraction of the second layer and the adsorbate binding height and first layer relaxation. As such, we suggest that further experimental analysis should be done to include the possibility of contraction of the second layer.

In Figures 6 and 7, we plot the CEM energy components and their sum for an atom in each layer of the surface. These plots provide insight into the energetics before and after chemisorption of H and N on the Fe(100) surface.

Let us first examine Figure 6 in detail for p(1x1) H on rigid Fe(100). Note that in Figure 6a the embedding energy of the unrelaxed surface atoms rises slightly upon chemisorption of H (due to an increased electron density overlap) while that for H is negative. In Figures 6b and 6c, the coulomb and correction energies for the Fe layers are lowered upon adsorption of H. Now, turn to the results for the relaxed surface. The expansion of the top layer away from the second layer lowers the embedding energies of both the first and second metal layers due to a decrease in the electron density overlaps. This is opposed by the rise in the coulomb energies. In contrast, the correction energies are nearly unchanged. Overall, in Figure 6d the potential (cohesive energy) of each layer atom shows that the second layer is slightly stabilized upon relaxation while the first layer is essentially unchanged. Thus, although there are very small changes in the energies, the relaxation induced by H seems to be driven by the second layer Fe atoms increasing their interaction with H. Note also from Figure 6d that the H binding energy (≈2.7 eV) is dominated by stabilization of the free H atom (≈2.0 eV or 74%) with smaller contributions from both the first (≈0.5 eV) and second (≈0.3 eV) layers of the Fe.

The p(1x1)N/Fe(100) system in Figure 7 shows similar but much more pronounced behavior of the energy components. First note that upon chemisorption of N the embedding energy of each layer atom increases much more than for H chemisorption. This is because N gets much closer to the Fe atoms on the surface and thus the density overlaps are much larger. The coulomb and correction energies are lowered considerably upon chemisorption of N. The changes in these energy components due to the induced relaxation are also very similar to H but much larger in magnitude. The embedding energies are lowered; the coulomb are raised; and, the correction are nearly unchanged. It is now clear in Figure 7d that the second layer is stabilized while the N atoms and the top Fe surface layer are slightly destabilized by the induced outward relaxation.

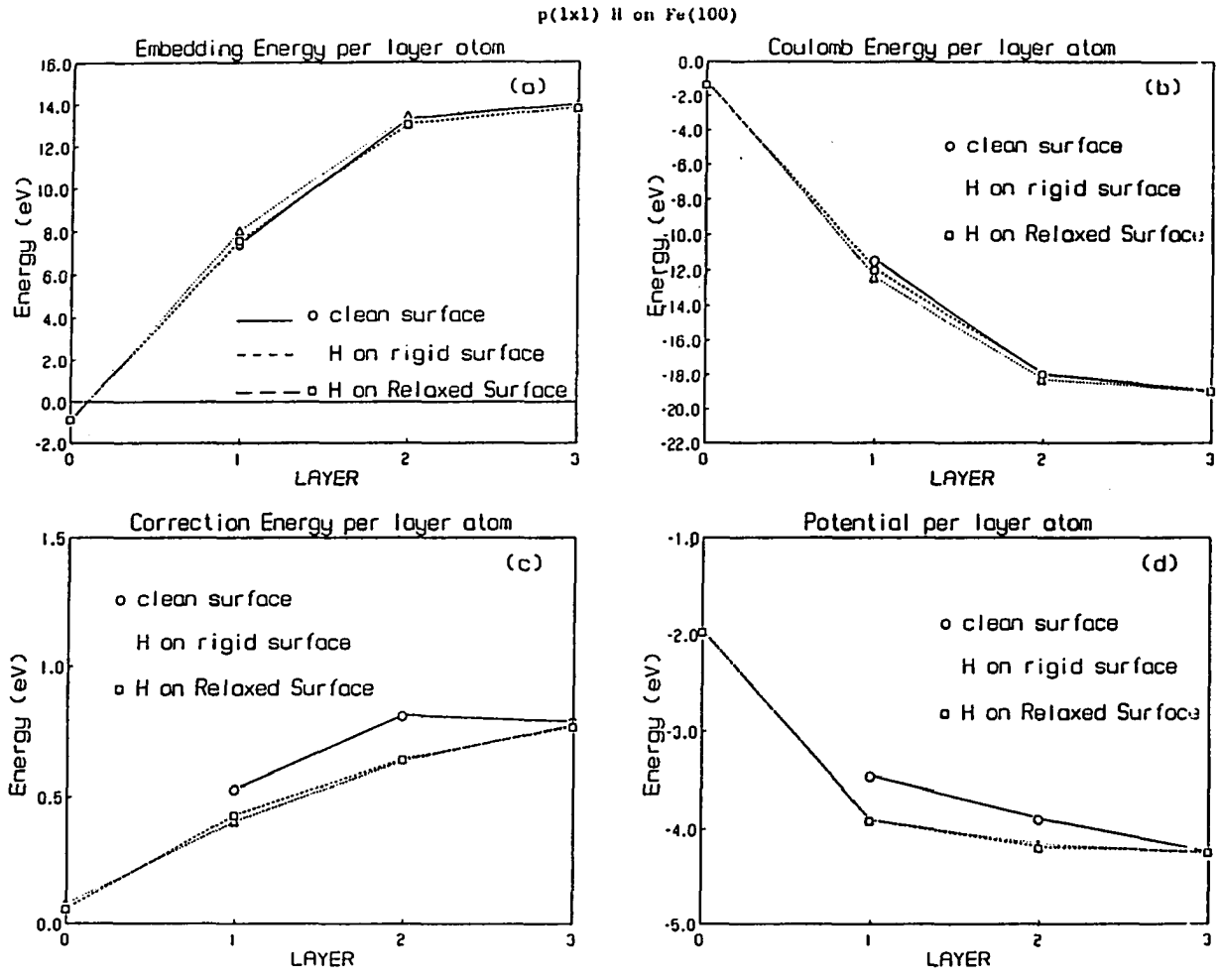

Fig. 6. The energy components for the clean Fe(100) surface (solid line with circles), H on rigid surface (dotted line with triangles) and non-rigid relaxed surface (dashed line with squares). (a) Homogeneous embedding energy. (b) Coulombic energy. (c) Correction energy. (d) Potential energy (sum of components a+b+c)

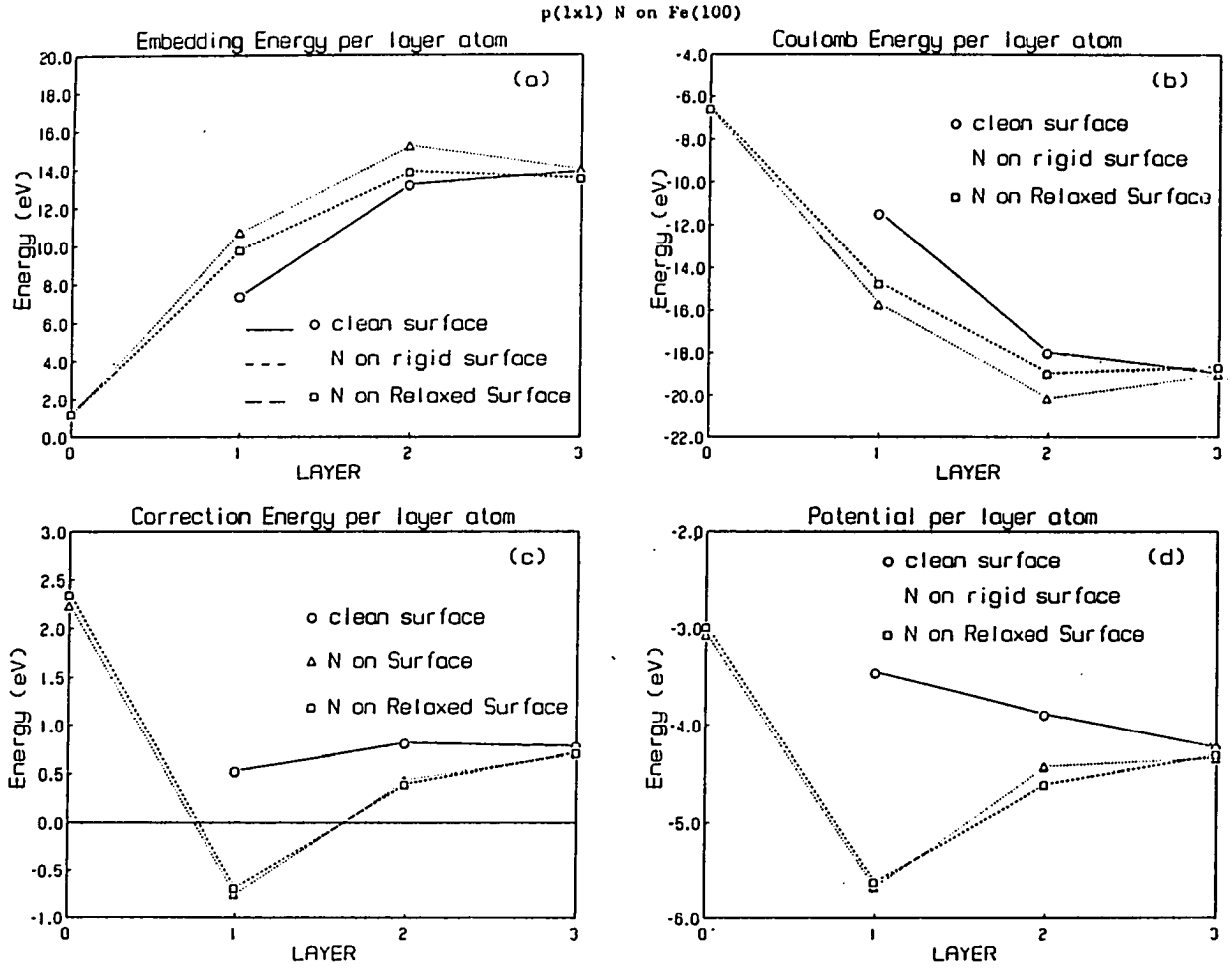

Fig. 7. Same as Fig. 6 except N on Fe(100)

The major difference between the N and H adsorption is illustrated by Figure 7d: a smaller fraction of the N binding energy comes from the stability (≈3 eV or 50%) of the N atom, with larger fractions from both the first (≈2¼ eV) and second (≈3/4 eV) layers of the Fe. It may be surprising that the strong interaction between adsorbates and the second substrate layer actually drives expansion. We have tested this by fixing the adsorbate on the bridge site and repeating the calculations. We find that neither H or N induce relaxation of Fe(100). This suggests that when chemisorption occurs on other surface faces where there is no second layer atom directly below the adsorbate, or if the second layer atom - adsorbate distance is large, no induced relaxation should be observed. We shall test this when we consider chemisorption on Fe(110) and W(110).

3.2.2. H and N on Fe(110)

We now consider the slightly more close packed Fe(110) surface as shown in Figure 4b. Two coverages, p(2x2) and p(2x1) in Figure 4d are examined to determine possible adsorbate interactions and coverage effects on adsorbate induced relaxation.

As for the (100) surface we first determine the extent of relaxation of clean Fe(110). We find that the top layer distance contracts by 1.5% relative to the ideal bulk termination distance. This is in good agreement with the experimentally determined [4] contraction of 1.5% ± 1.5. It is this surface geometry on which rigid surface chemisorption calculations are done. Later full relaxation of the surface is allowed.

We summarize in Table IV the calculated equilibrium binding heights, energies and relaxations for rigid (R) and non-rigid (NR) surfaces. In general, we find that the relative strengths of H and N binding on the (110) surfaces are weaker than seen on the (100) surface. This is due to two features. First, the (110) is slightly more closed than the (100) surface which implies that the cohesive energy of the surface atoms is larger on (110). Second, the lower coordination sites on (110) vs. the ≈5-fold coordination on (100) surface inhibits slightly the binding of H and N compared to the (100) surface. The larger change for N (0.26 eV or ≈4.3%) compared to H (0.1 eV or ≈3.6%) between the two surfaces is in accord with the stronger N binding to

subsurface Fe on the (100) surface, leading to a larger change in coordination for the N.

We find that H binds in both the three-fold center and long-bridge sites with equal strength and does not induce any relaxation of the surface layers. While it may appear that the N prefers the three-fold center site over the long-bridge site, we should reemphasize the point that such small energy differences are likely outside the accuracy of the CEM method. We do find that N induces a small amount of relaxation that is weakly dependent upon coverage.

Table IV Binding energies, heights and relaxation of the first layer distance of H and N on rigid (R) and non-rigid (NR) Fe(110)

	H			N			
	BE(eV)	H(Å)	$\%\Delta d_{12}$	BE(eV)	H(Å)	$\%\Delta d_{12}$	
(2x2) center[a]	2.64	1.48	-1.5	5.68	1.01	-1.5	R
	----[b]	----	----	5.69	1.00	-0.5	NR
(2x1) center[a]	2.65	1.48	-1.5	5.66	1.03	-1.5	R
	----[b]	----	----	5.67	1.02	0.0	NR
Expt.		0.90[c]					
(2x2) l-bridge[a]	2.64	1.49	-1.5	5.66	1.04	-1.5	R
	----[b]	----	----	5.68	1.02	-0.5	NR
(2x1) l-bridge[a]	2.65	1.49	-1.5	5.62	1.06	-1.5	R
	----[b]	----	----	5.64	1.03	0.0	NR
expt.	2.78[d]			6.03[d]			

[a] Site shown in Figure 4b.

[b] Induced relaxation not observed.

[c] Ref. [4].

[d] Ref. [8].

The calculated binding energy for H/Fe(110) is about 0.13 eV smaller than the experimental data [8], similar to the case on the (100) surface. Note though the excellent agreement with the bond weakening between the two surfaces, 2.75-2.65=0.10 eV for CEM vs. 2.87-2.78=0.09 eV for experiment. There has been some discussion in the literature dealing with the preferred H binding site. Recent LEED studies by Moritz et al. [4] indicate that H binds in the three-fold center site 0.90 Å above the surface at a temperature less than 270K. We predict a much higher binding height of 1.48 Å for this site. On the other hand, Barò and Erley [3] used HREELS to determine that H prefers the short-bridge site 1.49 Å above the surface at 130K. We predict a binding energy only 0.05 eV less in this site and a height of 1.62 Å. Finally, Bozso et al. [1] determined that the long-bridge site is most favorable for the H atoms but did not predict a value for the binding height. Obviously there is considerable disagreement on the assignment of the H binding site.

We are aware of only three other theoretical studies of this system. Using an embedded cluster method Muscat [57] determined that the center site is most stable. Later using a multiple scattering Xα theory [58] he determined the short-bridge site to be most stable. Unfortunately quantitative data were not given. Nørskov, using the effective medium EM method [29b,59], reports a H binding energy of around 2.7 eV for the most closed pack surface in the three-fold center site but unfortunately does not indicate the equilibrium binding height.

We find that both the three-fold center and long-bridge sites have the same binding energies and that the short-bridge site has a binding energy only 0.05 eV smaller. Furthermore, we calculate that the H binding potential is flat as far as 0.45 Å from the long-bridge site toward the three-fold center site. Allowing the surface to relax results in no changes in the above binding site preference. Based upon our calculations alone, we would suggest that it is likely that any of these sites can be occupied. The appearance of an ordered overlayer suggests that most likely the types of interactions that we do not include may play an important role in determining an equilibrium site.

The lack of H induced relaxation for either coverage supports our previous discussion on the (100) surface. The H atoms are so far away from the second layer

they do not significantly interact with these Fe atoms. With no strong interaction, inducement of an expansion of the first layer distance spacing cannot occur.

The calculated binding energy for N/Fe(110) is about 0.35 eV smaller than the experimental data, which is about twice the underestimate of 0.18 eV for the (100) surface. Thus, the bond weakening between the two surfaces is predicted to be 5.94-5.68=0.24 eV for CEM which is too large compared to the experimental value of 6.10-6.03=0.07 eV for experiment. The larger underestimation of the binding energy for (110) may indicate a slight adsorbate induced reconstruction. In addition, it indicates that dipole-dipole interactions, directional bonding or magnetic effects may stabilize the N/Fe(110) binding a little more than the N/Fe(100) binding.

As a simple test of the latter, we have repeated the CEM calculations utilizing a maximally spin polarized d-shell occupancy of Fe. (The spin-polarization can be included in the two limits within CEM but cannot be treated self-consistently since the atomic densities must be specified for the CEM method.) Negligible changes in the H binding resulted; for p(2x2)N/Fe(100) and p(2x1)N/Fe(110), the binding energy became 5.96 eV and 5.45 eV, respectively. Thus, the binding energy in Fe(110) is actually decreased, leading to even worse agreement with the experimental change of 0.07 eV. We believe that either directional bonding is more important in the N/Fe(110) system or that a substantial contribution from surface reconstruction may occur.

When relaxation of the metal surface is allowed we observe that N induces a much smaller relaxation of the (110) surface compared to the (100) surface. These small sizes of relaxation are in good agreement with our previous explanation about the driving force for adsorbate induced relaxation. Note that when N is in the long-bridge site the surface relaxes virtually the same as the center site relaxation. This makes sense since in both sites N is almost the same distance from the second layer Fe atoms.

Due to the lower stability and lack of adsorbate induced relaxation of the Fe(110) surface for both H and N adsorption, we do not show figures analogous to Figures 6 and 7. Instead, we just note a few details. First, only the top layer responds significantly to the adsorbate. Second, the H binding energy (≈2.7 eV) is dominated by stabilization of the free H atom (≈2.2 eV or 82%) with smaller contributions from both

the first (≈0.4 eV) and second (≈0.1 eV) layers of the Fe. For the N binding energy (≈5.7 eV), the analogous values are (≈4.2 eV or 74%) with smaller contributions from both the first (≈1.2 eV) and second (≈0.2 eV) layers of the Fe.

It is also interesting to note the stability of the l-bridge site on Fe(110). This is perhaps surprising since the second layer Fe is 2.03 Å below the surface and thus does not participate strongly in the binding. However, the participation is not negligible on the energy scale of importance for site-to-site variation, as demonstrated in the above paragraph.

From the above points, we can see why adsorbate binding on the Fe(110) surface is weaker than on the Fe(100) surface. For Fe(100) both H and N interact strongly with both the first and second layer and to a lesser degree with the third layer. On the other hand for Fe(110), only the first layer interacts strongly while second layer interacts in a weaker fashion. This also causes a much weaker effect on the surface relaxation of the Fe(110) surface.

3.2.3. H and N on W(110)

Finally, we examine the chemisorption of H and N on the W(110) surface. As for the Fe(110) surface, we consider two coverages, p(2x2) and p(2x1).

First we carried out calculations on the clean surface to determine the equilibrium structure before chemisorption. We calculate that the top layer contracts by 3% relative to the ideal bulk termination distance. One experimental observation indicates no relaxation [60] while another, more recent, measurement suggests a contraction of less than 2% [61]. This is the surface structure that rigid surface chemisorption calculations are done on. Later, relaxation of the surface is allowed to determine the extent of adsorbate induced relaxation on the W(110) surface.

We summarize in Table V the calculated equilibrium binding heights, energies and relaxations for rigid (R) and non-rigid (NR) surfaces. In general, we find that the relative strengths of H and N binding on the W(110) surfaces are stronger than on the Fe(110) surface by 0.22 eV and 0.75 eV, respectively. These differences are in excellent agreement with the experimental values of 0.28 eV and 0.69 eV, showing

that the CEM method is capable of a systematic description of binding to different metals. We also find that H does not induce relaxation while N does induce a weak coverage dependent relaxation of W(110). There is also a slight coverage effect on the N adsorbate binding energies which is absent for H. Chemisorption of H does not induce any relaxation of the surface but it is possible that H can induce small reconstructions that may change the barrier height.

Table V Binding energies, heights and relaxation of the first layer distance of H and N on rigid (R) and non-rigid (NR) W(110)

	H			N			
	BE(eV)	H(Å)	$\%\Delta d_{12}$	BE(eV)	H(Å)	$\%\Delta d_{12}$	
(2x2) center[a]	2.86	1.38	-3.0	6.44	0.98	-3.0	R
	----[b]	----	----	6.44	0.97	-2.5	NR
(2x1)	2.86	1.37	-3.0	6.41	0.99	-3.0	R
	----	----	----	6.42	0.97	-1.5	NR
(2x2) l-bridge	2.87	1.36	-3.0	6.40	1.03	-3.0	R
	----	----	----	6.41	1.02	-2.5	NR
(2x1)	2.87	1.35	-3.0	6.37	1.04	-3.0	R
	----	----	----	6.38	1.03	-1.5	NR
experiment	3.06[c]			6.72[d]			

[a] Site shown in Figure 4b.

[b] Induced relaxation not observed.

[c] Ref. [62].

[d] Ref. [63].

Reconstruction of the (110) surface is not studied in this paper but it is well documented [64] that H induces reconstruction on the W(100) surface.

The calculated binding energy of 2.87 eV for H on W(110) surface is a slight underestimation of the experimental [62] value of 3.06 eV, just as for the Fe surfaces. Binding to the three-fold center site is favored over the long-bridge site by only 0.01

eV, with the equilibrium three-fold center site in the unit cell located about 0.5 Å from the long-bridge. Experiments [65] indicate a long-bridge site binding but the short-bridge site has also been postulated in the past (see references in [65]). We find that binding to the short-bridge site is only 0.05 eV less stable, which makes it very difficult to assign any permanent binding site for H on W(110).

This small barrier appears in disagreement with an experimental [66] diffusion barrier of 0.20 eV that is weakly coverage dependent (increases with coverage). However, a quantum simulation of the diffusion is necessary to see whether this is the case. To help in such an undertaking, we present the binding curves for three different sites in Figure 8 and provide the energy values in Table VI. We also include data for H on Fe(110). At odds with a large diffusion barrier being intrinsic to the binding site energy variation is the fact that it has been difficult in general to observe experimentally ordered structures of H. Observations may be possible [67,68] at high coverages of around a full monolayer, indicating that adsorbate interactions may play a role in determining the equilibrium binding site for H atoms. We do not see any significant evidence of adatom interactions for coverages at or below a half monolayer but that does not mean they are not present at higher coverages. We did not do any calculations at a full monolayer for the (110) surfaces. Furthermore, as discussed in the adsorption on Fe(100), CEM does not treat dipole-dipole interactions and thus may not be accurate at high coverages. A dynamical simulation of the diffusion would utilize the potential in Table VI but should add on additional dipole interaction terms; the strength of the dipole could be estimated from the coverage dependence of the work function.

The calculated binding energy of 6.44 eV for N/W(110) is about 0.28 eV smaller than the experimental data [63]. This underestimate is in accord with all the other systems studied in this paper. As the coverage increases, the binding energy is lowered by 0.03 eV to 6.41 eV. This difference is still too small to be interpreted as evidence for a repulsive adsorbate interaction at half monolayer coverage. Calculations using other methods for N on Fe(110) have not been done to our knowledge.

Table VI CEM method calculated potential energy curves for H on rigid Fe(110) and W(110)

	W(110) sites			Fe(110) sites		
z(a.u.)	Atop	s-bridge	l-bridge	Atop	s-bridge	l-bridge
0.00	---[a]	5.11	0.10	---	1.38	-1.00
0.25	---	4.89	-0.08	---	1.18	-1.07
0.50	---	4.04	-0.37	---	0.78	-1.21
0.75	---	3.16	-0.76	---	0.24	-1.42
1.00	---	1.93	-1.18	---	-0.34	-1.63
1.25	---	0.74	-1.61	---	-0.90	-1.84
1.50	---	-0.38	-2.00	9.31	-1.38	-2.05
1.75	---	-1.24	-2.33	4.53	-1.76	-2.30
2.00	10.30	-1.88	-2.61	1.40	-2.07	-2.48
2.25	4.34	-2.35	-2.80	-0.43	-2.37	-2.58
2.50	0.88	-2.67	-2.86	-1.42	-2.51	-2.63
2.75	-1.10	-2.81	-2.85	-2.03	-2.57	-2.64
3.00	-2.10	-2.81	-2.81	-2.34	-2.59	-2.63
3.25	-2.60	-2.77	-2.76	-2.46	-2.57	-2.57
3.50	-2.71	-2.72	-2.68	-2.49	-2.50	-2.48
3.75	-2.68	-2.63	-2.58	-2.44	-2.41	-2.38
4.00	-2.63	-2.51	-2.46	-2.35	-2.27	-2.24
4.25	-2.51	-2.38	-2.32	-2.20	-2.13	-2.10
4.50	-2.38	-2.22	-2.17	-2.05	-1.98	-1.95
4.75	-2.20	-2.07	-2.02	-1.89	-1.83	-1.80
5.00	-2.03	-1.92	-1.87	-1.67	-1.56	-1.51
5.25	-1.85	-1.76	-1.72	-1.38	-1.32	-1.29
5.50	-1.67	-1.57	-1.53	-1.18	-1.15	-1.14
5.75	-1.46	-1.38	-1.35	-1.05	-1.04	-1.03
6.00	-1.27	-1.23	-1.21	-0.97	-0.96	-0.96

[a] Value not calculated.

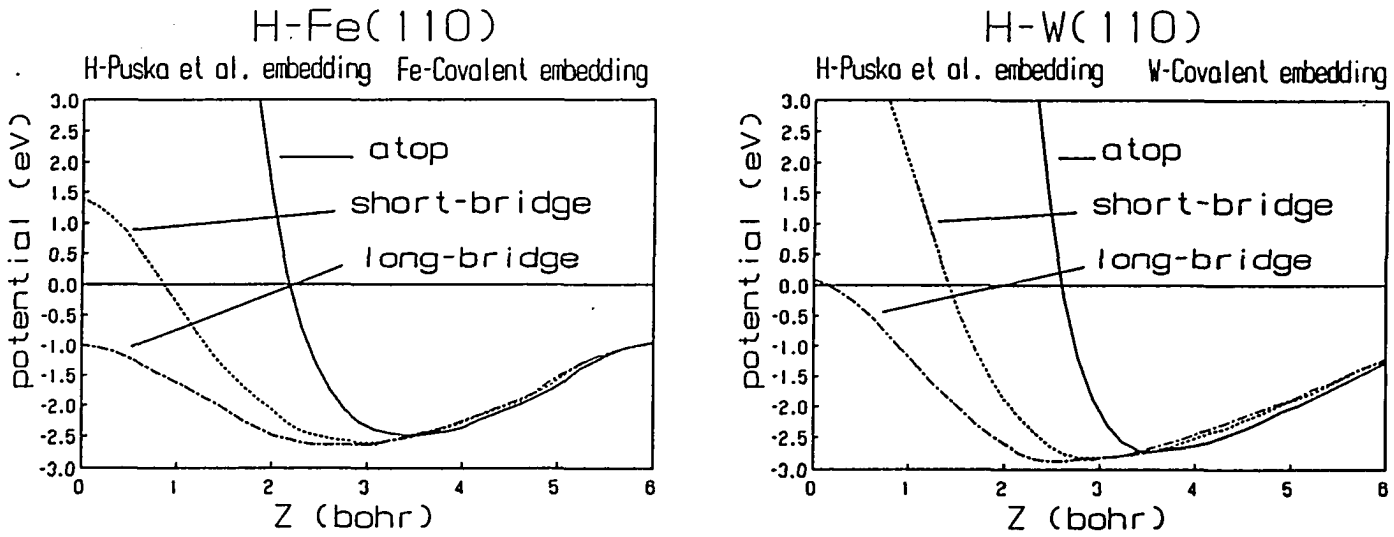

Fig. 8. **Calculated CEM binding potentials for H on Fe(110) and W(110) in the atop, short and long bridge sites using the $\Delta E_P(H)$ embedding energy function and the ΔE_C embedding energy functions for Fe and W**

We observe that N induces only a small relaxation of the W(110) surface, in accord with our previous explanation about the driving force for adsorbate induced relaxation. Note that when N is in the long-bridge site the surface relaxes virtually the same as the center site relaxation. This makes sense since in both sites N is almost the same distance from the second layer W atoms. The binding height is also very weakly dependent upon coverage and about the same for the two sites.

Due to the lack of adsorbate induced relaxation of the W(110) surface for both H and N adsorption, we do not show figures analogous to Figures 6 and 7. Instead, we just note a few details as in the Fe(110) case. First, only the top layer responds significantly to the adsorbate. Second, the H binding energy (≈2.9 eV) is dominated by stabilization of the free H atom (≈2.0 eV or 69%) with the remaining contribution from the first (≈0.9 eV) layer of the W. Third, for the N binding energy (≈6.4 eV), the analogous values are (≈4.3 eV or 67%) with smaller contributions from both the first (≈1.9 eV) and second (≈0.2 eV) layers of the Fe.

The slightly stronger H bonding to the W(110) surface compared to the Fe(110) surface comes from the top layer W atom stabilization of 0.9 eV being significantly larger than the 0.4 eV of the Fe; the H-atom stabilization is actually smaller by 0.2 eV on the W(110) surface. A similar explanation occurs for N in which the W is much more stable by 0.7 eV while the N is slightly more stable by 0.1 eV, as compared to the Fe(110) case. This interesting feature can be traced to a combination of two CEM energy components. The first is the higher electron density overlap with the W atoms compared to the Fe atoms. A higher electron density from W raises the overlap density and results in a higher H and N embedding energy. The second is the increased coulomb interaction of the adsorbates with W atoms. The combination of the two results in a slightly weaker H and only a slightly increased N stabilization energy. However, the coulomb interaction dominates for the surface stabilization and this then dominates the change. Physically, this makes sense since it indicates that adsorption on different metals varies mainly due to properties of the metals and only slightly due to properties of the adsorbates.

4. SUMMARY AND CONCLUSIONS

We have presented an extension and application of the CEM method to the chemisorption of overlayers. In the CEM method, the only flexibility arises from the choice of embedding function. Covalent embedding functions were used for all metals, as determined from the diatomic potential curve and the variation of bulk cohesive energy with NND. The SCF-LD embedding functions of Puska et al. [38] were used for the adsorbates. Thus the embedding functions used in all calculations were not adjusted to reproduce any experimental data used for comparisons in this paper. We calculated the relaxation of metal surfaces and then determined chemisorption energies and binding heights on these surfaces. We also carried out calculations in which both the surface relaxation and the adsorbate height were varied to determine the true potential energy minimum.

Results for chemisorption energies and binding sites were in general agreement with experimental data. However, the calculated binding heights and vibrational frequencies were not always in agreement. The vibrations frequencies were never very good and it is likely that without improvements the CEM method will never be able obtain correct frequencies. These drawbacks should not detract us from the added understanding the method can give us in chemisorption system. These calculations showed that the method can be successfully applied to both clean and adsorbate covered surfaces. In addition to providing a test of the CEM method, we determined a number of points about adsorbate induced relaxation. First, N induced a larger amount of outward relaxation of the Fe and W surfaces than did H. Second, Fe(100) was observed to relax the most and revealed a strong coverage dependence on the relaxation. Third, through detailed analysis of the CEM energy components and binding energy potential for each layer atom in the unit cell we have developed a simple rule for adsorbate induced relaxation:

> The interaction between the adsorbates and the second layer metal atoms drives the relaxation. In particular, the adsorbates' binding height tends to decrease in order to increase the adsorbates' interaction with the second layer. In response, the second layer forces the top layer to move away, leading to an expansion of the distance between the top and second layers.

This is very similar to our previous [34] explanation for the multi-layer relaxation of clean surfaces.

This led to the prediction that induced relaxation would not occur when either there were no second layer atoms directly below the adsorbate or the adsorbate binding height was large. Calculations on the Fe(110) and W(110) surfaces confirmed the above prediction. Analysis of the calculations also showed that the lack of a strong interaction (due to larger distances) of H or N with the second layer atoms resulted in weaker binding of the adsorbate.

We believe these calculations are the first to predict the significant effects adsorbates have on the structure of metal surfaces. Important effects are due not only to the type of adsorbate atom but also to the local geometry of the adsorbate and surface.

The CEM method has now been tested for both clean and adsorbate covered surfaces leading to the conclusion that both structures and energies can be predicted with good accuracy. This offers the opportunity for the study of a number of important types of systems. Current work is directed towards calculations on the chemisorption of metals on metals, in order to predict and describe the processes involved in growth of thin metal films.

5. ACKNOWLEDGEMENT

This work was supported by NSF grants CHE-8609832 and CHE8921099.

6. REFERENCES

[1] F. Bozso, G.Ertl, M. Grunze and M. Weiss, Appl. Surf. Sci. 1 (1977) 103.

[2] J. Benziger and R. J. Madix, Surf. Sci. 94 (1980) 119.

[3] A. M. Baró and W. Erley, Surf. Sci. 112 (1981) L759.

[4] W. Moritz, R. Imbihl, R. J. Behm, G. Ertl and T. Matsushima, J. Chem. Phys. 83 (1985) 1959.

[5] R. Imbihl, R. J. Behm and G. Ertl, Surf. Sci. 123 (1982) 129.

[6] F. Bozso, G. Ertl, M. Grunze and M. Weiss, J. Catalysis 49 (1977) 18.

[7] G. Wedler, G Steidl and D Borgmann, Surf. Sci. 100 (1980) 507.

[8] F. Bozso, G. Ertl and M. Weiss, J. Catalysis 50 (1977) 519.

[9] M. Grunze, M. Golze, W. Hirschwald, H. -J. Freund, H. Pulm, M. C. Tsai, G. Ertl and J. Küppers, Phys. Rev. Lett. 53 (1984) 850.

[10] P. H. Emmett, "The Physical Basis for Heterogeneous Catalysis' E. Drauglis and R. I. Jaffee, Eds. (Plenum Press, New York, 1975), p. 3 and references therein.

[11] P. Siegbahn, M. Blomberg, I. Panas and U. Wahlgren, Theor. Chim. Acta 75 (1988) 143.

[12] I. Panas, P. Siegbahn and U. Wahlgren, J. Chem. Phys. 90 (1989) 6791.

[13] J.E. Müller, Phys. Rev. Lett. 59 (1987) 2943.

[14] H. Yang and J. L. Whitten, "Reaction of CH_4 with Ni(111)", preprint.

[15] S. R. Chubb and W. E. Pickett, Phys. Rev. Lett. 58 (1987) 1248.

[16] R. Biswas and D. R. Hamann, Phys. Rev. Lett. 56 (1986) 2291.

[17] M. Weinert and J. W. Davenport, Phys. Rev. Lett. 54 (1985) 1547.

[18] C. Umrigar and J. W. Wilkins, Phys. Rev. Lett. 54 (1985) 1551.

[19] P. J. Feibelman and D. R. Hamann, Surf. Sci. 149 (1985) 48.

[20] G. W. Fernando and J. W. Wilkins, Phys. Rev. B35 (1987) 2995.

[21] P. J. Feibelman, Phys. Rev. Lett. 54 (1985) 2627.

[22] I. Panas, P. Siegbahn and U. Wahlgren, Chem. Phys. 112 (1987) 325.

[23] T.H. Upton and W. A. Goddard, III, "Chemistry and Physics of Solid Surfaces", eds. R. Vanselow and W. England (CRC Press, Cleveland, Ohio, 1985), Vol. III.

[24] C. W. Bauschlicher, J. Chem. Phys. 84 (1986) 250; Chem. Phys. Lett. 129 (1986) 586.

[25] N. A. Baykara, J. Andzelm, D. R. Salahub and S. Z. Baykara, Int. J. Quantum Chem. 29 (1986) 1025.

[26] T. H. Upton, P. Stevens and R. J. Madix, J. Chem. Phys. 88 (1988) 3988.

[27] A. Selmani, J. Andzelm and D. R. Salahub, Int. J. Quantum Chem. 29 (1986) 829.

[28] G. Blyholder, J. Head and F. Ruette, Surf. Sci. 131 (1983) 403.

[29] a) J. K. Nørskov and N. D. Lang, Phys. Rev. B21 (1980) 2136.
b) J. K. Nørskov, Phys. Rev. B26 (1982) 285.

[30] K. N. Jacobson, J. K. Nørskov and M. J. Puska, Phys. Rev. B35 (1987) 7423 and references therein.

[31] J. D. Kress and A. E. DePristo, J. Chem. Phys. 87 (1987) 4700.

[32] J. D. Kress and A. E. DePristo, J. Chem. Phys. 88 (1988) 2596.

[33] J. D. Kress, M. S. Stave and A. E. DePristo, J. Phys. Chem. 93 (1989) 1556.

[34] T. J. Raeker and A. E. DePristo, Phys. Rev. B39 (1989) 9967.

[35] M. J. Stott and E. Zaremba, Phys. Rev. B22 (1980) 1564.

[36] A. E. DePristo and J. D. Kress, Phys. Rev. A35 (1987) 438.

[37] O. Gunnarsson and B. I. Lundqvist, Phys. Rev. B13 (1976) 4274.

[38] a) M. J. Puska, R. M. Nieminen and M. Manninen, Phys. Rev. B24 (1981) 3037;
b) M. J. Puska (Provided unpublished embedding energy functions).

[39] J. N. Murrell, S. Carter, S. C. Farantos, P. Huxley and A. J. C. Varandas, "Molecular Potential Energy Functions" (John Wiley, New York, 1984).

[40] K. P. Huber and G. Herzberg, "Constants of Diatomic molecules" (Van Nostrand, New York, 1979).

[41] M. D. Morse, Chem. Rev. 86 (1986) 1049.

[42] a) J. R. Smith, J. H. Rose, J. Ferrante, and F. Guinea, in "Many-body Phenomena at Surfaces", edited by D. Langreth and H. Suhl (Academic Press, New York, 1984);
b) J. H. Rose, J. Ferrante and J. R. Smith, Phys. Rev. Lett. 47 (1981) 675.

[43] C. Kittel, "Introduction to Solid State Physics" (John Wiley, New York, 1986).

[44] D. R. Salahub, in "Transition-metal Atoms and Dimers", *Ab Initio* Methods in Quantum Chemistry, ed. by K. P. Lawley, (Wiley & Sons Ltd, London, 1987), Vol. II and references therein.

[45] V.L. Moruzzi, J.F. Janak, and A.R. Williams, "Calculated Properties of Metals", (Pergamon, 1978).

[46] a) M.S. Daw and M.I. Baskes, Phys.Rev. B29 (1984) 6443;
b) S.M. Foiles, M.I. Baskes and M. S. Daw, Phys. Rev. B33 (1986) 7983;
c) M.S. Daw, Phys. Rev. B39 (1989) 7441.

[47] a) E. Clementi, IBM J. Res. Develop. Suppl. 9 (1965);
b) P. S. Bagus, T. L. Gilbert and C. J. Roothan, J. Chem. Phys. 56 (1972) 5159.

[48] M. Schmidt and K. Ruedenberg, J. Chem. Phys. 71 (1979) 3951.

[49] S. Huzinaga, Prog. Theor. Physics Suppl. 40 (1967) 279.

[50] D. P. Chong, S. R. Langhoff, C. W. Bauschlicher, S. P. Walch and H. Partridge, J. Chem. Phys. 85 (1986) 2850.

[51] S. P. Walch and C. W. Bauschlicher, J. Chem. Phys. 78 (1983) 4597.

[52] A. E. Stevens, C. S. Feigerle and W. C. Lineberger, J. Chem. Phys. 78 (1983) 5420.

[53] P. Pyykko, J. G. Snijders and E. J. Baerends, Chem. Phys. Lett. 83 (1981) 432.

[54] P. E. M. Siegbahn and M. R. A. Blomberg, Chem. Phys. 87 (1984) 189.

[55] R. A. Wheeler, R. Hoffman and J. Strähle, J. Am. Chem. Soc. 108 (1986) 5381.

[56] I. Panas, J. Schule, P. Siegbahn, and U. Wahlgren, (1988) Chem. Phys. Lett. 149 (1988) 265.

[57] J. -P. Muscat, Surf. Sci. 118 (1982) 321.

[58] J. -P. Muscat, Surf. Sci. 139 (1984) 491.

[59] J. K. Nørskov, Physica B127 (1984) 193.

[60] B. W. Lee, A. Ingnatiev, S. Y. Tony and M. A. Van Hove, J. Vac. Sci. Technol. 14 (1977) 291.

[61] R. J. Smith, C. Hennessy, M. W. Kim, C. N. Whang, M. Worthington and Xu Mingde, Phys. Rev. Lett. 58 (1987) 702.

[62] P. W. Tamm and L. D. Schmidt, J. Chem. Phys. 54 (1971) 4775.

[63] P. W. Tamm and L. D. Schmidt, Surf. Sci. 26 (1971) 286.

[64] a) D. A. King and G. Thomas, Surf. Sci. 92 (1980) 201;
b) R. A. Barker and P. J. Estrup, J. Chem. Phys. 74 (1981) 1442;
c) J.J Arrecis, Y. J. Chabal and S. B. Christman, Phys. Rev. B33 (1986) 7906 and references therein.

[65] a) G. B. Blanchet, P. J. Estrup and P. J. Stiles, Phys. Rev. Lett. 44 (1980) 171;
b) G. B. Blanchet, N. J. DiNardo and E. W. Plummer, Surf. Sci. 118 (1982) 496.

[66] R. DiFoggio and R. Gomer, Phys. Rev. B25 (1982) 3490.

[67] J. M. Baribeau and J. D. Carette, Can. J. Phys. 60 (1982) 1008.

[68] K. J. Matysik, Surf. Sci. 29 (1972) 324.

PAPER III
MOLECULAR DYNAMICS SIMULATION OF METAL ADSORBATES ON METAL SURFACES RH ON AG(100)

Molecular Dynamics Simulations of Metal Adsorbates on Metal Surfaces: Rh on Ag(100).

Todd J. Raeker
David E. Sanders[1]
and
Andrew E. DePristo
Department of Chemistry
Iowa State University
Ames , Iowa 50010

[1] IBM Predoctoral Fellow

ABSTRACT

The mechanisms of thin metal film growth on metal surfaces are topics of considerable scientific and technological interest. We have studied the way in which a deposited metal adlayer behaves as a function of metal substrate temperature. Molecular dynamics simulations are used where the interaction energy and the corresponding forces are generated from the recently developed Corrected Effective Medium CEM method. In previous work the CEM method has been shown to predict the geometric and energetic properties of clean and adsorbate covered surfaces accurately.

In this paper we present results for the Rh on Ag(100) surface system. We show that Rh atoms penetrate the Ag(100) surface by exchanging with Ag atoms in the surface layer structure. Furthermore this phenomenon is found to depend on both the initial coverage of Rh atoms and the Ag substrate temperature. As the substrate temperature increases the number of Rh atoms exchanging with Ag atoms in the surface increases. Energetic and dynamical aspects of this system are used to understand the reasons why and also the way in which exchange takes place.

1. INTRODUCTION

The study of epitaxial growth of metals on metals has been the focus of considerable attention recently. The development of new technologies to deposit adatoms at a rate enabling monolayer deposition has catalyzed this fascinating field. The development of theoretical models to understand the static and dynamical properties of these systems has lagged behind experiment. Most theories have focused on the macroscopic kinetics and thermodynamics of epitaxial systems. An atomistic theory of epitaxial growth would play an important role in understanding the many new and interesting properties that occur when metals are deposited on other metals. Until very recently very few theoretical considerations of this type have been done.

While several recent attempts to model epitaxial growth of two and three dimensional Lennard-Jones systems have been reported [1], such pairwise additive potentials are inadequate for metals [2]. The simple empirical generalization to two and three-body interactions has been invoked to overcome this problem [3]. More promising and general methods have also been developed over the past decade to describe delocalized metallic bonding: the effective medium theory [4]; the embedded atom method [5]; the "glue" model [6] and the related approach of Finnis and Sinclair [7a] and Finnis *et al.* [7b]; and the corrected effective medium, CEM, method [8-10]. The reader is referred to a recent review of these new methods for a detailed presentation and discussion of general philosophy, methodology, theoretical similarities and differences [11]. The embedded atom method has already been applied to various problems in epitaxy [12].

In this paper, we utilize the CEM method in the simplest and computationally most efficient MD/MC-CEM form [13]. The CEM method provides accurate surface energies and relaxation of clean metal surfaces [9]. Extension to adsorbates and their effect on the structure of the surface was also examined with success [10]. The excellent agreement with experimental data provided motivation to apply the method to epitaxial systems.

We focus in this paper on initial results for Rh deposited on Ag(100) which has recently been observed [14] to exhibit an interesting and unexpected feature. After

deposition of Rh on Ag(100) at 300 K and subsequent annealing to 600 K, the Ag migrates through Rh to form an Ag film over the Rh film. The equilibrium structure is proposed to be that of an Ag-Rh-Ag(100) 'sandwich' that is suggested to be driven thermodynamically by the lower surface free energy of Ag(100) compared to the Rh(100) surface. We have carried out static and MD calculations on this system and have confirmed this sandwich structure to be more stable than Rh on top of Ag(100). Furthermore, we have discovered why a 'sandwich' and not a solid mixture occurs and have determined how such 'sandwich' formations could be inhibited by experimental modifications.

2. THEORETICAL MODEL

We employ the CEM method (in the MD/MC-CEM form [13] described below) to calculate the interaction energy and forces of a N-atom system in any geometrical configuration, $\{R_i\}$. Here we present the basic CEM energy relation, referring readers to previous work for details [8-11,13].

In CEM the interaction energy of N atoms is written as

$$\Delta E = \sum_{i=1}^{N} \Delta E_j(A_i;n_i) + \Delta G + \Delta V_c \tag{1}$$

$\Delta E_j(A_i;n_i)$ is the energy of embedding atom A_i into a homogeneous electron gas of electron density n_i, i.e., jellium. ΔG is an explicit correction for the kinetic-exchange-correlation energy difference between the inhomogeneous electron gas in the real N-atom system and the many effective atom-jellium systems. ΔV_c is the total interatomic coulomb energy.

Using the superposition of atomic electron densities approximation,

$$n(\vec{r}) = \sum n(A_i;\vec{r}-\vec{R}_i) \tag{2}$$

in Eq. (1) leads to

$$\Delta V_c = \frac{1}{2}\sum_i \sum_{j\neq i} V_c(i,j) \tag{3}$$

where $V_c(i,j)$ is the sum of electron-electron, electron-nuclear and nuclear-nuclear coulomb interactions between atoms A_i and A_j. Minimizing ΔG with respect to the $\{n_i\}$ yields, for unpolarized atomic electron densities,

$$n_i = \frac{\sum_{j\neq i} \int n(A_i;\vec{r}-\vec{R}_i)\, n(A_j;\vec{r}-\vec{R}_j)\, d\vec{r}}{2Z_i} \tag{4}$$

where Z_i is the atomic number.

We have constructed an even-tempered Gaussian basis [15] to represent the atomic densities that are generated from Slater-type atomic Hartree-Fock densities [16]. Use of Gaussians allows for efficient, analytic evaluation [17] of the $V_c(i,j)$ and the density overlaps in Eq. (4). The density due to p-orbitals had to be fit separately from the remaining density. For $Z_i>10$, the number of Gaussian functions was greater than 25 for both the spherical and p-densities.

Both the embedding and coulomb energies are thus very easy to evaluate, but the ΔG term involves a full three-dimensional numerical integration over the entire structure of the system of atoms and is thus very time consuming to evaluate. This evaluation is perfectly feasible using Becke's 'fuzzy cell' integration technique [18] for systems of up to about 1000 atoms for a small number of energy calculations. However, when one wants to do MD calculations with forces that are fast enough to evaluate many thousands of times the computational time involved in ΔG is too large for large systems.

There is a simple way to get around this difficulty. We have shown [12] that the ΔG term can be approximated as a function of n_i and thus Eq. (1) can be rewritten, using Eq. (3),as

$$\Delta E = \sum_{i=1}^{N} \Delta F_J(A_i;n_i) + \frac{1}{2}\sum_i \sum_{j\neq i} V_c(i,j) \tag{5}$$

where the ΔF_J are new 'effective' embedding energy functions. These are determined from experimental data on two different types of homonuclear systems, the diatomic and the bulk, which have very different magnitudes of n_i. The value of n_i for atoms in different size systems (i.e., clusters, surfaces) lies between these two limits and thus ΔF_J can be determined by simple interpolation. (This is exactly the same procedure as developed initially for determining the covalent embedding functions of the full CEM theory [8b].)

We call this new form of CEM the MD/MC-CEM method. Two advantages of the MD/MC-CEM method are that many-body interactions are an integral part of the method and high accuracy is obtained as revealed in Table I below for the face

dependent surface energies of several fcc transition metals.

Table I MD/MC-CEM calculated surface energies in j/m^2 for relaxed (111), (100) and (110) surfaces of various transition metals

	(111)	(100)	(110)	Expt.[a]
Ni	2.363	2.474	2.696	2.380
Cu	1.632	1.723	1.878	1.790
Rh	2.753	2.913	3.142	2.660
Pd	1.906	2.023	2.193	2.000
Ag	1.072	1.144	1.246	1.240
Pt	2.252	2.428	2.615	2.490
Au	1.423	1.543	1.664	1.500

[a] Average of a polycrystalline surface [21].

Another is that there are no adjustable parameters or empirical constructs once the embedding energies are determined solely from diatomic and bulk data on the respective homonuclear systems. Any further calculation on a mixed system is predictive, as is any other calculation on a homogeneous system. The coulombic energies are non-empirical. The reader may contrast this situation with the EAM and related methods, or may consult ref. [11] for a detailed discussion. We do want to mention that the atomic electron density configuration in the heterogeneous and homogeneous systems is assumed identical. While small changes will lead to negligible effects since the theory is correct through second order in any density variation, large changes due to a significant electron transfer will have effects [8]. We expect these to be negligible for mixing metals on the right hand side of the periodic table. There are other embedding functions which describe ionic bonding but at typical metallic densities, these functions do not differ from the covalent embedding functions. It is beyond the scope of this paper to discuss the situation further.

We summarize the steps involved in the MD/MC-CEM calculation, assuming

availability of the even-tempered Gaussian basis for the atomic densities:

1) compute density overlaps and evaluate $\{n_i\}$ in Eq. (4);

2) evaluate the embedding energies for jellium densities $\{n_i\}$ and compute coulomb energies;

3) compute derivatives of steps 2 and 3 and evaluate forces.

When the electron density around each atom is spherical and unpolarized, we have developed numerical smoothing plus polynomial evaluation techniques [19] such that steps 1-3 can be accomplished at a speed which is about half that for pairwise additive Lennard-Jones interactions.

3. RESULTS

We first present results of static calculations for clean Ag(100) and Rh(100) to test the MD/MC-CEM method. We find that Ag(100) does not relax and that the top layer distance for Rh(100) contracts by only 0.5%. The Rh contraction is in agreement with an observed 0% relaxation [20]. We are unaware of experimental studies of the Ag(100) surface. The surface energies for relaxed Ag(100) and Rh(100) are calculated to be 1.14 j/m^2 and 2.91 j/m^2 respectively. Good agreement is found with the experimental [21] results of 1.24 j/m^2 and 2.66 j/m^2 for polycrystalline surfaces for Ag and Rh.

We showed in a previous paper [9] that the cohesive energy for an atom in any layer can be calculated using CEM theory. The results presented in Table II for relaxed Ag(100) and Rh(100) indicate two important features.

Table II The MD/MC-CEM calculated layer cohesive energies[a] and layer distances for clean Ag(100) and Rh(100)

	Ag(100)		Rh(100)	
Layer	d(Å)	E_C(eV)	d(Å)	E_C(eV)
1	2.05	2.41	1.89	4.60
2	"	2.89	1.90	5.58
3	"	2.95	"	5.75
4	"	2.95	"	5.75
5	"	2.95	"	5.75

[a] The layer cohesive energy is the cohesive energy of any atom in the layer.

First, the correct experimental bulk cohesive energies and layer distance spacing are achieved by the third layer. Second, the cohesive energy for Rh atoms in the top layer is nearly twice that of Ag in its top layer. These features will be important in the equilibrium structures of the respective epitaxial systems.

The mixed systems were examined by depositing a full monolayer of an adlayer

metal on or in the substrate simply to ascertain whether the adlayer would be favored to be subsurface. We allowed the surface, down to 5 layers, to fully relax while the adlayer metal was forced to retain the in plane lattice constant of the respective substrate. Small incommensurate distances would be unimportant for the gross effects that these initial calculations were designed to test. Full MD-LE calculations on layers containing over 20 unit cells on a side showed no inclination to incommensurate structures; this does not rule-out the existence of such a structure but does indicate that it would be favored only very weakly over the commensurate one.

We stress that these static calculations are used only as a guide in helping to understand the dynamical calculations. These test if the MD/MC-CEM method can even predict a stable sandwich type structure.

In Table III we show the results of static calculations for Rh deposited on a Ag(100) surface. Here the four sets of data represent from left to right: 1) Rh on top of the Ag surface; 2) one Rh layer on the surface with one layer of Ag on top of the Rh layer in a sandwich Ag-Rh-Ag(100) configuration; 3) Rh on the surface with two layers of Ag on top of the Rh layer; and , finally, 4) Rh on the surface with three layer of Ag on top of the Rh layer. Several very interesting features appear in these data. Comparison of the sum between the first and second sets shows the Rh atoms clearly prefer to be below a Ag layer by 0.67 Ev/atom. Of equal importance is that the cohesive energy for the top Ag layer on one Rh layer in set 2 is 0.25 eV/atom more stable than for the top layer of the clean Ag surface in Table II. At the same time note that the third Ag layer in the second set is more stable than in the first set which in turn is more stable than for clean Ag(100) shown in Table II. All these imply that not only does Rh prefer to be below the Ag surface but that the presence of Rh atoms stabilizes the nearest and even the next nearest Ag layers as well. Thus from just energetics alone one can say that, if Ag were mobile enough, the equilibrium structures would have subsurface Rh. (This is also supported by our value of 2.2 eV for the energy gained by replacement of a Ag atom by a Rh atom in the Ag lattice, of which about 0.1 eV is due to lattice relaxation.) One might even expect that since the Rh prefers to bind to Rh instead of Ag, this would yield a sandwich type structure as suggested from experiments [7] by Thiel and coworkers.

Table III The MD/MC-CEM calculated layer (L) cohesive energies[a] and layer distances for Rh on Ag(100)

L	Rh on Ag(100) d(Å)	E_C(eV)	1 Ag-Rh-Ag(100) d(Å)	E_C(eV)	2 Ag-Rh-Ag(100) d(Å)	E_C(eV)	3 Ag-Rh-Ag(100) d(Å)	E_C(eV)
1	1.82	3.90 Rh	1.88	2.66	2.03	2.45	2.05	2.41
2	2.02	3.03	1.85	4.75 Rh	1.85	3.09	2.05	2.94
3	2.05	2.99	2.03	3.14	1.85	4.85 Rh	2.02	3.15
4	"	2.95	2.05	2.99	2.03	3.15	1.85	4.84 Rh
5	"	2.95	"	2.95	2.05	2.99	1.85	3.15
6	"	2.95	"	2.95	"	2.95	2.03	2.99
Total		18.77		19.44		19.48		19.47

[a] See Table II.

(The presence of mixed subsurface layers is not ruled out by the present calculations, but this is a topic for future work.) Note that the stability limit is almost reached when there is only 1 Ag layer on the Rh film, with 2 Ag and 3 Ag layers on the Rh film being of nearly equal stability. Diffusion processes then most likely limit how far Rh will penetrate and thus a dynamical treatment is required to examine this further.

Also of interest is the calculated layer distances with Rh on the Ag(100) surfaces. Note that in the first set the distance between the Rh layer and the Ag layer below it is 1.82 Å. This is much shorter than the ideal Ag-Ag distance of 2.05 Å and shorter by 0.07 Å than even the ideal Rh-Rh distance. This contraction occurs because the Rh in-plane lattice spacing is now expanded to retain the Ag substrate lattice constant. As a response to this strain of an expanded lattice layer, the Rh-Ag layer distance contracts. A similar situation occurs when Rh is the second layer in the second set where the both the Ag-Rh layer distances are contracted to 1.88 Å and 1.85 Å.

We show for completeness the similarly calculated layer cohesive energies for Ag deposited on the Rh(100) surface in Table IV. By comparison with Table II it is shown in the first set that the single Ag layer prefers to be over Rh(100) rather than Ag(100) (2.65 eV vs. 2.41 eV) but that the second layer which is Rh is not as stable if it had a Rh layer above it (5.34 vs. 5.58 eV). The second set shows that if Ag has one layer of Rh above it while on Rh(100) it is also more stable than the second layer that is

observed in Table II but that the total energy is raised by 0.88 eV/atom relative to Ag on Rh(100). Note that the Ag adlayer is constrained to retain the Rh substrate lattice constant. This results in the Ag-Rh layer distance being expanded since the Ag in plane lattice spacing is considerably compressed.

Table IV The MD/MC-CEM calculated layer cohesive energies[a] and layer distances for Ag on Rh(100)

	Ag on Rh(100)		1 Rh-Ag-Rh(100)	
Layer	d(Å)	E_C(eV)	d(Å)	E_C(eV)
1	2.08	2.65 Ag	2.03	4.19
2	1.91	5.34	2.05	3.23 Ag
3	1.90	5.68	1.91	5.43
4	"	5.75	1.90	5.69
5	"	5.75	"	5.75
6	"	5.75	"	5.75
Total		30.92		30.04

[a] See Table II.

From the above analysis of the data in Table III, it is clear that a Rh layer would be more stable underneath at least one layer of Ag when deposited on the Ag(100) substrate. And, the data in Table IV suggest that a Ag layer in turn would rather be on top of Rh(100) in agreement with experimental data [22]. What these calculations do not indicate is the time-scale to reach a final equilibrium structure of these epitaxial systems. If indeed Ag atoms were to migrate through the Rh adlayer they must be quit mobile and able to travel through or around the Rh adlayer. So far we have used only thermodynamic arguments to enable a simplistic prediction of what this system might really look like on an atomic scale.

To study the dynamics of this system we carried out three distinct sets of calculations that utilized the MD-Langevin equation technique [23]. In each case we used a square active zone of 15 atoms by 15 atoms in each of 5 layers. The edge

atoms have added friction and random forces to allow energy flow between the active zone and the remainder of the bulk. These atoms in turn are surrounded by 2 rows of fixed atoms 8 layers deep. The three sets of MD calculations involved:

1) colliding one Rh atom with an initial kinetic energy of 0.25 eV into a Ag(100) surface at a specified surface temperature;

2) depositing Rh on Ag(100) at a coverage of a half monolayer and then heating the system to a specified temperature;

3) depositing a full defect free monolayer of Rh on Ag(100) and then heating the system to a specified temperature.

These last two are done in order to simulate deposition at low surface temperatures followed by annealing of the surface. No other adsorbates, surface imperfection, etc. were allowed in this initial study although this is certainly possible within the MD/MC-CEM formalism and will be subjected to future work.

We show in Figure 1 a depth profile of the deposited Rh atom as a function of the Ag(100) substrate temperature. In this plot 'surface Rh' refers to Rh simply chemisorbed on the Ag(100) surface without penetration; 'Rh in 1st subsurface layer' refers to Rh exchange with a top layer Ag atom; and, 'Rh in 2nd subsurface layer' refers to Rh exchange with a second layer Ag atom. As the temperature increases the percentage of trajectories (Rh atoms) that simply chemisorb decreases while exchange with first layer Ag atoms increases. At higher surface temperature, the Ag becomes more mobile which makes it easier for the Rh atoms to displace Ag from the surface. At temperatures greater than 900 K limited exchange with second layer Ag atoms even occurs. This suggests that it may not only be the surface energy that drives penetration into the surface. Rather it may be the Rh cohesive energies shown in Table III driving the Rh atoms to be bulk or at least near-bulk atoms.

To examine the dynamical aspect of annealing, we heat an initially deposited half monolayer coverage of Rh atoms in a c(2x2) configuration on the surface. In Figure 2 we show snap shot pictures at 2 ps intervals of the surface once heating has begun.

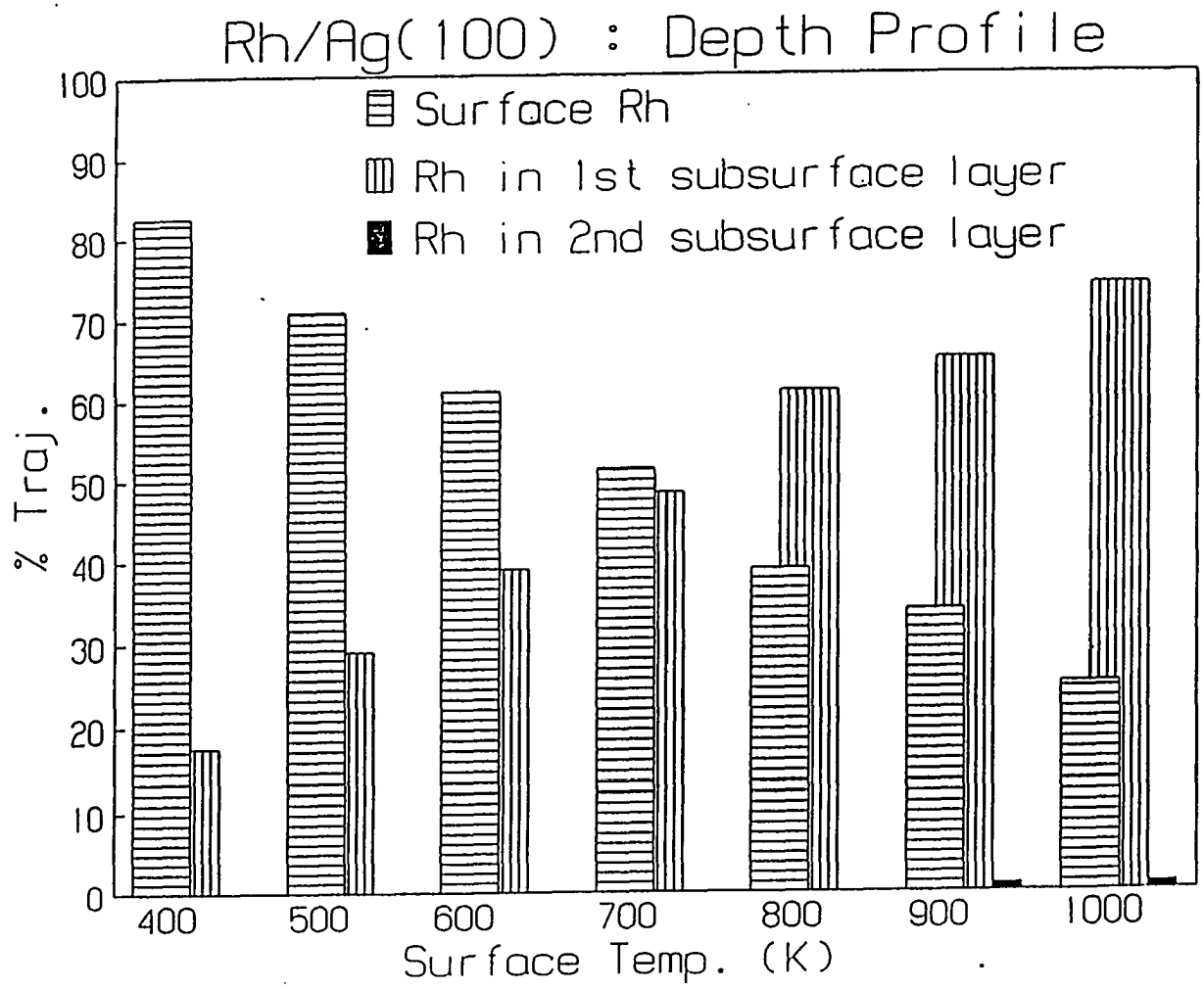

Fig. 1. **Depth profile from one Rh atom deposited on Ag(100) vs. surface temperature. The initial kinetic energy of Rh was 0.25 eV at normal incidence. At each temperature 200 trajectories were run to sample the aiming point in the unit cell and the thermal motion of the surface.**

128

As time goes on note that not only have several of the Rh atoms clustered together but that a number of them have penetrated into the Ag(100). Also note that the surface becomes disordered when this penetration occurs and that penetration occurs for groups or clumps of Rh atoms as well as for individual Rh atoms. In Figure 3 we show a depth profile of Rh atoms similar to that shown in Figure 1. The most striking feature is that the percentage of subsurface Rh atoms is less than that for single Rh atoms deposited in Figure 1. This must mean that even at a half monolayer coverage of Rh, the penetration of Rh into the Ag(100) surface is inhibited.

One question to ask is what is the rate of exchange of Rh atoms with Ag atoms? In Figure 4 we show the percentage of Rh atoms that have exchanged with the top layer Ag atoms as a function of time at two substrate temperatures of 600 K and 1000 K. The number of Rh atoms that have exchanged levels off quickly with time although the 1000 K surface is still active after 4 ps. The leveling is a direct consequence of a depletion of the originally deposited Rh layer on the surface. A resupply of Rh atoms on the surface would allow more of them to eventually exchange with Ag atoms. This will be examined in future work on this system.

These findings motivated a similar calculation for a defect free full monolayer coverage. Analysis shows that even at elevated temperatures of 1000 K no penetration into the surface occurs. In addition, the surface stays well ordered, there is no three dimensional clustering, and there is no exposure of the Ag(100) surface. This is somewhat unexpected since the half monolayer coverage showed considerable disorder only 4 to 6 ps after heating of the surface. The strong Rh-Rh bonding orders the adlayer and prevents the Ag atoms from exchanging with the Rh.

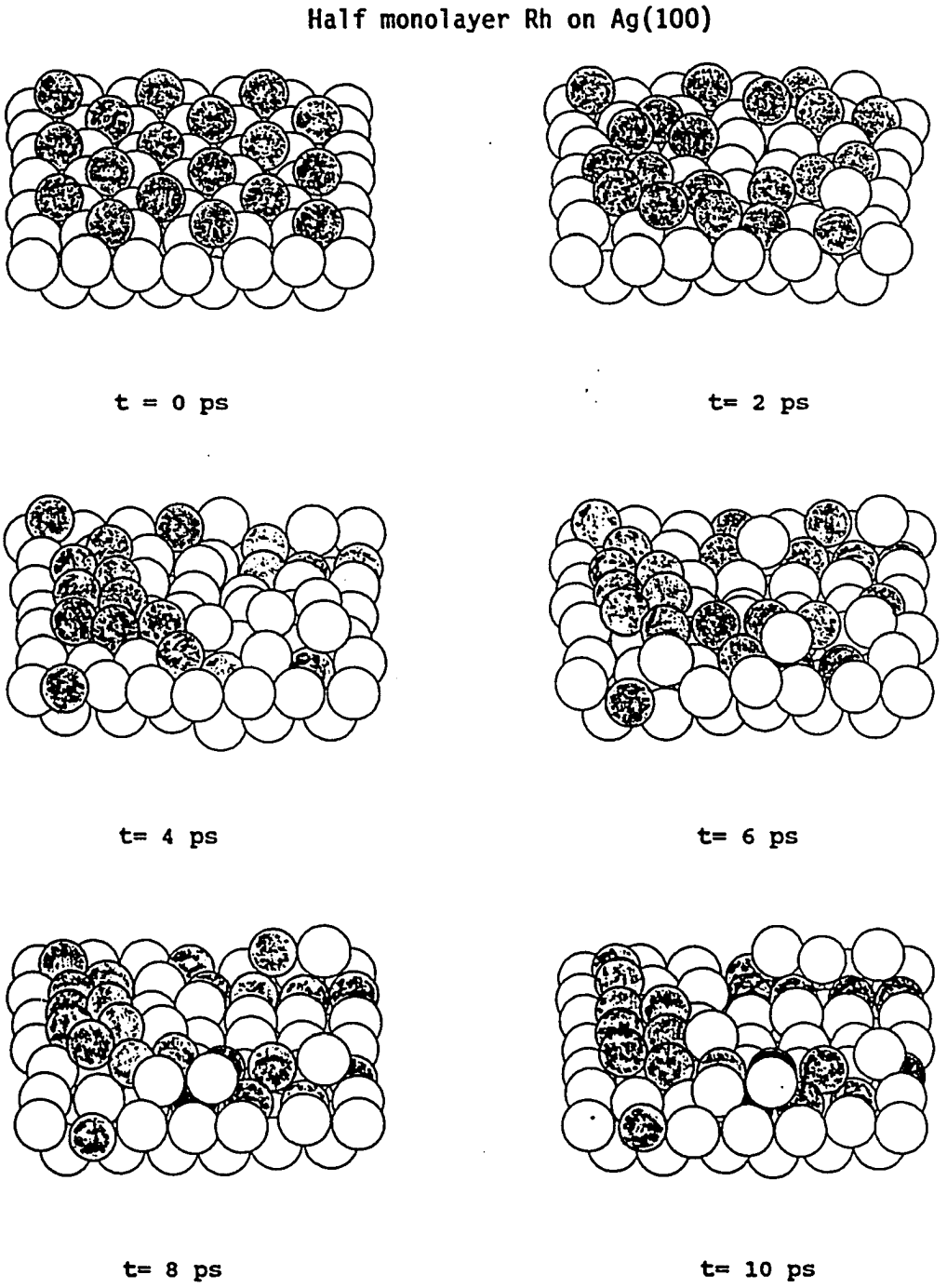

Fig. 2. Snap shot picture taken at 1 ps intervals after a half monolayer of Rh (solid circles) was deposited on cold Ag(100) and subsequent heating to 600K

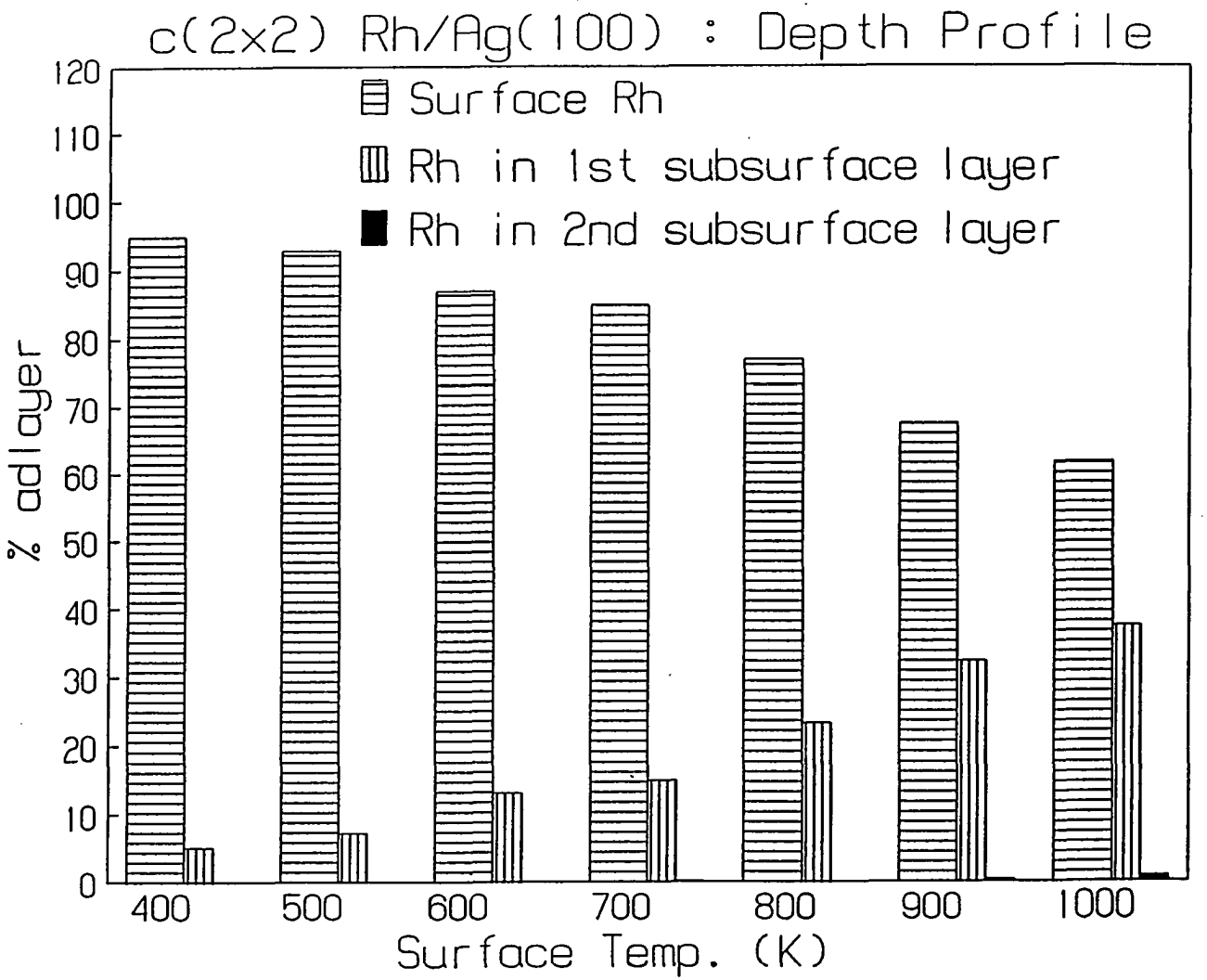

Fig. 3. Same as Fig. 1 except for an initial half monolayer coverage of Rh atoms and 50 trajectories.

131

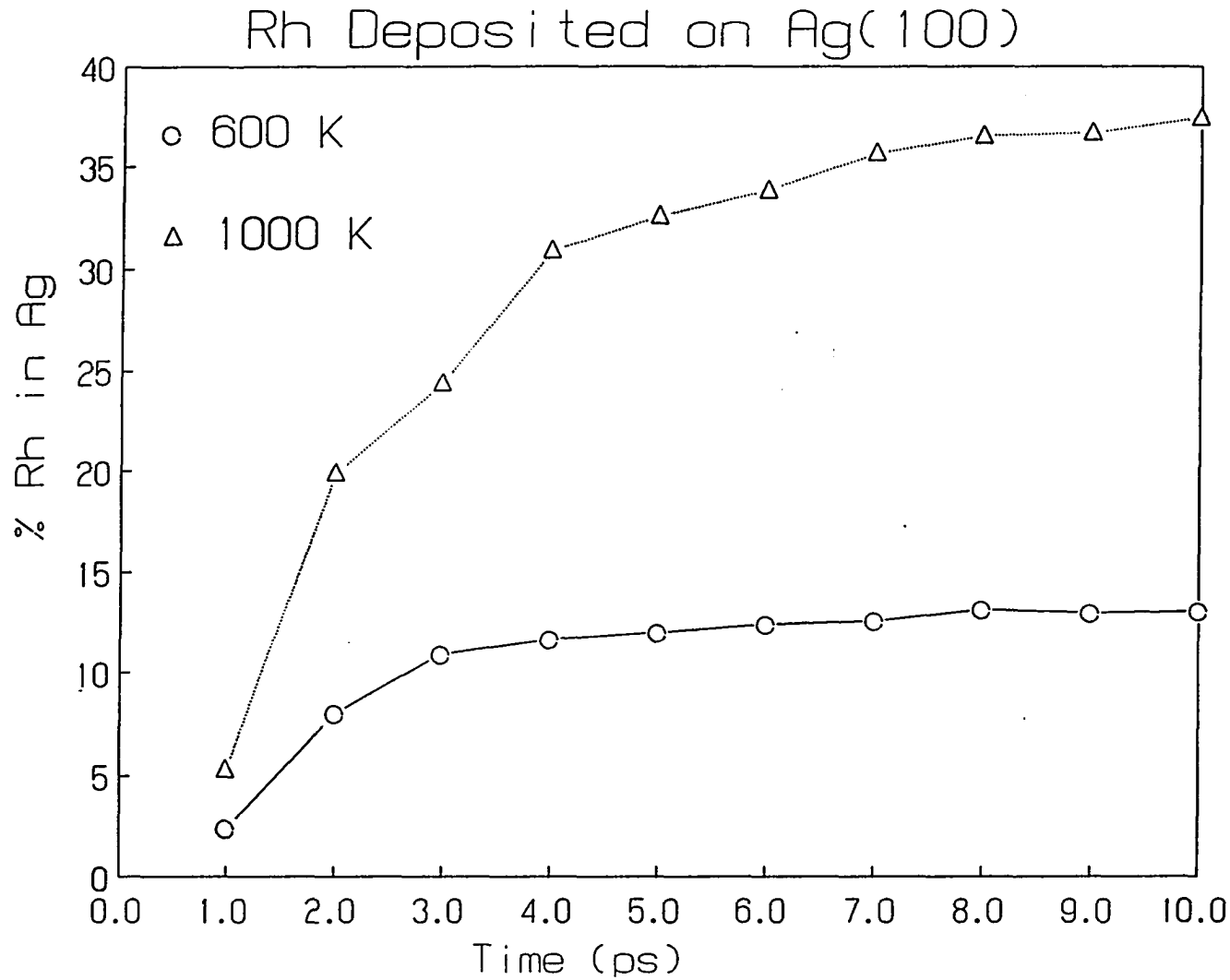

Fig. 4. Percentage of Rh atoms that have exchanged with the first layer Ag atoms at substrate temperatures of 600 K and 1000 K as a function of time after an initial half monolayer deposition.

4. SUMMARY AND CONCLUSIONS

We have presented results of calculations employing the MD/MC-CEM method to predict the surface energies of the clean Ag(100) and Rh(100) surfaces and agreement with experimental data was found to be good. In addition we calculated metal layer cohesive energies for the pure and mixed epitaxial systems. These calculations led to a prediction that, thermodynamically, Rh would prefer to lie below the Ag(100) surface rather than reside on top of the surface. These predictions supported experimental evidence that indeed Rh lies below at least one Ag layer.

Molecular dynamics calculations confirmed the findings by Thiel and coworkers that at least for initially low coverages of Rh, the Rh does indeed exchange with Ag and that this exchange is temperature dependent: an increase in substrate temperature results in an increase of exchange of Rh atoms with Ag atoms. If a full monolayer was used in the calculations no exchange occurred at any temperature. These results suggest that, in order for adlayer Rh atoms to exchange with Ag surface atoms, defects and/or holes must exist in the Rh layer that expose portions of the bare Ag(100) surface. These defects must also be present before annealing occurs since annealing does not induce clustering of the Rh layer. Two possible models were proposed by Thiel and coworkers to account for their experimental measurements. One model is for a low coverage of Rh atoms that allow portions of the Ag(100) surface to be exposed. This exposure gives Ag atoms a chance to migrate out of the surface layer and then onto the Rh adlayer. The other model suggests that cracks may exist in the Rh overlayer through which the Ag can migrate and eventually find their way over the Rh layer.

We believe these models are essentially correct. For regions of exposed Ag atoms, our calculations reveal that the Rh atoms actually burrow into the surface, forcing out the Ag atoms. In order for this to occur there must be room for Ag atoms to move. At a full monolayer coverage there is no room available and thus Rh cannot force the Ag atoms out of their lattice site. In addition, Rh-Rh bonding is so strong that it is very difficult for Ag to be forced through without some sort of open pathway. The strength of the bonds is such that not only would they be difficult to break, but also that Rh

would lose stability by bonding to Ag atoms rather than to other Rh atoms. Hence, the dynamical process is extremely slow even though it is significantly energetically favorable to have the Rh film covered by the Ag. This is why accurate dynamical calculations must be carried out, rather than relying just on static energy calculations.

We have not yet examined in detail the possibility of cracks in the Rh layer but expect that they would play an important role in not only opening up the Ag surface but also serving as a source of Rh atoms as well. Calculations are underway to examine this possibility and also the effect that 2 or more Rh layers have on the exchange of Rh with Ag atoms.

5. ACKNOWLEDGEMENT

Financial support from NSF grant CHE-8609832 is acknowledged as is an IBM predoctoral fellowship (DES). Partial support by the Petroleum Research Foundation administered by the American Chemical Society has also been received on grant 21690-AC5,C. In addition, we are pleased to acknowledge a generous grant of Cray YMP computer time at the Pittsburgh Supercomputer Center from Cray Research, Inc.

6. REFERENCES

[1] a) M. Schneider, A. Rahman and I.K. Schuller, Phys. Rev. Lett. 5 (1985) 604;
b) M. Schneider, A. Rahman and I.K. Schuller, Phys. Rev. B34 (1986) 1802;
c) S. Das Sarma, S. M. Paik, K. E. Khor and A. Kobayashi, J. Vac. Sci. Technol. B5 (1987) 1179;
d) S. M. Paik and S. Das Sarma, Phys. Rev. B39 (1989) 1224.

[2] D. P. Jackson in "Interatomic Potentials and Simulations of Lattice Defects", (Plenum Press, New York, 1972) and ref. therein.

[3] a) E. Pearson, T. Takai, T. Halicioglu and W. A. Tiller, J. Cryst. Growth 70 (1984) 33;
b) T. Halicioglou, H. O. Pamuk and S. Erkoc, Surf. Sci. 143 (1984) 601.

[4] a) K. W. Jacobsen, J. K. Nørskov, and M. J. Puska, Phys. Rev. B35 (1987) 7423;
b) K. W. Jacobsen, Comments Condens. Matter Phys. 14 (1988) 129;
c) J. K. Nørskov and N. D. Lang, Phys. Rev. B21 (1980) 2131;
d) M. J. Stott and E. Zaremba, Phys. Rev. B22 (1980) 1564.

[5] a) M. S. Daw, Phys. Rev. B39 (1989) 7441;
b) M. S. Daw, and M. I. Baskes, Phys. Rev. B29 (1984) 6443.

[6] a) F. Ercolessi, M. Parrinello, and E. Tosatti, Surf. Sci. 177 (1986) 314;
b) F. Ercolessi, A. Bartolini, M. Garofalo, M. Parrinello, and E. Tosatti, Surf. Sci. 189-190 (1987) 636;
c) F. Ercolessi, A. Bartolini, M. Garofalo, M., Parrinello, and E. Tosatti, Phys. Scr. T19B (1987) 399;
d) F. Ercolessi, M. Parrinello, and E. Tosatti, Philos. Mag. A58 (1988) 213.

[7] a) M. W. Finnis and J. E. Sinclair, Phil Mag. A50 (1984) 45;
b) M. W. Finnis, A. T. Paxton, D. G. Pettifor, A. P. Sutton, and Y. Ohta, Philos. Mag. A58 (1988) 143.

[8] a) J. D. Kress and A. E. DePristo, J. Chem. Phys. 88 (1988) 2596;
b) J. D. Kress, M. S. Stave and A. E. DePristo, J. Phys. Chem. 93 (1989) 1556.

[9] T. J. Raeker and A. E. DePristo, Phys. Rev. B39 (1989) 9967.

[10] T. J. Raeker and A. E. DePristo, Surf. Sci. 235 (1990) 84.

[11] T. J. Raeker and A.E. DePristo, "Theory of Chemical Bonding based upon the Atom-Homogeneous Electron Gas System", Int. Rev. Phys. Chem., in press.

[12] a) B. W. Dodson, Phys. Rev. B36 (1987) 6288;
b) B. W. Dodson, Surf. Sci. 184 (1987) 1;
c) S. M. Foiles, Surf. Sci. 191 (1987) 329;
d) C. M. Gilmore, J. A. Sprague, J. M. Eridon, and V. Provenzano, Surf. Sci. 218 (1989) 26;
e) A. F. Voter, Proc. SPIE-Int. Soc. Opt. Eng. 821 (1988) 214.

[13] M. S. Stave, D. E. Sanders, T. J. Raeker and A. E. DePristo, "Corrected Effective Medium Method: V. Simplifications for Molecular Dynamics and Monte-Carlo Simulations", J. Chem. Phys., (accepted 1990).

[14] P. J. Schmitz, W. -Y. Leung, G. W. Graham and P. A. Thiel, Phys. Rev. B40 (1989) 1.

[15] M. W. Schmidt and K. J. Ruedenberg, Chem. Phys. 71 (1979) 3951.

[16] a) E. Clementi, IBM J. Res. Develop. Suppl. 9 (1965) 9;
b) P. S. Bagus, T. L. Gilbert and C. J. Roothan, J. Chem. Phys. 56 (1972) 5195.

[17] S. Huzinaga, Prog. Theor. Physics Suppl. 40 (1967) 279.

[18] A. D. Becke, J. Chem. Phys. 88 (1988) 2547.

[19] D.E. Sanders, M.S. Stave and A.E. DePristo, "SCT89: a computer code for atomic and molecular scattering from clean and adsorbate covered surfaces", J. Comp. Phys., (submitted).

[20] P. R. Watson, F. R. Shepard, D. C. Frost and K. A. R. Mitchell, Surf. Sci. 72 (1987) 562.

[21] W. R. Tyson and W. A. Miller, Surf. Sci. 62 (1977) 267.

[22] a) Y. KIm, H. C. Peebles, and J. M. White, Surf. Sci. 114 (1982) 363;
b) H. C.Peebles, D. D. Beck, J. M. White, and C. T. Campbell, Surf. Sci. 150 (1985) 120.

[23] A. E. DePristo and H. Metiu, J. Chem. Phys. 90 (1989) 1229.

PAPER IV
THEORETICAL STUDIES OF DYNAMICAL PHENOMENA IN EPITAXIAL SURFACE SYSTEMS

Theoretical studies of dynamical phenomena in epitaxial surface systems.

Todd J. Raeker
and
Andrew E. DePristo
Department of Chemistry
Iowa State University
Ames , Iowa 50010

ABSTRACT

The increasing resolution of scanning tunneling microscopy techniques is beginning to reveal new interesting aspects of atomic behavior at surfaces. The ability to monitor diffusion of even single atoms is one dynamical example. This atomic scale resolution enables a close connection to theory, which plays an important role in uncovering the driving forces and mechanisms behind these dynamical events.

In this paper we briefly discuss the theoretical foundations of the Corrected Effective Medium (CEM) method and its application to the epitaxy of metals on metals. Static interaction energy and dynamical Monte-Carlo (MC) and molecular dynamics (MD) calculations are employed to examine equilibrium structures and the mechanisms in which equilibrium is obtained. Three specific applications are considered:

1) the mechanism for the formation of the ordered c(2x2) Au/Cu(100) surface alloy;
2) The formation of Ag/Rh/Ag(100) "sandwich" structures;
3) The growth of Au on Ag(110).

1. INTRODUCTION

Recent studies of the deposition of metals on metals have revealed many interesting and novel structures. The advanced resolution of scanning tunneling microscopy equipment allows visualization of atoms in particular structures. However, these techniques cannot (yet) show how these structures are formed and, if the formation process occurs on the time scale of atomic motion (10^{-14} - 10^{-9} sec), it will be many years before such direct dynamical imaging becomes possible. Theory can play a critical role in understanding the energetics and dynamics of the formation process. In particular, MD and MC calculations allow simulations of the deposition and growth in microscopic detail. In combination with computer visualization and animation, these provide unique insight.

The theoretical study of the epitaxy of metals on metals has focused generally on the prediction of the type of growth mode and the final structure. These models use the relative surface energies of the respective metals [1] to discriminate between layer-by-layer and 3D island growth. Such models are useful but limited, since they neither provide the microscopic reasons for formation of equilibrium structures nor predict the presence of non-equilibrium structures. Recent attempts employing rate equation [2] and birth-death equation [3] approaches have provided more insight. However, all the microscopic processes cannot be included in such kinetic schemes, and even the rates for many processes are unknown. So one can quickly get lost in examining the effects of various parameters, making interpretation of the results very complicated. Direct MD and MC simulations can also help in the development of kinetic models, which are capable of describing processes on much longer time scales than 10^{-9} sec.

The difficult part of atomistic simulations is assuring that the interaction energies and forces describe accurately the real system. For metal surfaces where many atoms are present, the choice of the potential used must satisfy two important criteria:

1) proper description of the interactions among all the atoms, including the variations in coordination between surface and bulk atoms.

2) computationally simple to evaluate.

Even when "2" is satisfied, the forces become very time-consuming to evaluate for large systems, thus limiting the length of the simulation to 10^{-12} - 10^{-9} seconds.

The simplest approach involves a pairwise interaction form such as the well known Morse and Lennard-Jones type potentials. Unfortunately, these do not properly describe the interactions present in both bulk metal and surface systems [4]. This is not at all surprising since the main justification of these forms is that they reproduce the diatomic binding curves quite well around the minimum. One may also include 3-body terms [5].

For metallic bonding, ideas based on the atom-jellium system have been developed over the past decade. These include the Effective Medium Theory [6], the Embedded-Atom-Method [7], the "glue" model [8] and the Corrected Effective Medium (CEM) method [9-13]. These methods are connected by the similar approach of embedding an atom in a homogeneous electron gas as the fundamental energy term. They differ in the way of introducing additional non-atom-jellium interactions, such as electrostatic terms for example. We use the CEM method throughout this paper for reasons detailed in Sections II and III.

In this paper we examine three epitaxial systems displaying different phenomenon as discovered experimentally. The first involves formation of a surface alloy after deposition of ½ monolayer of Au on Cu(100) at room temperature [14-16]. The second entails production of a "sandwich" type structure in the Rh/Ag(100) system: a film of Ag atoms forms over the initial Rh adsorbate after annealing at 600K [17]. The last involves the formation of 3D islands at low coverages in a bilayer structure of Au on Ag(110) [18]. Most of this paper is dedicated to the Au on Cu system while for the other two systems we only summarize our results to date.

The rest of this paper is broken into four sections. In Section II we present the CEM method for calculating energies and forces. Section III contains computational details about the description of surfaces and the use of MC and MD calculations. Results on all three epitaxial systems are presented and discussed in Section IV. Finally, in Section V we summarize the results and discuss future directions.

2. INTERACTION POTENTIAL

We employ the CEM method (in a form suitable for use in large scale MD and MC calculations) to determine the interaction energy and forces of a N-atom system in any geometrical configuration. As already mentioned the basic approach is to first replace the interaction of one atom with the N-1 other atoms by the interaction of the atom with jellium. This is illustrated in Figure 1 where the atomic electron densities of the surrounding atoms are used to provide the background jellium electron density around the center atom.

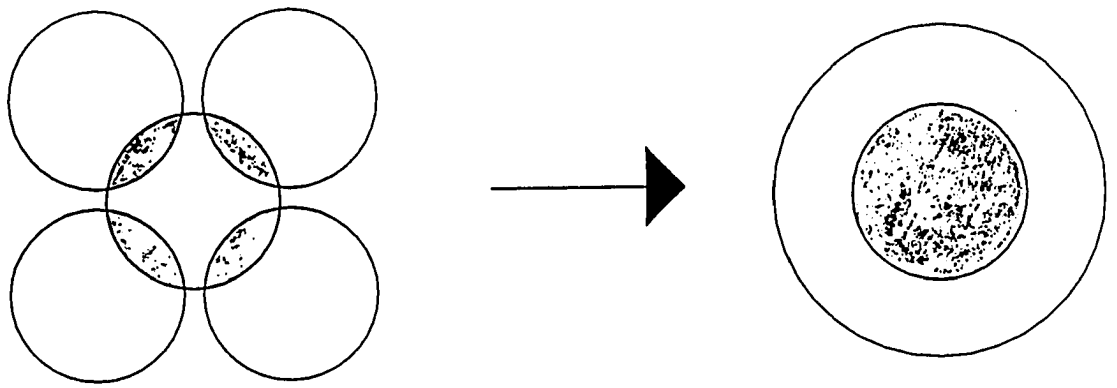

Fig. 1. Schematic of the embedding of one atom in the electron density of the surrounding atoms. This enables the replacement of the atomic interactions with atom-jellium one.

The process is repeated for each atom, thus simplifying the N-body problem considerably to a set of N one-body problems.

In CEM the interaction energy of N atoms is written as

$$\Delta E = \sum_{i=1}^{N} \Delta E_f(A_i;n_i) + \Delta G + \Delta V_c \tag{1}$$

$\Delta E_f(A_i;n_i)$ is the energy of embedding atom A_i into a homogeneous electron gas of electron density n_i, (i.e., jellium). ΔG is an explicit correction for the kinetic-exchange-correlation energy difference between the inhomogeneous electron gas in the real N-atom system and the many effective atom-jellium systems. ΔV_c is the total interatomic coulomb energy. These last two terms account for the presence of atoms instead of atom-jellium systems.

Using the superposition of atomic electron densities approximation,

$$n(\vec{r}) = \sum n(A_i;\vec{r}-\vec{R}_i) \tag{2}$$

in Eq. (1) leads to

$$\Delta V_c = \frac{1}{2}\sum_i \sum_{j\neq i} V_c(i,j) \tag{3}$$

where $V_c(i,j)$ is the sum of electron-electron, electron-nuclear and nuclear-nuclear coulomb interactions between atoms A_i and A_j:

$$V_c(i,j) = \int \frac{[n(A_i;\vec{r}-\vec{R}_i)-Z_i\delta(\vec{r}-\vec{R}_i)][n(A_j;\vec{r}\,'-\vec{R}_j)-Z_j\delta(\vec{r}\,'-\vec{R}_j)]\,d\vec{r}\,d\vec{r}\,'}{|\vec{r}-\vec{r}\,'|} \tag{4}$$

Minimizing ΔG with respect to the $\{n_i\}$ yields, for unpolarized atomic electron densities,

$$n_i = \frac{\sum_{j\neq i} \int n(A_i;\vec{r}-\vec{R}_i)\,n(A_j;\vec{r}-\vec{R}_j)\,d\vec{r}}{2Z_i} \tag{5}$$

where Z_i is the atomic number. This form of determining the jellium density is appealing since it is a measure of the real atomic electron density felt by atom "i" from all the other atoms.

The overlaps and coulomb energies are both pairwise in Eqs. (3b) and (4). When the atomic densities are spherical, they can be evaluated once for each pair of atoms on a grid of radial separations and interpolated for efficient energy and force evaluations [12]. Unfortunately the ΔG term in Eq. (1) involves a full three-dimensional numerical integration over the entire system of atoms and is thus very time consuming. For example evaluation of ΔG for a 100 atom cluster requires 99% of the CPU time (about 4 hours on a 4 MFLOP computer). It is feasible to perform such calculations for systems of up to around 1000 atoms for a small number of energy calculations. However, to do MD calculations with forces that are fast enough to evaluate many thousands of times, the time involved in ΔG is not acceptable for large systems.

We, however, have developed an approximate way to get around this difficulty. We have suggested [12,13] that the ΔG term can be approximated as an empirical function of n_i and the type of atom just as for the ΔE_J term in Eq. (1). With this in mind Eq. (1) can then be rewritten as

$$\Delta E = \sum_{i=1}^{N} \Delta F_J(A_i;n_i) + \Delta V_c \qquad (6)$$

where the ΔF_J are new 'effective' embedding energy functions. The simplest way to determine these embedding functions is to use experimental data on two different types of homonuclear systems. The first is for a homonuclear diatomic and the second for atoms in a bulk lattice. These two configurations have very different magnitudes of n_i and thus provide a wide range of electron densities in which ΔG can be approximated.

The above approximation relies on the assumption that the value of n_i for atoms in different size systems (i.e., clusters and surfaces) lies between these two limits. We shall see later that this approximation is not always appropriate for systems containing different types of atoms. In this regard, one should carefully distinguish

between the full CEM theory in which the ΔG term accounts for electron inhomogeneity, but the electron density is not adjusted self-consistently, and the MD/MC-CEM theory in which consideration of electron inhomogeneity does not enter. One must regard the MD/MC-CEM method as a semi-empirical theory designed to approximate the full CEM calculations at much higher computational speed. Thus, one might expect that flexibility in the choice of ΔF_J should be used to ensure close agreement between CEM and MD/MC-CEM calculations. We will have more to say about this later.

The MD/MC-CEM method allows evaluation of energies and forces at computational speeds over 50% of that using the simple Lennard-Jones(12,6) potentials and forces [19]. We call this new form of CEM the MD/MC-CEM method. The advantages of the MD/MC-CEM method are that many-body interactions are still an integral part of the method and good accuracy is obtained as shown in Table I for some of the surface energies for the metals of interest in this paper.

We now summarize the steps involved in the MD/MC-CEM calculation:

1) Construct atomic densities from Hartree Fock tabulated values;

2) Compute density overlap and evaluate n_i;

3) Evaluate the embedding energies for jellium density n_i and compute the coulomb energies for energy calculations;

4) Compute derivatives of steps 2 and 3 and sum for the total force on atom i.

There are no adjustable parameters to reproduce various alloy properties. In addition, the overlap and coulomb integrals are totally determined from the electron densities of HF calculations on atoms. Any further calculation on a mixed system is completely predictive, as is any other calculation on a homogeneous system.

3. COMPUTATIONAL DETAILS

In this section we discuss some of the computational details involved in the simulations. These involve the methodology in both MC and MD techniques and the treatment of the surface. For the latter, we have used slabs of various thicknesses and layer sizes without the use of periodic boundary conditions. Each layer in the slab may contain atoms which can be moved (i.e., active) and atoms which are fixed. The fixed atoms ensure that the surface slab stays as a slab and does not reorganize to form a cluster of presumably near-spherical geometry. In the MD simulations, the moving atoms obey Newton's equations with extra random and local frictional forces on the boundary atoms to the fixed atoms. The latter ensures that the surface can be kept at any finite temperature and that unphysical reflection of energy does not occur at the boundary of the active atoms [20].

Different types of MC methods were used to help the simulation obtain equilibrium with minimum computational effort. In all cases, the number of each type of atom was conserved throughout the calculation. Mixing of different species was simulated by allowing exchange of atoms types between existing atoms in the slab. Mixing with open or vacant surface sites was also employed to allow for extended defect formation during mixing. Finally, a continuous change in atomic positions was used to allow for relaxation of the atomic positions in the new environment. Of course, the fixed atoms were not allowed to move.

The above MC simulations used a slab of two active and two fixed layers. The layers were of varied extent with the largest giving a total of about 1600 atoms and 300 ghost atoms (movable empty lattice sites). Different sized slabs gave qualitatively different results, a point which will be discussed in the next section. We note however that increasing the number of layers does not significantly effect the results.

The MD calculations of Au on Cu(100) used a slab with 4 active and 3 fixed layers. We carried out the calculations for various size layers, containing from 200 to 1200 atoms, in order to determine the effect that slab size and edges may have on the results. We shall discuss these in the next section. Newton's equations were solved

using the Verlet algorithm [21] with a time step of 10^{-14} seconds, which was found to be quite adequate.

4. RESULTS

We now examine the energetics and dynamics of three epitaxial systems, employing both static and dynamical calculations. The former are used to better understand the energetics underlying the dynamical processes present in each system. Two different types of MD/MC-CEM embedding functions are determined. The first follows previous work and utilizes experimental data on the homonuclear bulk and diatomic systems, with interpolation between the large and small density regime. The second utilizes experimental data on the homonuclear bulk and CEM calculations on the top layer of surface atoms. In particular, the new embedding function is defined by

$$\Delta F_C(A_\alpha;n_\alpha) = \Delta E_C(A_\alpha;n_\alpha) + \Delta G(A_\alpha)_{ws(\alpha)} \tag{7}$$

where α denotes an atom in the surface layer and WS(α) indicates that the integration region is the generalized Wigner-Seitz cell of a surface atom [10,11]. The use of bulk and surface data eliminates the ability to treat the diatomic molecule but increases the accuracy in the surface region. The two different ways to determine ΔF_C are referred to as MD/MC-CEM I and MD/MC-CEM II, respectively. The latter method should agree with the full CEM method results most and it is these that we measure the quality of the embedding energy functions.

The three systems are Au/Cu(100), Rh/Ag(100) and Au/Ag(110). These display interesting varieties of cohesive energy and lattice constant: Au (3.81 eV/atom, 4.08 Å), Cu (3.49 eV/atom, 3.61 Å), Ag (2.95 eV/atom, 4.09 Å), Rh (5.75 eV/atom, 3.80 Å). For Au/Cu(100), the adsorbate is much larger and there is a slight favoring of the adsorbate to be in a bulk environment. For Au/Ag(110), the adsorbate and substrate are equally large and there is substantial favoring of the adsorbate to be a bulk environment. For Rh/Ag(100), the adsorbate is actually smaller than the substrate and there is an extremely large favoring of the adsorbate to be in a bulk environment.

4.1. Au on Cu(100)

Experimentally, the deposition of a half monolayer of Au atoms on Cu(100) results in a surface alloy in which the top layer is a 50:50 mixture of Au and Cu. The first LEED structure by [14] of the Au-Cu surface alloy displayed a c(2x2) pattern. Further experimental work [16] also determined a c(2x2) LEED pattern but apparently with streaking. Detailed LEED intensity analysis [15] demonstrated that the Au atoms bind about 0.1 Å above the plane of the Cu atoms, forming a c(2x2) pattern.

It is important to place these findings in context. Since the cohesive energy of Au is 0.3 eV/atom greater than Cu, one would intuitively think that a simple switching of atoms types should indeed result in the mixed layer being lower in energy than the pure Cu(100) slab. Also, the larger size of the Au atom should limit the concentration to something below a full monolayer. Thus, part of the experimental data is rather understandable. However, the 0.1 Å distance is quite surprising since the lattice constant of Au is 4.08 Å while that of Cu is 3.61 Å. Simple geometric arguments about the packing of hard spheres of such different size leads one to expect a buckling height of around 0.94 Å.

First, we carried out static calculations on the Cu, Au, and Au/Cu systems with the results in Tables I and II.

Table I Surface energies of various metals of interest in this paper as calculated by full CEM and two types of MC/MD-CEM

	Surface energy (j/m^2)			
Surface	CEM	MD/MC-CEM I[a]	MD/MC-CEM II[b]	experiment[c]
Cu(100)	1.50	1.72	1.39	1.79
Au(100)	1.29	1.54	1.33	1.50
Ag(100)	0.99	1.14		1.24
Rh(100)	2.56	2.91		2.66

[a] The embedding function is determined from bulk and diatomic data on the homogeneous system following previously discussed CEM references.

[b] The embedding function is determined from bulk data and surface CEM calculations on the homogeneous system. See text for details.

[c] The experimental data are an average of a polycrystalline surface from W. R. Tyson and W. A. Miller (1977), Surf. Sci. 62, 267.

Table II Binding energies for p(1x1) and c(2x2) Au on Cu(100) as calculated by full CEM and Two types of MC/MD-CEM

	Energy (eV/atom)		
Phase	CEM	MC/MD-CEM I	MC/MD-CEM II
p(1x1)	3.97	3.49	3.36
c(2x2)	3.90	2.96	3.38

The results indicate that the MD/MC-CEM I method overestimates the surface energies and the stability of the Au adlayer p(1x1) phase while the MD/MC-CEM II method is generally much better when compared to the CEM results. The lower accuracy of the former for surface problems can be traced to the inaccuracy of the assumption that ΔG of the surface atoms lies on the assumed smooth curve between the diatomic and bulk atom correction energies. This is evident in Figure 2 for Cu as an example. The surface correction energies do indeed lie between the diatomic and bulk limits but not on the assumed smooth interpolation curve.

A comparison of the embedding functions for Cu and Au is shown in Figure 3. Clearly, the inclusion of the surface points changes quantitatively the lower density region of the curves. Ignoring the diatomic data has no significant consequences in the current calculations since we are not dealing with isolated diatomics. In addition, there were no surface or bulk atoms that had an electron density environment as low as for an atom in a diatomic.

It is worthwhile to emphasize that the results in Table II indicate that not only are both pure surfaces described much better by MD/MC-CEM II but also that the Au is equally stable in both close packed p(1x1) and more open c(2x2) structures.

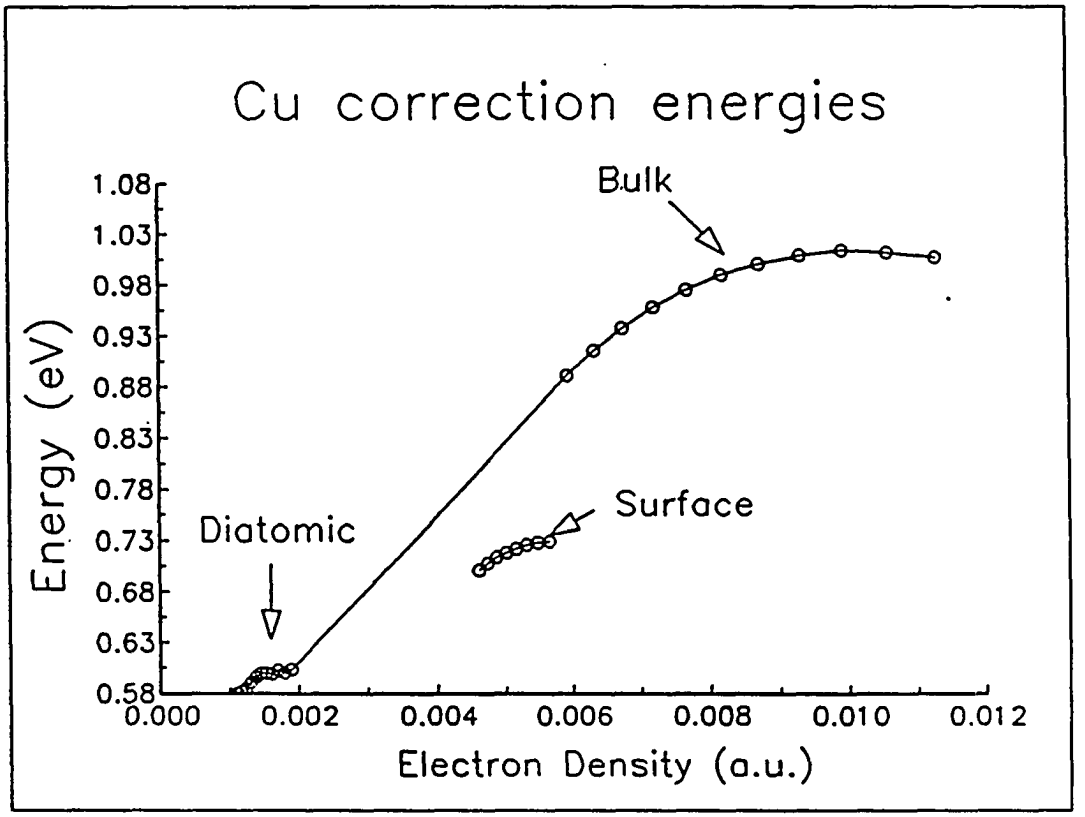

Fig. 2. The correction energy, ΔG, for Cu in diatomic, fcc(100) surface and bulk fcc lattice. The points from the diatomic and bulk are connected by straight line for clarity.

This may help the formation of a surface alloy. It is important to point out that we are not adjusting the embedding energy functions from any alloy data. We are only forcing the MD/MC-CEM II method to be closer to the full CEM method for the homogeneous surfaces. The MD/MC-CEM II method still does not achieve the same absolute binding energies of Au on Cu(100) as full CEM.

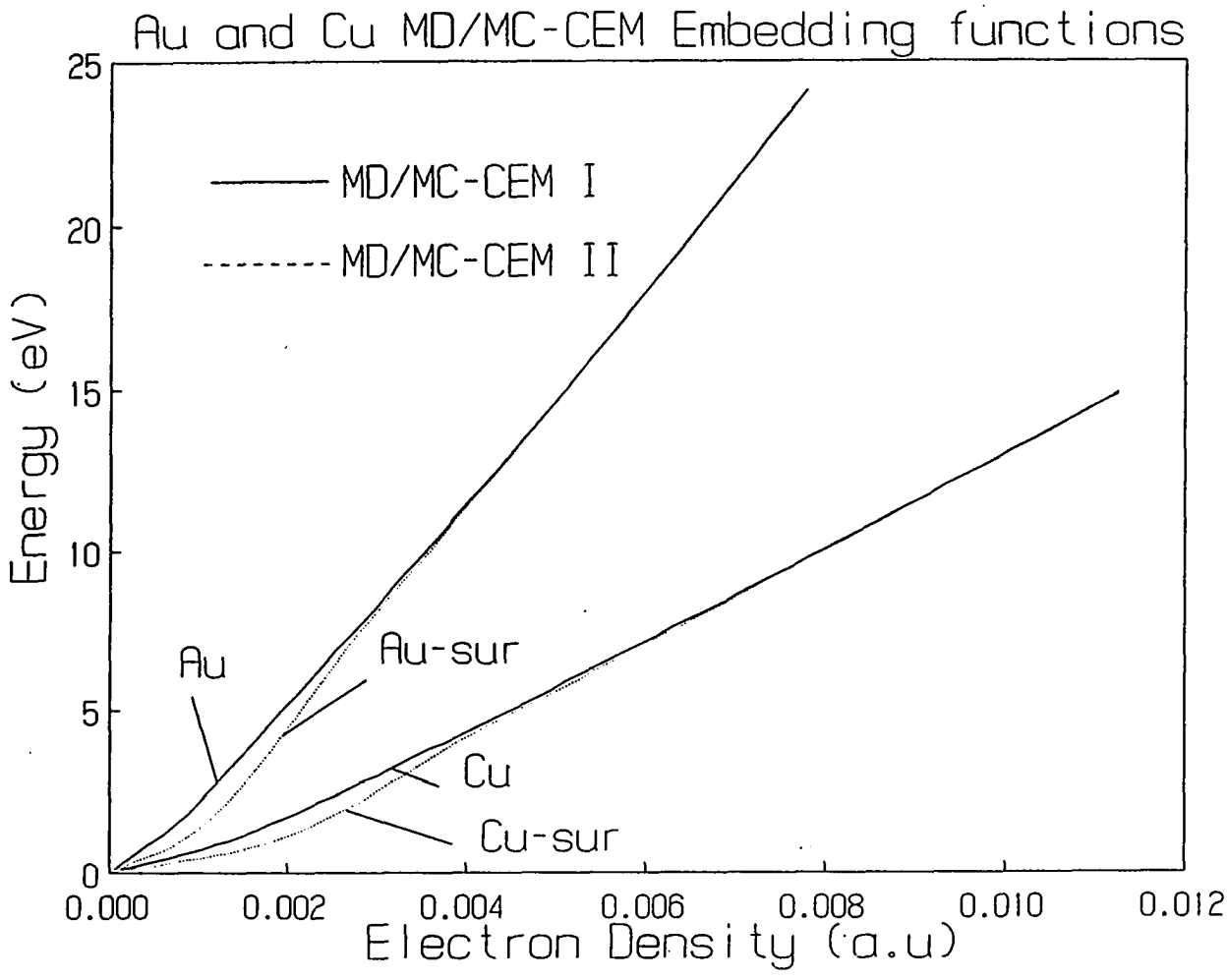

Fig. 3. **Two different embedding functions for MD/MC-CEM theory. The solid line is the original function which interpolates between the diatomic and bulk systems. The dashed line is the new embedding function which uses the bulk system and CEM calculations on the surface atoms to determine the embedding function. See text for more details.**

The correction energy is more accurately mimicked for surfaces in the MD/MC-CEM II approach but is still not described exactly. The surface energy for Cu(100) is too small. This can be traced to the fact that ΔG for the second layer Cu atoms is not the same as for the first layer atoms. There is simply no way to take a complex functional of the electron density and gradients and replace it by a function of the jellium density without some loss of accuracy. Indeed, ΔG is also clearly a function of the bonding formed from mixed atom types, at least for Au and Cu. Nevertheless, the relative energetics may be described well enough by MD/MC-CEM II to capture the essence of full CEM.

Static calculations are useful for guidelines but do not simulate the process by which the surface alloy layer is formed. We have carried out both MD and MC calculations in an attempt to understand how the surface alloy is indeed formed. Due to current limitations of computer speeds and dynamical methodologies the MD calculations can only simulate events occurring in less than about 10^{-9} sec. We can examine the initial stages of the alloy formation, but not necessarily the development of the final equilibrium (or non-equilibrium) structure. MC calculations are employed to alleviate this difficulty in a crude way; these are unable to describe non-equilibrium kinetic effects which we have already observed [22] to be an important feature in the Rh on Ag(100) system.

First, we report the results using the MD/MC-CEM I embedding function, which we expect will not describe the Au/Cu(100) system accurately based upon the static calculations in Table II. This is important since it allows one to correlate the behavior of bimetallic systems with the adsorbate binding energy variation with coverage.

We did two types of MC runs at temperatures of 300 K and 600 K each. The first was with a preexisting 50-50 adlayer mixture of Au-Cu on the surface with no ghost atoms present. All results showed almost complete segregation of Au and Cu atoms on the surface, with no alloy equilibrium structure. When a similar run was done with ghost atoms instead of adlayer Cu we found that some substrate Cu atoms mixed with the Au adlayer atoms. The Au atoms that were originally dispersed on the surface formed large islands having a (1x1) structure with 2-5% of mixed Cu atoms with a small amount of Cu clustering among the adlayer Au islands. Some adsorbate Au

atoms occupied sites in the substrate that were vacated by Cu atoms. However, we never observed the formation of a surface alloy of long range order having a c(2x2) structure.

To investigate the cluster size dependence of these results, we repeated the above ghost atom runs but with nearly twice as many atoms in the slab. This resulted in a 5-10% mixture of Cu atoms in the Au adlayer. There seemed to be a weak dependence of the amount of mixing with the size of the cluster. MD simulations resulted in no mixing of Cu and Au even for temperatures as high as 800K. Interestingly enough, compact islands of Au having a clear hexagonal arrangement were observed with large areas of the Cu(100) surface being exposed. This indicates that in MD/MC-CEM the Au-Au interactions dominate the Au-Cu ones since the adlayer is forming a close-packed face even though the substrate provides a (100) template.

It is clear from the above behavior that our interpretation of the static calculations in Tables I and II is correct. The MD/MC-CEM I method does not describe the interaction between the Au and Cu with sufficient accuracy, greatly overestimating the strength of the Au-Au interaction relative to that of Au-Cu. In conjunction with the larger size of the Au atoms, this greatly inhibits formation of a surface alloy.

Next, we performed calculations with the MD/MC-CEM II embedding function, which we expect describes the Au/Cu(100) system much better. Figure 4 displays results from two different MD calculations in which an initial 0.25 monolayer coverage of Au on Cu(100) at 600K and 800K were run for 900 psec using 1000 atoms/layer slabs. We use higher temperatures to speed-up the rate of alloy formation so that the process can be simulated in a reasonable amount of computer time. Figure 4a is a snapshot picture of the surface after annealing at 600K for 900 psec then cooling to 300K for 3 psec. The Au atoms have clustered with little mixing of Cu. It would appear that the initial stage of the formation of the surface alloy may first involve the formation of Au islands followed by alloying. This is more easily seen from Figure 4b for a run at 800K.

0.25 monolayer Au on Cu(100)

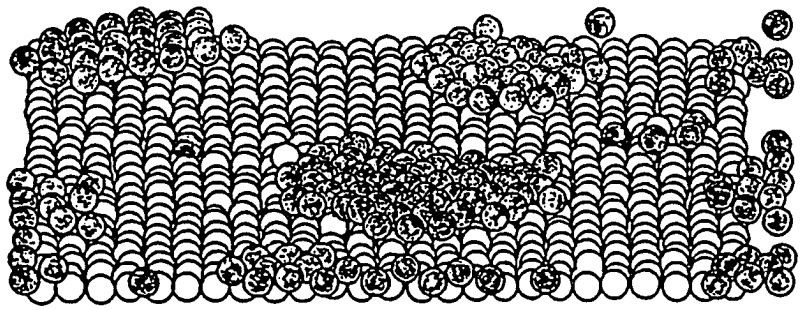

900 ps at 600K

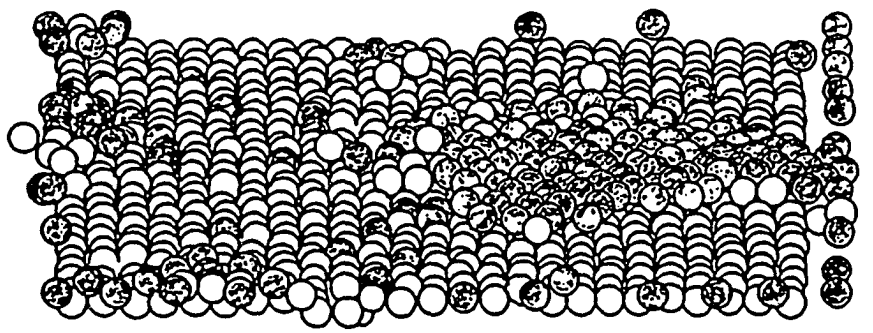

900 ps at 800K

Fig. 4. Snap shot pictures of a MD simulation of a ¼ monolayer Au coverage on Cu(100), initially in a p(2x2) structure, after 900 psec molecular dynamics simulation at 600 K and 800 K.

While island formation is still apparent, the open Cu(100) exposed areas display a significant amount of Au mixing with the Cu surface atoms and these Au atoms are not grouped together as when on the surface. Note also that most of the alloying in the adlayer occurs near the edges of the Au islands. This is a feature that appears for all the simulations we have done on this system and suggests that islands and their edges are required in order to form the surface alloy. Thus, alloy formation in this system may actually occur by either a similar or identical mechanism to that found recently in the O/Cu(100) system [23]: Cu atoms diffuse from the steps and surround the O atoms, forming a new surface.

Figures 5a and 5b show results of similar calculations for an initial 0.5 monolayer coverage of Au. At 600K in Figure 5a we see only a few Cu atoms mixed with the Au islands but at 800K we see a significantly greater amount of mixing, which is nevertheless still smaller than the experimentally observed 50% mixture.

If left to run for long enough times both coverages would eventually show significantly more mixing of Au and Cu atoms. However, we cannot say for sure that a c(2x2) structure would be formed. Since we ran the dynamics for $\approx 10^{-9}$ sec, it is likely that formation of the alloy is a slow process which cannot be modeled by any dynamical calculation in an economically feasible time. In addition, the ordered alloy may be formed more readily during deposition which can not be simulated on any realistic time scale.

As an alternative, we did a MC calculation using the MD/MC-CEM II embedding functions and found a mixture at 600K of 15-20% of Cu and Au atoms in both surface islands and in the substrate. A 50:50 mixture was not found and segregation was still present. It is perhaps appropriate to mention that our high temperature simulations could have missed the formation of the ordered alloy if the c(2x2) phase may is a metastable state.

We are aware of one theoretical attempt to examine this system [24] employing the Embedded Atom Method for the interaction potential. Foiles carried out a MC simulation on a Cu(100) slab at room temperature in which MC steps involved changing the identity of surface Cu and Au atoms. The total number of atoms of the slab was conserved but the number of each type was not.

0.5 monolayer Au on Cu(100)

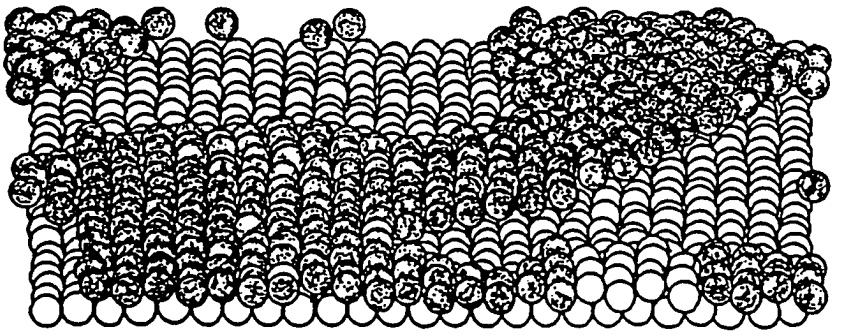

900 ps at 600K

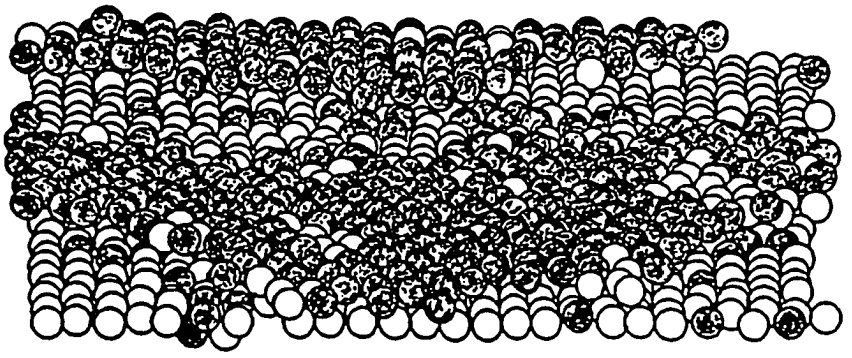

900 ps at 800K

Fig. 5. Same as Fig. 4 except for a ½ monolayer coverage of Au, initially in a c(2x2) structure.

In addition, atom coordinate relaxation and site switching were allowed in order to relax the surface as a response to creating Au atoms in the surface. The results of this calculation were that a 50:50 surface mixture of Au and Cu was stable in an ordered c(2x2) structure with thesurface buckled by 0.18 Å. The EAM potentials used the dilute heat of mixing for the parametrization. There was no attempt to simulate the process by which the surface alloy layer is formed.

4.2. Rh on Ag(100)

Experimentally it has been observed by Schmitz et al. [17] that annealing at 600K, of a Rh film previously deposited on Ag(100) results in a thin film of Ag forming on top of the original Rh layer. This film formation is complete and no significant mixing of the two metals is observed. In other words the respective Rh and Ag layers are homogeneous in content. We have carried out extensive MD simulations for sub-monolayer coverages of Rh on Ag(100) to investigate the initial mechanisms for the formation of this "sandwich" structure. We have published results of these calculations recently [22] and shall only summarize them here.

We used a cluster slab with about 200 atoms/layer plus fixed atoms to ensure maintenance of the fcc(100) surface structure. Runs at temperatures ranging for 300K to 1000K were done in order to examine the effects of temperature on the rate of formation of the observed structure. We show in Figure 6 a plot of depth profiles for three different cases at the above mentioned temperatures. The first simulates the deposition of a single Rh atom impinging on the Ag(100) surface; the second, a 0.25 monolayer coverage of Rh initially in a p(2x2) configuration; and the third, a 0.50 monolayer coverage initially in a c(2x2) structure.

The results in Figure 6 are puzzling at first glance. The single atom deposition is much more efficient at exchanging with surface Ag than annealing of deposited Rh. In contrast, the 0.25 monolayer coverage leads to less exchange than the 0.50 monolayer

coverage. Clearly the single atom deposition/exchange is quite different than a single atom exchange in an already deposited layer. This is understandable since about 4.5 eV is gained in chemisorbing a single Rh atom. This energy leads to considerable collision induced local distortion of the Ag lattice, increasing the probability for Rh to find a large enough gap in the Ag surface to begin pushing aside Ag atoms and eventually exchanging positions with one of them. Thus, chemisorption energy gained in attaching Rh to the Ag surface provides a great increase in exchange; this is not surprising since this energy corresponds to a very large increase in the surface temperature, which also increases the exchange probability.

For annealing of an adsorbed layer, the small oscillations of the Ag surface limit the initial exchange of Rh until a relatively high annealing temperature is reached. Rh atom exchange with Ag is an isolated and rare event. However, each exchange of a single Rh atom with a Ag atom causes other nearby Rh atoms to follow quickly; Rh prefers to bind subsurface and with other Rh atoms as compared to on the surface and with Ag atoms. In a sense the exchange at higher coverages is self-propagated by one Rh dragging other nearby Rh atoms under the Ag surface. This quickly spreads and continues until the supply of Rh atoms on the surface is exhausted. In essence our calculations confirm the experimental "sandwich" structure and also shed light on the mechanism behind this structure.

4.3. Au on Ag(110)

Recent experimental data [18] has indicated that deposition of low coverages of Au atoms on Ag(110) results in bilayers being formed at room temperature. This suggests that growth of Au on Ag(110) proceeds in a 3D island growth mode rather than layer by layer. Since it has been established that Au grows layer by layer on both Ag(111) [25] and (100) [26], this new data represents an interesting deviation. One must be careful in making assumptions for one surface based on known phenomena on others.

We shall examine the energetics as well as the dynamics of this system in order to understand why the Ag(110) surface behaves differently from the (100) and (111) surfaces. This low coverage experimental study is ideal for comparison to the present

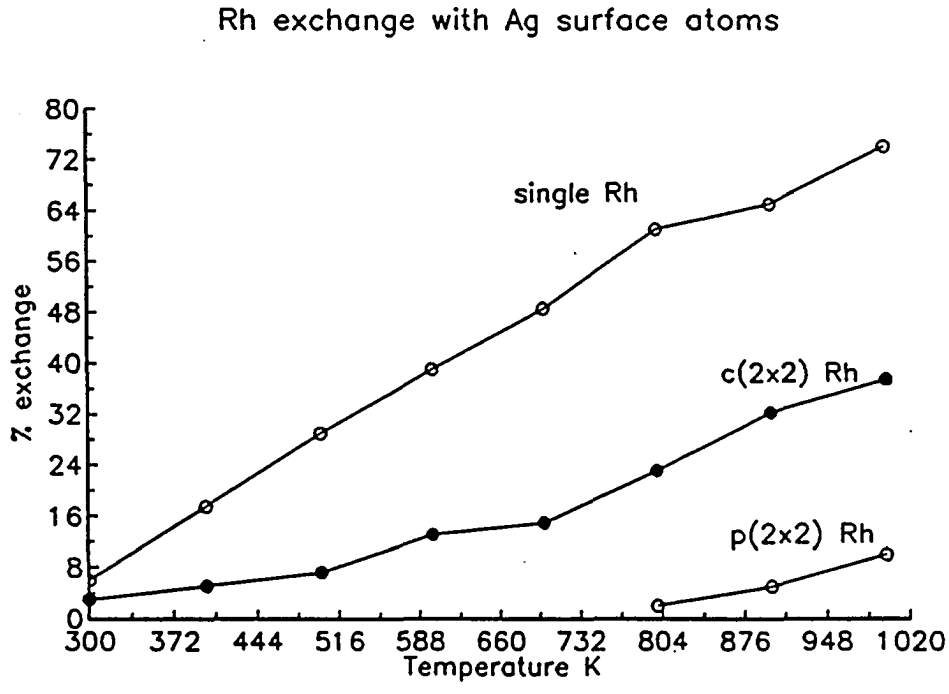

Fig. 6. Percent of place exchange of surface Ag atoms with Rh atoms for single Rh atom deposition, annealing of an initial p(2x2) Rh coverage for 10 psec, and annealing of an initial c(2x2) Rh coverage for 10 psec.

calculations. High coverage large scale structures are not present here.

First, we examine the relative surfaces energies of Au and Ag in Table III to see if anything can be learned. In Table III we show results of full CEM and both types of MD/MC-CEM for the surface energies of the (111), (100) and (110) surfaces of Ag and Au. In order for layer by layer growth to occur, the surface energy of the adlayer must either be smaller or at least only slightly larger (interfacial energy may be negative) than that of the substrate. From Table III we can see that the latter case holds. The question is how much larger can the adlayer surface energy be than the substrate. The difference between surface energies calculated by CEM are 0.26 J/m^2, 0.30 J/m^2 and 0.31 J/m^2 for the (111), (100) and (110) surfaces respectively. The MD/MC-CEM results show the same general trend although the values are all 0.10 J/m^2 larger. Clearly there are no overwhelming differences among these surfaces. Considering that Au deposition on the (111) and (100) Ag surfaces proceeds in a layer by layer mode, one might from these data alone predict the same growth mode for deposition on the Ag(110) surface.

However, knowledge of the surface energies is not sufficient when these values are close since then one must also know the interfacial energy. This is typically ignored as small although it is usually negative in value. To estimate the relative magnitude of this parameter for the three surfaces, we show in Table IV the CEM calculated binding energies of a full monolayer coverage of Au on each Ag surface. From the CEM values, it is clear that the binding strength on the (110) surface is the weakest. This indicates that the interfacial energy for deposition on Ag(110) is most likely smaller than for deposition on the (111) and (100) surfaces. Indeed, the energy increase of 0.09 eV/atom between (100) and (110) corresponds to an added surface energy of 0.12 J/m^2 on the (110) surface. This makes the effective surface energy difference for Au(110) and Ag(110) even larger, about 0.43 J/m^2, and distinguishes the (110) surface from the (111) and (100) ones. This larger surface energy difference favors 3D island growth.

Table III Surface energies of the (111), (100) and (110) surfaces of Au and Ag as calculated by full CEM and both types of MD/MC-CEM

		Surface Energy (j/m^2)			
	FACE	CEM	MD/MC-CEM I[a]	MD/MC-CEM II[b]	Expt.[c]
Ag	(111)	0.94	1.07	0.91	
	(100)	0.99	1.14	0.95	1.24
	(110)	1.07	1.25	1.07	
Au	(111)	1.20	1.42	1.26	
	(100)	1.29	1.54	1.33	1.50
	(110)	1.38	1.66	1.46	

[a] The embedding function is determined from bulk and diatomic data on the homogeneous system following previously discussed CEM references.

[b] The embedding function is determined from bulk data and surface CEM calculations on the homogeneous system. See text for details.

[c] The experimental data are an average of a polycrystalline surface from W. R. Tyson and W. A. Miller (1977), Surf. Sci. 62, 267.

From an atomistic viewpoint, the more closed packed nature of the (111) and (100) surfaces increases the binding of the Au atoms to the substrate. For these two surfaces the Au atoms attain nearly their bulk cohesive energy (3.81 eV) at a full monolayer coverage, or when (1x1) islands are formed. On the other hand, the Au atoms' binding energy on the (110) surface is not as close to the bulk cohesive energy and thus may attempt to attain larger binding by forming a second layer of Au even at low coverages (i.e., mimicking the bulk environment). We confirmed this by calculating the binding energy of an additional monolayer of Au atoms on a one monolayer thick film of Au on Ag(110) to be 3.84 eV/atom from CEM. Similar calculations for the other two surfaces result in the same binding energy. Thus, bilayer growth on the (110) surface gains about 0.1 eV/atom more than on the (111) and (100) surfaces. Results from MD/MC-CEM II show the same trend although the absolute magnitudes are slightly smaller and the differences in Table IV not as distinct.

Table IV Binding energies per Au atom of a full monolayer of Au on Ag(111), (100) and (110) as calculated by CEM and the two types of MD/MC-CEM

	Binding Energy (eV)		
	CEM	MD/MC-CEM I[a]	MD/MC-CEM II[b]
(111)	3.67	3.40	3.45
(100)	3.64	3.29	3.37
(110)	3.55	3.13	3.25

[a] See Table III.

[b] See Table III.

We cannot at this time say that growth is occurring in 3D island fashion. However, we do believe that the static energy calculations provide a plausible explanation for the results of Fenter and Gustafsson [18].

5. SUMMARY AND CONCLUSIONS

We have applied the recently developed CEM and MD/MC-CEM methods to three different thin film systems: Au/Cu(100), Rh/Ag(100) and Au/Ag(110). Static interaction energy as well as dynamical MD and MC calculations were used to investigate the energetics and dynamics of the initial growth modes in these systems at the atomic level. The new theoretical development involved utilizing and contrasting two different types of MD/MC-CEM embedding functions. The first was determined from experimental data on the homonuclear bulk and diatomic systems. The second was determined from experimental data on the homonuclear bulk and CEM calculations on the top layer of surface atoms. The former described a larger range of systems but was not as accurate as the latter for surfaces and mixtures of metals at surfaces. The non-universality of the MD/MC-CEM embedding functions arises directly from the neglect of the explicit kinetic-exchange-correlation energy correction for inhomogeneity of the electron density distribution in the real N-atom system.

It is worthwhile to emphasize a few of the general conclusions found in these studies. First, the Au on Cu system, with a larger adsorbate and little energy gain in making the adsorbate move subsurface, is unlikely to form surface mixtures by adsorbate-substrate place exchange. Instead, it is much more likely that the substrate envelopes the adsorbate via diffusion of adsorbate atoms from steps [23]. Second, the Rh on Ag system, with a smaller adsorbate and large energy gain, undergoes rapid exchange of Rh and Ag atoms which are catalyzed by the existence of subsurface Rh. Third, the Au on Ag system, with equal sized adsorbate and substrate and moderate energy gain, can display more complex behavior that depends upon the geometrical arrangement of the substrate atoms. This changes the interfacial surface energy which plays a dominant role when the surface energy differences are small.

It is useful to try and place these results in the context of previous work on the characteristics of epitaxial growth in fcc(100) systems obeying Lennard-Jones potentials [27]. These potentials are characterized by a size parameter, σ, and a strength parameter, ε. For the substrate-substrate, film-film and film-substrate potentials, there are six parameters, (σ_{ss}, ε_{ss}), (σ_{ff}, ε_{ff}) and (σ_{fs}, ε_{fs}), respectively. The

system behavior is determined by the two energy and two size ratios: $\varepsilon_{ff}/\varepsilon_{ss}$, $\varepsilon_{fs}/\varepsilon_{ss}$, σ_{ff}/σ_{ss}, σ_{fs}/σ_{ss}. The two size ratios are not independent since the hard-sphere type interpolation, $\sigma_{fs}=(\sigma_{ff}+\sigma_{ss})/2$, is expected to hold to good accuracy. Thus one size ratio suffices, and is conveniently expressed as $\eta=(-1+\sigma_{ff}/\sigma_{ss})$ with $-1<\eta<\infty$.

To our knowledge, the general system behavior has not been analyzed in this three parameter space. Instead, the most thorough investigations [27] have made the additional simplification that $\varepsilon_{ss}=\varepsilon_{ff}$. Then, only one energy ratio, $W=\varepsilon_{fs}/\varepsilon_{ss}$, is needed. The assumption of equal substrate-substrate and film-film interactions severely limited the generality of these investigations.

The cases $\eta\geq 0$, equal or larger film than surface atoms, have been investigated in great detail [27]. For $\eta=0$, 3D islands grow for $W<1$ and layer-by-layer growth for $W>1$. For $\eta>0$, 3D islands grow for $0<W<W_c(\eta)$ and 3D islands on top of layer-by-layer grow for $W_c(\eta)<W<\infty$. The critical strength ratio, $W_c(\eta)$, is a strongly increasing function of η. In this work, no qualitative differences were found between rigid and non-rigid substrates.

For the systems in the present work, the energy and size ratios can be estimated from MD/MC-CEM II and experimental data. However, we do caution that these are not Lennard-Jones systems so the system behavior may not correspond precisely to that found in ref.[27] even when the parameter ratios are similar. The values are:

Au/Cu ($\varepsilon_{ff}/\varepsilon_{ss}$, $\varepsilon_{fs}/\varepsilon_{ss}$, σ_{ff}/σ_{ss}) = (3.81/3.49, ≈3.4/3.49, 4.08/3.61)

Rh/Ag ($\varepsilon_{ff}/\varepsilon_{ss}$, $\varepsilon_{fs}/\varepsilon_{ss}$, σ_{ff}/σ_{ss}) = (5.75/2.95, ≈4.5/2.95, 3.80/4.09)

Au/Ag ($\varepsilon_{ff}/\varepsilon_{ss}$, $\varepsilon_{fs}/\varepsilon_{ss}$, σ_{ff}/σ_{ss}) = (3.81/2.95, ≈3.3/2.95, 4.08/4.09)

Only the Au/Cu system approximately obeys the restriction $\varepsilon_{ff}=\varepsilon_{ss}$. And, in this case, $W<1$ and $\eta\approx 0.1$. Our finding that the Au/Cu(100) system forms islands of Au is in accord with the Lennard-Jones based categorization, although the coverages were too low and the MD simulations too short to allow formation of 3D islands.

The Rh/Ag and Au/Ag cases do not come close to satisfying $\varepsilon_{ff}=\varepsilon_{ss}$, while the former also has $\eta<0$ which was not investigated in the Lennard-Jonesian systems. From our results, it is clear that *when the film-film and film-substrate interactions are stronger than that of the substrate-substrate and when the film atoms are smaller, complex behavior such as "sandwich" formation is possible.* Indeed, we believe that the

restrictions of the Lennard-Jones investigations to equal film-film and substrate-substrate interaction strengths, equal or larger film than substrate atoms and, especially rigid substrates, eliminated much of the interesting surface chemistry that can occur in metal on metal systems. These investigations simply categorized the classical growth modes in terms of microscopic parameters without providing clues to the rich behavior possible in other types of systems.

The present investigations are based upon describing the interatomic energies and forces in metallic systems by accurate semi-empirical methods. As such, the intent is not to categorize different behaviors of model systems, (i.e., perform computer experiments), but to predict phenomena in real systems. It is important to understand the limitations in such work. The accuracy of the present semi-empirical interactions may be insufficient to describe phenomena depending upon small energies, with comparisons to experiment necessary to delimit the predictive ability. The present results indicate both areas of caution, the Au/Cu mixed layer at ½ monolayer coverage may not be predicted correctly (or may not form via a place exchange mechanism), and success, "sandwich" structure formation in Rh/Ag and growth mode dependence upon Ag surface in Au/Ag.

Based upon our results, we expect that other systems will also display "sandwich" structures. These should involve small adsorbates with much larger cohesive energies than the substrate, for example Rh/Pd, Rh/Au, Pt/Ag and Pt/Au. An interesting investigation would involve Rh/Cu and Rh/Ni since the adsorbate becomes increasing larger than the substrate but the former is still favored to exist in bulk environments.

6. ACKNOWLEDGEMENT

We would like to thank Susan Sinnott for providing CEM and MD/MC-CEM surface energies prior to publication. Financial support was received from NSF grant CHE-8609832 and CHE-8921099. Partial support by the Petroleum Research Foundation administered by the American Chemical Society has also been received on grant 21690-AC5,C. In addition, we are pleased to acknowledge a grant of Cray YMP computer time at the Pittsburgh Supercomputer Center from Cray Research, Inc.

7. REFERENCES

[1] a) E. Bauer, Z. Kristallogr. 110 (1958) 372;
b) E. Bauer and H. Poppa, Thin Solid Films 12 (1972) 167;
c) E. Bauer, Appl. Surf. Sci. 11/12 (1982) 479;
d) R. W. Vook, Intern. Metals Rev. 27 (1982) 209;
e) S. Stoyanov, Surf. Sci. 172 (1986) 198.

[2] a) J. A. Venables, G. D. T. Spiller and M. Hanbucken, Rep. Prog. Phys., 47, (1984) 399;
b) J. A. Nieminen and K. Kaski, Phys. Rev. A40 (1989) 2088;

[3] a) P. I. Cohen, G. S. Petrich, P. R. Pukite, G. J. Whaley and A. S. Arrott, Surf. Sci. 216 (1989) 222;
b) B. Shizgal and J. C. Barrett, J. Chem. Phys. 91 (1989) 6505.

[4] D. P. Jackson in "Interatomic Potentials and Simulations of Lattice Defects", (Plenum Press, New York, 1972) and ref. therein.

[5] a) E. Pearson, T. Taki, T. Halicioglu amd W. A. Tiller, J. Cryst. Growth 70 (1984) 33;
b) T. Halicioglu, H. O. Pamuk and S. Erkoc, Surf. Sci. 143 (1984) 601.

[6] a) K. W. Jacobsen, J. K. Nørskov, and M. J. Puska, Phys. Rev. B35 (1987) 7423;
b) K. W. Jacobsen, Comments Condens. Matter Phys. 14 (1988) 129;
c) J. K. Nørskov and N. D. Lang, Phys. Rev. B21 (1980) 2131;
d) M. J. Stott and E. Zaremba, Phys. Rev. B22 (1980) 1564.

[7] a) M. S. Daw, Phys. Rev. B39 7441 (1989);
b) M. S. Daw, and M. I. Baskes, Phys. Rev. B29 (1984) 6443.

[8] a) F. Ercolessi, M. Parrinello, and E. Tosatti, Surf. Sci. 177 (1986) 314;
b) F. Ercolessi, A. Bartolini, M. Garofalo, M. Parrinello, and E. Tosatti, Surf. Sci. 189-190 (1987) 636;
c) F. Ercolessi, A. Bartolini, M. Garofalo, M., Parrinello, and E. Tosatti, Phys. Scr. T19B (1987) 399;
d) F. Ercolessi, M. Parrinello, and E. Tosatti, Philos. Mag. A58 (1988) 213.

[9] a) J. D. Kress and A. E. DePristo, J. Chem. Phys. 88 (1988) 2596;
b) J. D. Kress, M. S. Stave and A. E. DePristo, J. Phys. Chem. 93 (1989) 1556.

[10] T. J. Raeker and A. E. DePristo, Phys. Rev. B39 (1989) 9967.

[11] T. J. Raeker and A. E. DePristo, Surf. Sci. 235 (1990) 84.

[12] M. S. Stave, D. E. Sanders, T. J. Raeker and A. E. DePristo, "Corrected Effective Medium Method: V. Simplifications for Molecular Dynamics and Monte-Carlo Simulations", J. Chem. Phys. (accepted).

[13] T. J. Raeker and A.E. DePristo, "Theory of Chemical Bonding based upon the Atom-Homogeneous Electron Gas System", Int. Rev. Phys. Chem., in press.

[14] P. W. Palmberg and T. N. Rhodin, J. Chem. Phys. 49 (1968) 134.

[15] Z. Q. Wang, Y. S. Li, C. K. C. Lok, J. Qiunn, F. Jona and P. M. Marcus, Solid State Communications 62 (1987) 181.

[16] G. W. Graham, Surf. Sci. 184 (1987) 137.

[17] P.J. Schmitz, W. -Y. Leung, G. W. Graham and P. A. Thiel, Phys. Rev. B40 (1989) 1.

[18] P. Fenter and T. Gustafsson, Phys. Rev. Lett. 64 (1990) 1142.

[19] D. E. Sanders, M. S. Stave, and A. E. DePristo, "SCT89: a computer code for atomic and molecular scattering from clean and adsorbate covered surfaces", J. Comp. Phys. (submitted October 1990).

[20] a) A. E. DePristo and H. Metiu, J. Chem. Phys. 90 (1989) 1229;
b) M. Berkowitz and J. A. McCammon, Chem. Phys. Lett. 90 (1982) 215;
c) C. L. Brooks III and M. Karplus, J. Chem. Phys. 79 (1983) 6312;
d) R. Lucchese and J. C. Tully, Surf. Sci. 137 1570 (1983); J. Chem. Phys. 80, (1984) 3451.

[21] L. Verlet, Phys. Rev. 159 (1967) 98.

[22] T. J. Raeker, D. E. Sanders and A. E. DePristo, J. of Vac. Sci. Technol. A8 (1990) 3531.

[23] D. J Coulman, J. Wintterlin, R. J. Behm, and G Ertl, Phys. Rev. Lett. 64 (1990) 1761.

[24] S. M. Foiles, Surf. Sci. 191 (1987) 329.

[25] R. J. Culbertson, L. C. Feldman, P. J. Silverman and H. Boehm, Phys. Rev. Lett. 47 (1981) 657.

[26] T.C. Hsieh, A. P. Shapiro and T. -C. Chiang, Phys. Rev. B31 (1985) 2541.

[27] a) M. H. Grabow and G. H. Gilmer, Mat. Res. Soc. Symp. Proc. 94 (1987) 15;
b) M. H. Grabow and G. H. Gilmer, Surf. Sci. 194, 333 (1988).

GENERAL SUMMARIES AND CONCLUSIONS

In the introduction I derived the basic CEM interaction energy relation, Eq. (6), for any N-atom system. Papers I and II develops CEM formalisms specific for high symmetry cases of bulk metals, clean and adsorbate covered surfaces. By making use of symmetry I was able to simplify significantly the cumbersome interaction energy of a N-atom system to that of select 'focus' atoms interacting with a semi-infinite system of atoms. This eliminates edge effects when one is trying to examine properties of infinite systems.

Clean Surfaces

Paper I presents an expression for the bulk cohesive energy of any metal atom in a monatomic lattice. Analysis of the calculations based on this expression when using the SCF-LD embedding energy functions of Puska *et al.* [4] suggested that these embedding energy functions represent an ionic interaction of the atom with jellium. This type of interaction is not appropriate for a homogeneous system with covalent bonding. As a result, a semi-empirical embedding energy function was constructed to represent covalent or metallic bonding for these systems.

Further use of symmetry for clean surfaces resulted in a very simple expression for the surface energy. The minimization of the surface energy with respect to interplaner distances allowed prediction of multi-layer relaxation for various surfaces. The good agreement of the predicted surface energies led to confidence in the multilayer relaxation predictions. For open surfaces, the oscillatory relaxations extended deeper into the surface than experiments have been able to probe.

It was confirmed that the top layer of a metal surface contracts toward the second layer. The second layer in turn expands away from the layer below it due to the excess interaction from the top layer contraction. In addition, if the second layer expansion is large the third layer itself may contract towards the fourth layer below. This oscillatory pattern continues in a dampened fashion as one goes further below the

top layer.

The excellent results obtained for the clean surfaces led me to further extensions of the method that included adsorbates on the metal surface. This was the topic of Paper II. I we showed that the binding energy for any adsorbate in an ordered overlayer can be calculated quite readily. Again the use of a semi-infinite model eliminated the undesirable feature of edge effects inherent in cluster models and enabled a direct comparison to experimental data.

Chemisorption on Surfaces

The binding of H and N atoms on various Fe surfaces and W(110) was examined in detail. Minimization of the binding energy with respect to the metal surface layer distances (as in Paper I), as well as the adsorbate binding height, demonstrated that some adsorbates can influence considerably the structure of the surface. The degree of influence is dominated by two features of adsorbate binding. The first is the strength of the adsorbate-second metal layer interaction and the second is the coverage. In general the magnitude of induced surface relaxation was found to increase with both the binding strength and coverage.

It is the interaction of the adsorbate with the second layer metal atoms that governs the relaxation. The adsorbate tends to decrease its binding height to enhance its interaction with the second layer atoms. If the adsorbate gets close enough, and interacts strongly, the second layer will push the first layer away. In essence the second layer is willing to sacrifice interaction with metal atoms above for a stronger interaction with the adsorbate. This is in contrast to the traditional thinking that adsorbates heal the surface [14]. The dangling bonds left on the clean surface cause the surface to contract. Adsorbates then fill these dangling bonds and the surface relaxes away from the second layer. The healing idea makes intuitive sense but I have shown that this is not a complete picture of the adsorbate induced relaxation of metal surfaces.

The above calculations were all static in nature: an ordered structure was guessed and the energy was calculated. This process was repeated until the energy was minimized with respect to only a few degrees of freedom describing the surface. The

effects of disorder, temperature and many more degrees of freedom were not examined in Papers I and II. The purpose of Papers III and IV were to address these and extend the CEM method to very large and less symmetric systems.

Molecular Dynamics of Metal Adsorbates

In Paper III, I described the initial mechanisms involved in the formation of the equilibrium structures of Rh atoms deposited on the Ag(100) surface. Many simulations of temperature annealing of predeposited Rh atoms were done to examine in detail how atoms move in order to form an equilibrium structure. I have determined that the dominant motion is Rh atoms exchanging places with surface Ag atoms. Higher temperature annealing enhanced the rate and overall amount of place exchange. This confirmed experimental data [15] that suggest a sandwich type structure is formed after annealing at 600 C of a Rh deposited film on the Ag(100) surface.

My calculations indicated that the initial stages of the formation of a sandwich structure is a self-catalyzing mechanism at around half monolayer coverages. The mechanism has two stages. First, the rare event of a Rh-Ag place exchange has to have taken place. Then once this is accomplished, other nearby Rh atoms still on top of the surface are drawn into the surface by the previous Rh atoms that have already exchanged. If there are no nearby Rh atoms, then the original exchange is a single isolated event.

Paper IV examined the thin film dynamics of two systems. The dynamics of the structural formation of Au atoms deposited on Cu(100) at half and quarter monolayer coverages was examined. The Rh/Ag(100) system was examined again with the results providing further support of the previous findings in Paper III.

The molecular dynamics simulations of the Au/Cu(100) system also gave insight on the initial stages of the formation of an ordered surface alloy of Au and Cu on the Cu(100) surface. Unlike the Rh/Ag(100) system, place exchange of Au and Cu does not occur on the time scale of around 1000 ps. Rather, Au and Cu atoms most likely simply mix on the surface where Cu atoms from step edges diffuse into existing Au islands. The same can occur for Au atoms diffusing into Cu step edges from these

same Au islands. This phenomenon has recently been experimentally postulated [16] for O chemisorbed on Cu(110). Although this type of phenomena is much to slow to be examined completely by a molecular dynamics simulation, such short time scale calculations have shed light on the initial mechanism involved in forming equilibrium structures.

Paper IV also examined the energetics of Au deposited films on Ag(110) system. Only static calculations were done here. The results indicated that Au atoms may have an energetic preference to form bilayer rather than single monolayer islands on the Ag(110) surface. Thus at low coverages, Au atoms may migrate onto an existing Au island and form a two layer island. There is an energetic advantage to form the second layer rather than bind on the Ag surface. This confirmed recent experimental evidence [17] suggesting bilayer island growth of Au on the Ag(110) surface.

The CEM method is fast evolving into an efficient predictive tool for several areas of scientific research. The method is particularly applicable to extended systems where the electron density distributions more closely resemble that of jellium. Papers I and II of this thesis presented results that can be compared directly to available experimental data. The quantitative predictions agreed very well with available experiment data. This success of the method thus builds confidence for future applications.

Papers III and IV presented results that, even without quantitative comparison to experimental data, do qualitatively help in the interpretation of new and existing experimental work. Many areas in the materials sciences pose problems which are ideal for the MD/MC-CEM method. I must reemphasize that the molecular dynamics simulations should not be used to determine the overall equilibrium structures. Rather, one should use MD simulations as a tool in identifying and quantifying the various processes that eventually form an equilibrium structure.

There are limitations of the CEM method that should be mentioned. The most obvious is that the method is not self-consistent. Thus electronic properties are not accessible. This self-consistency problem may never be addressed since making CEM self-consistent defeats the purpose: to provide a simple, very fast and accurate method. There are however a few steps that can be taken to make the CEM method more in

touch with real systems or at least even more reliable.

First the use of free atom HF electron densities turns out to be a problem in some cases. More recent calculations by another member of the research group and me [18] on the relaxation of clean metal surfaces have resulted in the loss of CEM's ability to predict oscillatory relaxation of open surfaces. Only top layer contraction is predicted to occur. This is in contrast to my original calculations in Paper I. The only difference between these sets of calculations was in the form of the Gaussian fit to the HF atomic electron density. Paper I utilized the first Gaussian form Eq. (23) and the more recent results utilized the second in Eq. (25). As already discussed, the first form of the fit had electron density tails higher in magnitude than the second. Surprisingly, improving the quality of the fit and, supposedly a better calculation, resulted in poorer results.

The reason for this discrepancy is that in bulk systems the electron density is less localized around an individual atom than in free space. Thus the first fit had mimicked in a crude way this delocalization of the electron density which in turn made the atoms more sensitive to small displacements such as layer relaxation. This indicates to me that the proper representation of the atomic electron density is indeed important. One way in which to better describe extended systems such as surfaces is to fit the Gaussian expansion to atomic electron densities derived from bulk systems rather than from the free atom. Some properties of surfaces, such as relaxation, are sensitive to small changes in the electron density distributions. We cannot easily relax the electron densities but at least we can better approximate them for a given configuration of atoms (i.e., bulk and surface systems).

Second, the MD/MC-CEM method is ideal for molecular dynamics calculations and far superior to empirical pair-potentials. This is so even though there are some disagreements in energetics compared to experimental data and the full CEM method. Remember that the correction energy ΔG is approximated quite simply as a function of the jellium electron density environment and is empirically constructed. It is apparent that a more sophisticated approximation of ΔG will surely improve the accuracy over the simplistic approach.

One way to improve upon the approximation is to make ΔG depend also on some

average gradient of the electron density environment;

$$\Delta G = \sum_{i}^{N} [\Delta G(n_i) + \Delta G_i(\langle\langle \nabla n(\vec{r}) \rangle\rangle)] \tag{34}$$

The first term is the current empirical approximation (not the exact values) and the second term depends the gradient correction of the electron density environment. This approximation is much more reasonable since the correction energy ΔG was designed to correct for electron inhomogeneities (gradients) in the first place.

One must however be careful not to make the above gradient correction too complicated since molecular dynamics of large systems requires a potential that is fast to evaluate and differentiate. Thus the ideal case would be to use something that is already calculated or at least easily derived from existing information. The electron density overlaps in Eqs. (21) and (22) may lend themselves to such an approach.

ACKNOWLEDGEMENT

I would like to first thank my parents who, during my childhood, recognized my interest in science and encouraged me in learning about and doing science. I would also like thank my major professor, Dr. Andrew DePristo, for giving me the freedom to work on problems in surface science that are of most interest to me. His excitement towards scientific research is, I believe, one of the most important attitudes a teacher can pass on to students. I hope I can live up to his example. Finally, I would like to thank my new wife Maide for giving me support and providing additional motivation to finish up this thesis and get on with my career.

REFERENCES

[1] W. Kohn and L. J. Sham, Phys. Rev. A140 (1965) 1133.

[2] For good and informative surveys see a) "*Theory of the Inhomogeneous Electron Gas*", edited by S. Lundqvist and N. H. March, Plenum, New York, 1983 and;
b) R. G. Parr and W. Yang, "*Density-Functional Theory of Atoms and Molecules*",Oxford University Press, New York (1989).

[3] D. R. Salahub and M. C. Zerner, *The challenge of d and f electrons: Theory and Computation*, 1989, (ACS Symposium Series).

[4] M. J. Puska, R. M. Nieminen, and M Manninen, Phys. Rev. B24 (1981) 3037.

[5] T. J. Raeker and A. E. DePristo, *Theory of Chemical Bonding based on the Atom-Homogeneous Electron Gas System*, Int. Rev. Phys. Chem, (in press).

[6] J. D. Kress and A. E. Depristo, J. Chem. Phys. 88 (1988) 2596.

[7] P. A. M. Dirac, Proc. Camb. Philos. Soc., 26 (1930) 376.

[8] O. Gunnarsson and B. I. Lundqvist, Phys. Rev. B13, (1976) 4274.

[9] A. E. DePristo and J. D. Kress, Phys. Rev. A 35 (1987) 438.

[10] a) L. H. Thomas, Proc., Camb. Philos. Soc. 23 (1927) 542;
b) E. Fermi, Rend. Accad., Lincei, 6 (1928) 602;
c) E. Fermi, Z. Phys. 48 (1928) 73;
d) E. Fermi, Rend. Accad., Lincei, 7 (1928) 342.

[11] M. Schmidt and K. Ruedenberg, J. Chem. Phys. 71 (1979) 3951.

[12] S. Huzinaga. Proc. Theor. Phys. Suppl. 40 (1967) 279.

[13] Stepit is a self-sufficient fortran routine that can find the local minima of a smooth function with respect to parameters defining the function. The code was obtained through the Quantum Chemistry Program Exchange, Dept. of Chemistry, Indiana University, Bloomington, Indiana 47401.

[14] a) P. J. Feibman and D. R. Hamann, Surf. Sci. 234 (1990) 377;
b) V. Bortolani, A. Franchini, G. Santoro, J. P. Toennies, Ch. Woll and G. Zhang, Phys. Rev B 40 (1989) 3524;
c) A. P. Baddorf, I. -W. Lyo, E. W Plummer and H. L. Davis, J. Vac. Sci. Technol. A 5 (1987) 782.

[15] P. J. Schmitz, W. -Y. Leung, G. W. Graham and P. A. Thiel, Phys Rev. B 40 (1989) 1.

[16] D. J. Coulman, J. Wintterlin, R. J. Behm and G. Ertl, Phys. Rev. Lett. 64 (1990) 1761.

[17] P. Fenter and T Gustafsson, Phys. Rev. Lett. 64 (1990) 1142.

[18] S. Sinnott, T. J. Raeker, and A. E. DePristo, (manuscript in preparation).